Catalysis by oxides: conversion of light organic molecules

Ioan-Cezar Marcu

UNIVERSITY OF BUCHAREST

FACULTY OF CHEMISTRY

CATALYSIS BY OXIDES:
CONVERSION OF LIGHT ORGANIC MOLECULES

HABILITATION THESIS

Dr. Ioan-Cezar Marcu

Associate Professor

2013

My URLs: http://www.unibuc.ro/e/prof/marcu_i_c/ (in English)

http://www.unibuc.ro/prof/marcu_i_c/ (in Romanian)

“If we knew what it was we were doing, it would not be called research, would it?”

Albert Einstein

This page intentionally left blank

To my mentor, Prof. Ioan Săndulescu,

whose human and professional qualities inspired me to become both a researcher and a teacher.

This page intentionally left blank

ABSTRACT

In this thesis I present my most relevant research work I performed as a main author from 2002 until these days in the field of Catalysis by Oxides by grouping it on a thematic basis. Consequently, each chapter in *Section A* presents a research direction which corresponds to several papers. I tried to avoid technical details in the text and illustrate the main ideas using results and their discussion. It is worth noting that the results presented here were mainly obtained in the Laboratory of Chemical Technology and Catalysis from the University of Bucharest but also in laboratories abroad where I worked or we are collaborating with.

Chapter I presents the most relevant of my results on the subject of the oxidative dehydrogenation (ODH) of light alkanes following two main directions: i) enhancing the ODH selectivity of highly active catalysts and ii) developing new effective catalysts for ODH of light alkanes. Thus, we have shown that the ODH reaction of *n*-butane over highly active and selective TiP_2O_7 catalysts can be further improved by addition of CO_2 in the feed and that phosphating ceria produces an increase in ODH selectivity mainly at the expense of total oxidation products. We studied new rare earth and transition metal-containing mixed-oxides obtained from layered double hydroxides (LDH) precursors as ODH catalysts. We have shown first that the use of the LDH-derived Mg-containing mixed oxides as catalysts in the ODH reaction favored the desorption of alkenes, and, consequently, improved the ODH selectivity. Among them the Co-containing system was the most active and selective for propane ODH. In this case we have shown that the well-dispersed cobalt species with tetrahedral coordination played a main role in the ODH reaction of propane into propene, the highest propene yields being obtained with the catalysts containing 7.5-9 at % Co with respect to cations.

Chapter II is dedicated to the study of total oxidation of short-chain alkanes over different novel oxide-based catalysts with the aim of finding highly active catalysts for volatile organic compounds (VOCs) destruction, capable to replace the precious metal catalysts presently used. Thus, we have studied Pb and Ba titanates, LDH-derived transition metal-containing mixed oxides and Ni and Co ferrospinels. The most active and stable catalyst in the total oxidation of methane was the LDH-derived Cu-containing system. In this case we have shown that the active sites were the highly reducible copper species, their optimum dispersion being observed for the

catalyst containing ~ 12 at % Cu with respect to cations. We have also shown for the first time that Co ferrite was highly active and stable in the total oxidation of propane as a VOC model.

Chapter III is focussed on the study of oxidation catalysts by electrical conductivity measurements, a powerful technique for catalysts characterization that can provide information on the nature of surface oxidizing species, of structure defects and of the oxidic phase involved in the catalytic reaction which allows us to explain the catalytic behavior of the catalysts studied and to propose a reaction mechanism. Thus, we studied by electrical conductivity measurements ceria and phosphated ceria, catalysts for isobutane ODH, Pb and Ba titanates, catalysts for methane total oxidation, and vanadium antimonate and mixed vanadium and iron antimonate, catalysts for propane ammoxidation, the relationship existing between their redox and catalytic properties being evidenced and their catalytic behavior explained.

Chapter IV is devoted to the study of catalytic processes involving the acid-base properties of the catalyst, such as conversion of ethanol into higher added value products over LDH-derived mixed oxides, cyanoethylation of methanol over transition-metal containing Mg-Al hydrotalcites and their corresponding mixed oxides and esterification of *n*-butanol with acetic acid over almina-supported molibdena and vanadia catalysts. Thus, we have shown that the Pd-containing LDH-derived mixed oxide was active for ethanol conversion into *n*-butanol while the Cu-based catalyst oriented the transformation towards *n*-butanol or 1,1-diethoxyethane depending on the reaction conditions and on the copper content. In the cyanoethylation reaction of methanol MgAlO system showed the best catalytic performances which diminished after introduction of the transition metal cations, the equilibrium between basic and acid sites being a key factor. Finally, we have shown that molybdena supported on γ-alumina acts as an efficient stable solid acid catalyst for the esterification of acetic acid with *n*-butanol, while vanadia supported on γ-alumina loose its activity because of the leaching of the active component.

In *Section B* a plan for my research and academic career development is emphasized, different research topics in the field of Catalysis by Oxides that I intend to tackle in the future being described and justified based on a literature survey.

REZUMAT

În această teză sunt prezentate cele mai relevante rezultate ale activității mele de cercetare efectuată în calitate de autor principal în domeniul Cataliză pe Oxizi din 2002 până în prezent, grupate pe baze tematice. Astfel, fiecare capitol din *Secțiunea A* prezintă o direcție de cercetare careia îi corespund mai multe publicații. Am încercat să evit detaliile tehnice în text şi să ilustrez ideile principale cu rezultate şi discuția acestora. De notat ca rezultatele prezentate aici au fost obținute în principal in Laboratorul de Chimie Tehnologică şi Cataliză al Universității din Bucureşti dar şi în alte laboratoare în care am lucrat sau cu care colaborăm.

Capitolul I prezintă cele mai relevante dintre rezultatele mele pe tema dehidrogenării oxidative (DHO) a alcanilor inferiori urmărind doua direcții principale: i) îmbunătățirea selectivității pentru DHO a catalizatorilor foarte activi şi ii) obținerea de noi catalizatori eficienți pentru DHO a alcanilor inferiori. Astfel, am arătat că DHO a *n*-butanului pe catalizatorii foarte activi şi selectivi TiP_2O_7 poate fi încă ameliorată prin adăugarea de CO_2 în amestecul reactant precum şi faptul că fosfatarea dioxidului de ceriu are ca rezultat o creştere a selectivității pentru DHO în principal pe seama produşilor de oxidare totală. Am studiat drept catalizatori pentru DHO noi oxizi micşti cu lantanoide şi metale tranziționale obținuți din precursori hidroxizi dubli lamelari (HDL). Am arătat în primul rand că utilizarea oxizilor micşti cu Mg obținuți din precursori HDL drept catalizatori în DHO favorizează desorbția alchenelor şi, în consecință, creşte selectivitatea pentru DHO. Printre aceştia sistemul cu Co s-a dovedit a fi cel mai activ şi selectiv pentru DHO a propanului. În acest caz am arătat că speciile de Co înalt dispersate cu coordinare tetraedrică joacă un rol important in DHO a propanului în propenă, cele mai bune randamente pentru propenă fiind obținute cu catalizatorii ce conțin 7.5-9 at % Co față de cationi.

Capitolul II este dedicat studiului oxidării totale a alcanilor inferiori în prezența unor noi catalizatori pe bază de oxizi metalici cu scopul de a găsi catalizatori cu activitate ridicată în distrugerea compuşilor organici volatili (COV) capabili să înlocuiască catalizatorii de metale nobile utilizați în prezent. Astfel, am studiat titanați de Pb si Ba, oxizi micşti ce conțin cationi de metale tranziționale obținuți din precursori HDL şi ferite spinelice de Ni şi Co. Cel mai activ şi stabil catalizator în oxidarea totală a metanului s-a dovedit a fi sistemul pe bază de Cu obținut din precursori HDL. În acest caz am arătat că centrii activi sunt speciile de cupru înalt reductibile, dispersia optimă a acestora fiind observată pentru catalizatorul cu ~ 12 at % Cu față de cationi.

Am arătat, de asemenea, pentru prima dată că ferita de Co este foarte activă şi stabilă în oxidarea totală a propanului ca model de COV.

Capitolul III este centrat pe studiul catalizatorilor de oxidare prin măsurători de conductivitate electrică, o tehnică excelentă de caracterizare a catalizatorilor care poate da informații despre natura speciilor oxidante superficiale, a structurii defectelor şi a fazei oxidice implicate în reacția catalitică, permițându-ne astfel explicarea comportamentului catalitic al catalizatorilor studiați şi elaborarea unui mecanism de reacție. Astfel, am studiat prin măsurători de conductivitate electrică dioxidul de ceriu pur şi fosfatat, catalizatori pentru DHO a izobutanului, titanații de Pb şi Ba, catalizatori pentru oxidarea totală a metanului precum şi antimoniatul de vanadiu şi antimoniatul mixt de vanadiu şi fier, catalizatori pentru amonoxidarea propanului, fiind evidențiată relația existentă intre proprităţile lor redox şi catalitice şi explicat comportamentul lor catalitic.

Capitolul IV este consacrat studiului unor procese catalitice care implică proprietăţile acido-bazice ale catalizatorilor, cum ar fi conversia etanolului în produşi cu valoare adaugată ridicată pe catalizatori oxizi micşti derivați din HDL, cianoetilarea metanolului pe catalizatori HDL cu Mg, Al şi metale tranzitionale şi oxizii micşti corespunzători precum şi esterificarea *n*-butanolului cu acid acetic pe catalizatori de oxid de molibden si oxid de vanadiu suportați pe alumina. Astfel, am arătat că oxidul mixt cu Pd derivat din HDL este activ pentru conversia etanolului în *n*-butanol în timp ce catalizatorul pe bază de Cu orientează transformarea fie către *n*-butanol sau 1,1-dietoxietan în funcție de condițiile de reacție şi de conținutul de Cu. În reacția de cianoetilare a metanolului, cele mai bune performanțe catalitice le-a avut sistemul MgAlO acestea diminuându-se în urma introducerii de cationi de metale tranziționale în oxidul mixt, echilibrul dintre centrii acizi şi bazici fiind un factor cheie. În sfârşit, am arătat că oxidul de molibden suportat pe γ-alumină este un catalizator solid acid eficient şi stabil pentru esterificarea acidului acetic cu *n*-butanol, în timp ce oxidul de vanadiu suportat pe γ-alumină îşi pierde activitatea ca urmare a pierderii componentei active.

In *Secțiunea B* este prezentat un plan de dezvoltare al carierei mele academice şi de cercetare, fiind descrise şi justificate pe baza unui examen al datelor de literatură diferite subiecte de cercetare din domeniul Cataliză pe Oxizi pe care intenționez să le abordez în viitor.

AKNOWLEDGEMENTS

First of all I warmly thank Prof. Ioan Săndulescu, *the Professor*, for encouraging me and supporting both my research and my didactic work, for giving me the freedom to pursue my own ideas all along my university career and for his great generosity of spirit. Each working experience with the Professor was for me not only a lesson of chemistry but also a lesson of humanity.

My special warm thanks go to my former PhD co-supervisor Dr. Jean-Marc Millet from IRCELYON, France, for encouraging and helping me all these last years and for restarting our collaboration (we will publish soon!). I owe a lot to Jean-Marc who is a man of sound advice and a good friend for me.

I am very much grateful to Dr. Jean-Marie Herrmann from IRCELYON, France, who initiated me in applying electrical conductivity measurements to the characterization of oxide-based catalysts and encouraged me to develop this technique in my laboratory. Thanks to him and to Jean-Marc, my first work after my PhD thesis was the study by electrical conductivity measurements of antimonate-based catalysts.

I feel very much enriched by my post-doc experience in the Laboratory of Advanced Materials for Catalysis and Health at Institute Charles Gerhardt of Montpellier, France, especially as it was the starting point of a long-term and fruitful collaboration with our laboratory in Bucharest. It was and it is still an honor and a pleasure for me to work with Dr. François Fajula, Dr. Nathalie Tanchoux and Dr. Didier Tichit. I am very glad to have had the chance to interact with all the people of the Laboratory of Advanced Materials for Catalysis and Health. My note of gratitude goes to Thomas Cacciaguerra and Geraldine Layrac in particular.

I deeply appreciate the long-term and fruitful collaboration with Prof. Ákos Rédey and his research team from the University of Pannonia at Veszprém, Hungary. I am very thankful to Prof. Rédey for his constant encouragement, for his kindness and his willingness to help me. A special note of gratitude goes to everyone at the University of Pannonia, in particular Tatiana Yuzhakova, Éva Mako, Jozsef Kovacs and Oravetz Dezsö.

I am also grateful to Stéphane Loridant from IRCELYON, France, for his seriousness and for his ongoing availability to help me with the Raman spectroscopy studies.

Special thanks to Prof. Vasile Pârvulescu for his confidence in my research work and for his collaboration on the oxidative dehydrogenation over phosphated ceria. I greatly appreciate his effort for creating good research conditions and a stimulating environment in our laboratory.

My warmest personal thanks go to my colleague and friend Ionel Popescu, the architect of the electrical conductivity measurements set-up in our laboratory, for his patience and meticulousness but also for all the hours of exciting discussions, not only on catalysis after all.

I am very grateful to my colleagues and close collaborators Gheorghița Mitran who has done most of the experimental work on the oxidative dehydrogenation and esterification, and Adriana Urdă and Octavian-Dumitru Pavel for their co-operation on the total oxidation and cyanoethylation, respectively.

I would also like to thank all my colleagues from the Laboratory of Chemical Technology and Catalysis at the University of Bucharest, in particular Mihaela Florea, Mădălina Săndulescu, Bogdan Cojocaru and Simona Coman for their collegiality and availability to help me with different catalysts characterizations.

This work is also based on the collaboration with several of my best former students from the University of Bucharest but also from Toulouse Institute of Technology who worked in our laboratory starting from 2006 within the frame of the Erasmus Program. I am particularly indebted to Florentina Urlan, Adrien Herraïz, Marcel Nicu Urlan and Ioan-Teodor Trotuş. I am also indebted to Serghei Tanasoi, the last PhD student of my Professor, who worked with me on the total oxidation of methane.

Most of the research work presented in this monograph was more or less financed within the frame of several projects by the Romanian National Authority for Scientific Research – Executive Agency for Higher Education, Research, Development and Innovation Funding (CNCS-UEFISCDI) which is greatly acknowledged.

Last but not least, I am very grateful to my wife Mirela and my son Sebastian for their ongoing support and for their great understanding for my extended working hours…

TABLE OF CONTENTS

This page intentionally left blank

SECTION A. SCIENTIFIC ACHIEVEMENTS

SECTION A. SCIENTIFIC ACHIEVEMENTS

This page intentionally left blank

I. CATALYTIC OXIDATIVE DEHYDROGENATION OF LIGHT ALKANES

A potential route for short-chain alkane (C_2-C_4) valorization is their conversion to unsaturated hydrocarbons which are largely used as starting materials in chemical industry.

Dehydrogenation of light alkanes is an equilibrium endothermic reaction that requires relatively high temperature to obtain a high yield of alkenes. However, the alkane conversion is limited by thermodynamic equilibrium and the high reaction temperature favors thermal cracking reactions of the alkane and coke formation, resulting in a decline in product yield and an increase in catalyst deactivation [1].

Oxidative dehydrogenation (ODH) of light alkanes may offer a promising alternative for the production of alkenes compared to the dehydrogenation process. ODH has the advantage of an exothermic reaction, without thermodynamic limitations and with a low risk of catalyst deactivation through coking because the reaction is run in an oxidative environment. In spite of being intensively studied for a long time, the conventional oxidative dehydrogenation of light alkanes is still far from industrial application [2]. Nevertheless, it is worth noting that the concept of oxydehydrogenation is already used in industry to convert propane into propene in a two-step process. For example, in the STAR process (UHDE) a conventional dehydrogenation step is followed by an oxidation step in which oxygen is admitted to the system for converting hydrogen into water and thus shifting the equilibrium of the dehydrogenation reaction to the products side [3].

The main difficulty in obtaining high alkenes yields by conventional ODH of the corresponding alkanes arises from the fact that alkenes are more reactive than alkanes, thus being prone to further oxidation to produce carbon oxides. Therefore the catalytic oxidative dehydrogenation of light alkanes with high yields remains a challenge, the key aspect being the development of catalysts capable to accelerate only the sequence of consecutive elementary steps leading to the desired product (alkene) and suppress all other possible elementary steps, parallel or consecutive [4].

Due to the above-reported considerations my research work was oriented in the direction of developing and studying new active and selective catalysts for oxidative dehydrogenation of light alkanes. Taking into consideration that for being effective, a catalyst needs first of all to be selective (i.e. to produce minimal amounts of undesirable products), its activity being the second concern, we paid a special attention to improve the oxidative dehydrogenation selectivity. The most relevant results of my work in the field of ODH of light alkanes are presented below following two main directions: i) enhancing oxidative dehydrogenation selectivity of highly active catalysts and ii) developing new effective catalysts for oxidative dehydrogenation of light alkanes.

It is worth noting that the research work presented in this chapter was a natural continuation of my PhD research work as the oxidative dehydrogenation was the subject of my PhD thesis entitled "Oxidative dehydrogenation of *n*-butane over metal pyrophosphates based catalysts" and defended in 2002 at *Université Claude Bernard Lyon I*, France. It is available in full-text form at the URL http://tel.ccsd.cnrs.fr/documents/archives0/00/00/14/74/index_fr.html

I.1. ENHANCING THE OXIDATIVE DEHYDROGENATION SELECTIVITY

I.1.1. Enhancing the oxidative dehydrogenation selectivity with carbon dioxide as soft co-oxidant

Carbon dioxide is a promising nonconventional oxidant (or co-feed gas) for catalytic oxidative dehydrogenation of light alkanes to alkenes [5-19] and ethylbenzene to styrene [19-24]. The CO_2 serves as a medium for supplying heat for the endothermic dehydrogenation reaction, as a diluent for enhancing the equilibrium conversion of light alkanes and as an agent for the removal of coke formed on the catalyst. On the other hand, contrarily to what is traditionally believed, CO_2 is not inert in the oxidation reaction. Oxygen species produced by its dissociation can modify the oxidation state of the atoms on the surface of the catalysts and can directly participate in the oxidation of the hydrocarbon [14-17]. The oxidative dehydrogenation of light alkanes and ethylbenzene in the presence of carbon dioxide has been reviewed in Refs. [25, 26].

Several studies on *n*-butane oxidative dehydrogenation in the presence of CO_2 [9-13] showed that the effect of carbon dioxide was rather benefic in this reaction. This is why we studied the oxidative dehydrogenation of *n*-butane over two different titanium pyrophosphates, TiP_2O_7-M1 and TiP_2O_7-M2, in the presence of carbon dioxide and we compared the results with those obtained in our previous studies where we have shown that titanium pyrophosphate was an active and selective catalyst for the oxidative dehydrogenation of *n*-butane to butenes and butadiene [27, 28]. This work has been published in Ref. [29].

We have shown that, over all the range of temperatures considered, addition of CO_2 in the feed slightly decreased *n*-butane conversion but strongly increased the selectivity to dehydrogenation products at the expense of carbon oxides and cracking products, for both titanium pyrophosphates studied (Fig. I.1). For example, on TiP_2O_7-M1 at 530 °C, the conversion passed from 25 % in absence of CO_2 to 20 % in presence of CO_2, whereas the total selectivity for butenes and butadiene passed from 56 % to 83 %. These results were in line with those obtained by Ge et al. [12] over a V-Mg-O catalyst and may be explained by the fact that the addition of

CO_2 in the feed leads to the competition between molecular O_2 and CO_2 adsorption on the active sites and the decrease of the amount of adsorbed molecular O_2 which is believed to be responsible for the total oxidation. Furthermore, CO_2 may poison the non-selective sites on the catalyst surface resulting in the decrease of the deep oxidation [12]. Nevertheless, it is noteworthy that Dury et al. [15] observed during oxidative dehydrogenation of propane over $NiMoO_4$ based catalysts that the addition of CO_2 had a contrary effect: an increase in the conversion of propane accompanied by a decrease in the selectivity for propylene. Therefore, it seems that the effect of the addition of CO_2 in the feed on the catalytic performances depends on the nature of the catalyst.

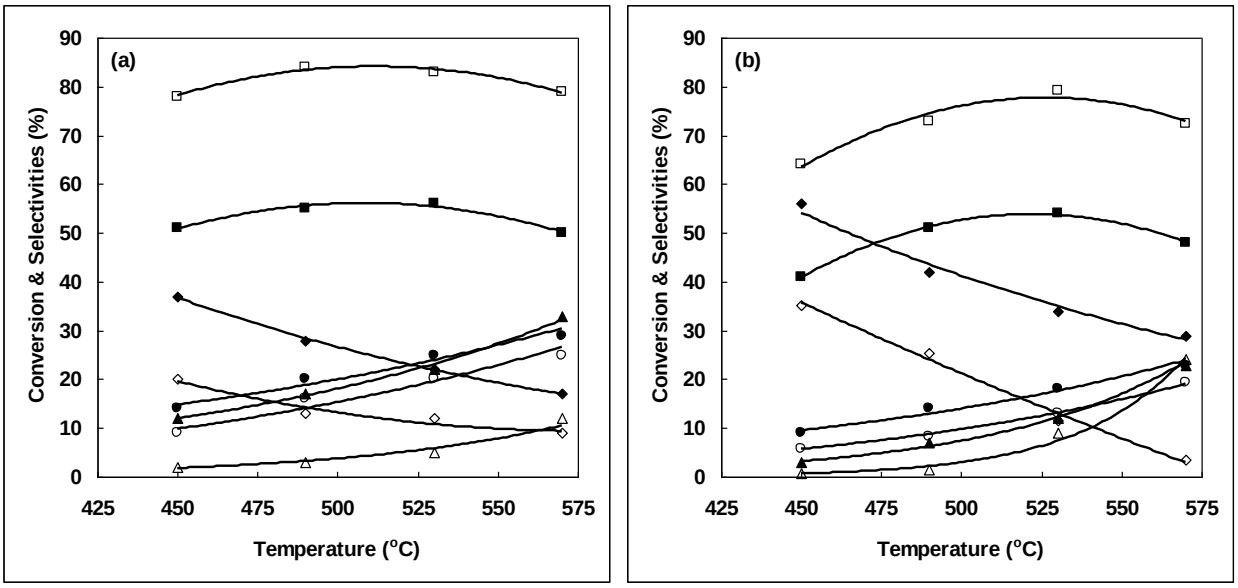

Figure I.1. Catalytic performances of TiP_2O_7-M1 (a) and TiP_2O_7-M2 (b) in the oxidative dehydrogenation of n-butane with air, in absence (solid symbols) and presence (open symbols) of CO_2. Reaction conditions: temperature range 450-570 °C, the molar ratios in absence and presence of CO_2 were air/n-butane = 5/1 and air/*n*-butane/CO_2 = 5/1/0.5, respectively, and the VHSV with respect to *n*-butane was equal to 1000 h^{-1}. ●, ○ – conversion; ■, □ – total dehydrogenation selectivity; ♦, ◊ – CO_x selectivity; ▲, Δ – cracking selectivity.

The rates of formation of dehydrogenation products, cracking products and total oxidation products for the reaction over both pyrophosphates at 530 °C, in the absence and in the presence of carbon dioxide, were calculated and are presented in Table I.1. It can be observed that, over

TiP_2O_7-M1 in the presence of carbon dioxide, the rates of formation of cracking products and total oxidation products decreased 5.7 and 2.3 times, respectively, while the rate of formation of dehydrogenation products increased only 1.2 times. For the reaction over TiP_2O_7-M2 in the presence of carbon dioxide, the rates of formation of cracking products and total oxidation products decreased 1.8 and 4.0 times, respectively, while the rate of formation of dehydrogenation products increased 1.1 times. This suggests that the observed loss in the overall activity in the presence of carbon dioxide is due to reduction of the reaction rates towards both cracking products and total oxidation products.

Table I.1. The rates of formation of dehydrogenation products, cracking products and total oxidation products for the reaction at 530 °C, in the absence and in the presence of CO_2.

Catalyst	Reaction mixture	Reaction rate (10^7 mol g^{-1} s^{-1}) towards:		
		Dehydrogenation	Cracking	CO_x
TiP_2O_7-M1	with CO_2	24.0	1.4	03.5
	without CO_2	20.2	8.0	08.0
TiP_2O_7-M2	with CO_2	22.3	2.6	03.3
	without CO_2	20.9	4.6	13.2

In our previous studies [27, 28] we have shown for the reaction with air in the absence of CO_2, that the catalytic performances of the crystalline titanium pyrophosphate phases were better than those of the similar amorphous compounds. This observation seems to remain valid for the reaction in the presence of CO_2 when TiP_2O_7-M1, a crystalline compound, was more active and selective than TiP_2O_7-M2, an amorphous compound. As we have already shown, the activity of the catalysts depends almost exclusively of the ability of the titanium to undergo oxido-reduction [27] and the crystalline pyrophosphate is more reducible than the amorphous one [27, 30]. On the other hand, the lower selectivity of the amorphous pyrophosphate compared to the crystalline pyrophosphate may be due to the overoxidation of the reaction products in the pores which presence was related to its high surface area [27].

It is noteworthy that the selectivity vs. conversion data for the reactions in the presence and in the absence of CO_2 showed that the presence of CO_2 in the reaction mixture inhibits the parallel reaction of *n*-butane leading to carbon oxides. This result is in line with the hypothesis that the addition of CO_2 in the feed leads to the competition between molecular O_2 and CO_2 adsorption on the active sites resulting in a decrease of the amount of adsorbed molecular O_2 which is believed to be responsible for the total oxidation.

When air was replaced with CO_2 over TiP_2O_7-M1 catalyst (Fig. I.2 compared with Fig. I.1(a)), an important decrease of the catalytic activity was observed within all the range of temperatures considered, even though accompanied by an important increase of the dehydrogenation selectivity. We have shown that at temperatures higher than 450 °C, the activity of TiP_2O_7 catalyst in the oxidative dehydrogenation of *n*-butane depends on the degree of reduction of the catalyst [27, 28, 31]. So, this fall of activity observed when air was replaced with CO_2 would be explained by the fact that the catalyst reduced by *n*-butane is very difficult to be reoxidized by CO_2. On the other hand, by studying the *n*-butane oxidative dehydrogenation on the TiP_2O_7-M1 catalyst in the TAP reactor [31] we observed that a strong adsorption of carbon dioxide on the catalyst surface takes place. This may be another important factor that has to be considered for explaining the loss of activity observed when air was replaced with CO_2.

Fig. I.2 shows the comparison of dehydrogenation with N_2 (data from ref. [32]) and with CO_2 over TiP_2O_7-M1. It can be observed that in the dehydrogenation with carbon dioxide the *n*-butane conversion was lower than in the dehydrogenation with nitrogen, within all domain of temperature. This could be explained by the strong adsorption of carbon dioxide on the catalyst surface, as observed by studying the *n*-butane oxidative dehydrogenation on the TiP_2O_7-M1 catalyst in the TAP reactor [31], which may compete with that of *n*-butane. At temperatures lower than 550 °C, the selectivity for dehydrogenation products was much higher in the dehydrogenation with carbon dioxide compared with the dehydrogenation with nitrogen. At temperatures higher than 550 °C, when the cracking reaction became important in both dehydrogenation with nitrogen and carbon dioxide, the differences between the selectivities for dehydrogenation products are not significant. Yet again, these results clearly show that carbon dioxide is not an inert gas for the dehydrogenation of *n*-butane, improving the dehydrogenation selectivity in particular at lower temperatures.

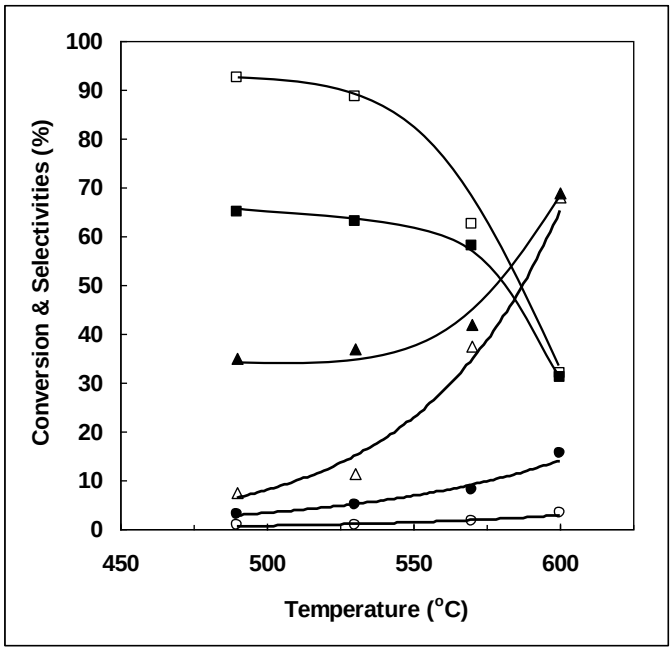

Figure I.2. Catalytic performances of TiP_2O_7-M1 in the dehydrogenation of *n*-butane with N_2 (solid symbols) and with CO_2 (open symbols). Reaction conditions: temperature range 490-600 °C, the molar ratios N_2/*n*-butane and CO_2/*n*-butane were kept at 5/1 and the VHSV with respect to *n*-butane was equal to 1000 h^{-1}. ●, ○ – conversion; ■, □ – total dehydrogenation selectivity; ▲, Δ – cracking selectivity.

In conclusion, the oxidative dehydrogenation of *n*-butane over TiP_2O_7 catalysts can be successfully improved by addition of CO_2 in the feed. It leads to the competition between molecular O_2 and CO_2 adsorption on the catalyst surface and the decrease of the amount of adsorbed molecular O_2 which is believed to be responsible for the total oxidation. On the other hand, when air was replaced with carbon dioxide as unique oxidant, an important decrease of the catalytic activity was observed probably due to the fact that the catalyst reduced by *n*-butane is very difficult to be reoxidized by CO_2. Another factor that has to be considered for explaining this loss of activity is the strong adsorption of carbon dioxide on the catalyst surface.

I.1.2. Enhancing the oxidative dehydrogenation selectivity of ceria-based catalysts using phosphorus as additive

The literature demonstrates that phosphorus, and surface-phosphorus in particular, plays a crucial role in phosphate based catalytic systems. There is yet no consensus on the precise nature of the role that surface phosphorus plays in these catalytic systems, but the results presented in the literature suggest that adding phosphorus to certain phosphate based catalysts may improve their catalytic performances [33-35]. Consistent with this, it was found [36-39] that catalytic activity could be significantly improved by adding phosphate to certain oxide catalyst surfaces through pretreatment with triethylphosphate, phosphoric acid or ammonium phosphate, but there are not many studies reported in the literature in this direction up to now and the role of surface phosphorus is yet not totally understood. Thus, for explaining the enhanced dehydrogenation reaction of ethane over tin(IV)-phosphorus catalysts Argent et al. [36] considered that highly nucleophilic surface phosphorus oxide sites favor hydrogen abstraction. Maiti et al. [37] also showed that, in the oxidative dehydrogenation of ethane over phosphated silica and alumina, the activation barriers for the rate-limiting steps were lowered by ~10 kcal/mol in the presence of phosphorus. Kaddouri et al. [38] showed that the addition of P_2O_5 to the Ni-Mo-O system increased its performance in terms of both propene selectivity and propane conversion. They claimed that phosphorus acts as a promoter preventing propene degradation. El-Idrissi et al. [39] showed that the addition of phosphorus to Cr/TiO_2 resulted in a remarkable increase in the activity and ethylene selectivity. They attributed these improvements to the fact that phosphorus contributes to the stabilizing octahedral Cr^{3+} species in a well defined environment and adjusts in an advantageous way the acid properties of the active surface.

On the other hand, CeO_2 is an important active component of the combustion catalysts due to its large concentration of oxygen vacancies, fast exchange of surface oxygen with gas phase oxygen and high diffusion rates of bulk oxygen toward the surface [40-42]. For selective oxidative dehydrogenation the mobility of the lattice oxygen in the catalyst must be low enough to inhibit the successive oxidation of alkene. The phosphatation of ceria could have as an effect a substantial increase in the selectivity for oxidative dehydrogenation at the expense of the total oxidation. This could be explained by a reduction of the mobility of the lattice oxygen as a result of the interaction of ceria with the phosphate phases formed at the catalyst surface. In this

manner, particularly selective catalysts could be obtained. This is in line with the results obtained by Larese et al. [43, 44] which showed that the amount of labile surface and bulk oxygen and the bulk oxygen diffusion rates were significantly reduced and the reduction of Ce(IV) present in the CeO_2 solid was affected when ceria was contaminated with phosphorus. The monazite phase present in the surface and subsurface region of the solid has been proposed to be responsible for these effects.

Oxidative dehydrogenation of isobutane

Taking into consideration the above literature data, we studied the oxidative dehydrogenation of isobutane over surface-phosphated ceria catalysts containing two different amounts of phosphorus, the catalytic performances of the phosphated ceria being compared with those of pure ceria [45]. The physico-chemical characteristics of the catalysts studied are resumed in Table I.2. Note that cubic CeO_2 fluorite phase was observed in all the catalysts. The presence of cerium (III) phosphate, $CePO_4$, was also evidenced in the phosphated samples.

Table I.2. The physico-chemical characteristics of the catalysts.

Catalyst	Surface area (m^2/g)	Atomic composition evaluated by EDX (%)			Surface atomic ratio evaluated by XPS		H_2 consumption by TPR ($\mu mol\ g^{-1}$)
		P	Ce	O	P/Ce	Ce(IV)/Ce	
CeO_2	6.4	-	35.4	64.6	-	1.00	216.5
$1.1P/CeO_2$	3.3	2.6	43.1	54.3	0.57	0.36	203.8
$2.2P/CeO_2$	2.6	6.9	33.5	59.6	0.83	0.47	154.7

The catalytic properties are presented in Table I.3. It can be observed that, by adding phosphorus to ceria and with increasing the phosphorus content in the catalyst, the catalytic activity in the reaction of isobutane decreased, this decrease being less significant as the temperature increase in the range considered, so that at 570 °C the activity remained almost constant for the three catalyst samples. At higher temperatures, i. e. 610 °C, the catalytic activity in the reaction of isobutane increased by adding phosphorus to ceria and with increasing the phosphorus content in the catalyst. This corresponds to a compensation effect in catalysis [46] as shown in Fig. I.3 where the Arrhenius plots for the isobutane conversion on the three catalysts are presented.

Table I.3. Catalytic performances of the ceria and phosphated ceria catalysts in the reaction of isobutane.[a]

Catalyst	Reaction temperature (°C)	Isobutane conversion (%)	Selectivities (%)			
			Isobutene	CO	CO_2	Cracking
CeO_2	450	07.0	24.2	05.1	54.1	16.6 (15.9)[b]
	490	08.0	34.2	06.1	40.1	19.6 (18.0)
	530	09.0	42.0	08.6	25.9	23.5 (22.3)
	570	10.5	35.2	12.4	16.8	35.6 (32.7)
	610	11.8	26.1	16.6	10.2	47.1 (36.6)
1.1P/CeO_2	450	04.5	72.7	06.0	10.9	10.4 (07.2)
	490	06.5	71.2	04.4	08.1	16.3 (11.0)
	530	08.5	69.4	02.0	04.2	24.4 (15.5)
	570	11.1	67.6	01.5	03.6	27.3 (16.5)
	610	13.5	49.2	01.7	03.5	45.6 (25.2)
2.2P/CeO_2	450	03.5	94.0	01.0	03.0	2.0 (1.2)
	490	05.5	90.0	03.3	04.1	2.6 (2.2)
	530	08.0	88.0	03.9	03.8	4.3 (3.9)
	570	11.0	87.0	03.0	02.7	7.3 (6.4)
	610	14.7	68.4	02.6	02.5	26.5 (16.1)

[a] Reaction conditions: air to isobutane molar ratio equal to 2.5, VHSV with respect to isobutane equal to 1000 h^{-1}.

[b] Propene selectivity in the cracking products.

The apparent activation energies on CeO_2, $1.1P/CeO_2$ and $2.2P/CeO_2$ catalysts are increasing, i. e. 4.2 kcal/mol, 8.7 kcal/mol and 11.4 kcal/mol, respectively, and are comparable with those reported in the literature for the same reaction [47]. These results suggest that adding phosphorus to ceria new catalytic sites for the isobutane reaction are created but less strong. Phosphorus acts as a poison for ceria in the isobutane reaction at temperatures lower than 570 °C, point that corresponds to the isokinetic temperature. At temperatures higher than the isokinetic point phosphorus acts as a promoter for ceria in the isobutane reaction, in line with the observed compensation effect.

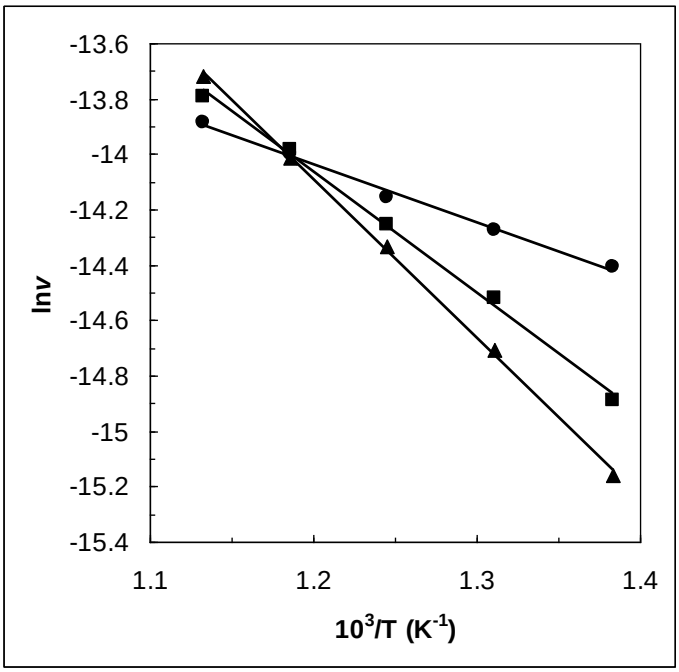

Figure I.3. Arrhenius plots for the isobutane conversion on the CeO_2 (●), $1.1P/CeO_2$ (■) and $2.2P/CeO_2$ (▲) catalysts.

It has already been shown [48] that surface Ce(IV) species in interaction with $CePO_4$ are able to activate isobutane. Thus, we consider that low reducible Ce(IV) species in interaction with surface phosphorous evidenced by H_2-TPR (Fig. I.4) are the new catalytic sites formed at ceria surface that could explain the observed compensation effect in the catalytic reaction. Moreover, the observed decrease of the isobutane conversion at temperatures lower than 570 °C by adding phosphorus to ceria and with increasing the phosphorus content is correlated with the observed

shift of the reduction temperature to higher temperatures in the TPR experiments: lower the reduction ability of Ce(IV), lower the catalytic activity.

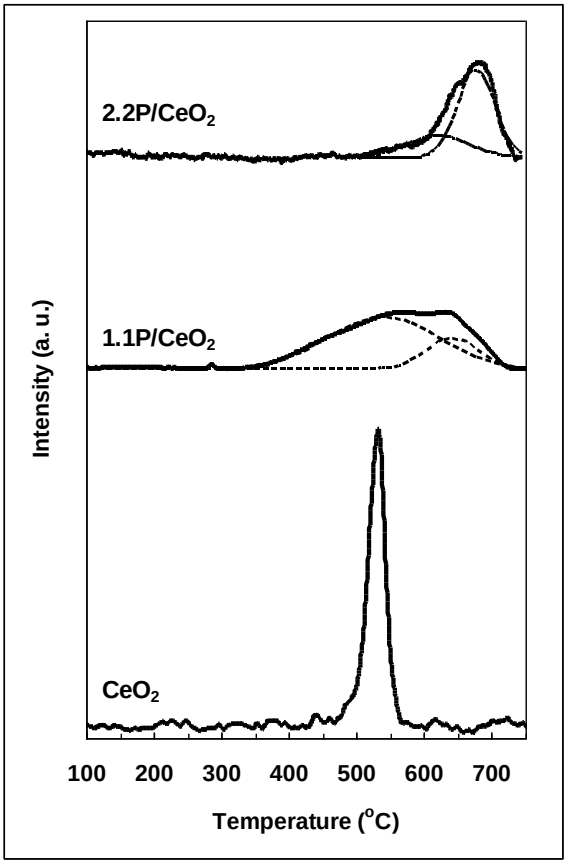

Figure I.4. TPR profiles for the CeO_2, 1.1P/CeO_2 and 2.2P/CeO_2 catalysts.

On the other hand, by adding phosphorus to ceria and by increasing its content, an important increase of the selectivity for isobutene (the oxidative dehydrogenation product) at the expense of the carbon oxides and the cracking products was also observed. This is well evidenced for the reaction at 570°C where the conversion was almost constant and equal to approximately 11 % for all three catalysts (isoconversion): the selectivity for isobutene passes from 35.2 to 67.6 and 87.0 % for CeO_2, 1.1P/CeO_2 and 2.2P/CeO_2 catalyst, respectively. At the same time, the selectivity for carbon oxides passes from 29.2 to 5.1 and 5.7 %, and the selectivity for the cracking products, from 35.6 to 27.3 and 7.3 %. This increase in isobutene selectivity can be correlated with the observed decrease of the H_2-TPR cerium reducibility, in line with what has been postulated by Michalakos et al. for vanadium based catalysts [49].

In conclusion, adding phosphorus to ceria, on one hand, and increasing phosphorus content, on the other hand, results in a modification of the physico-chemical characteristics of the catalyst. Among these, the redox ability of the catalytic material strongly decreases. In line with this, the catalytic activity decreases with an important increase of the selectivity for isobutene mainly at the expense of the combustion products. On the other hand, the formation of low reducible Ce(IV) species in interaction with surface phosphorous in the phosphated catalysts explains the compensation effect in catalysis observed.

Oxidative dehydrogenation of propane

In spite of being intensively studied for a long time, the conventional oxidative dehydrogenation of propane is still far from industrial application [2]. The main difficulty in obtaining high propene yields by ODH of propane arises from the fact that propene is more reactive than propane, thus being prone to further oxidation to produce carbon oxides.

In order to meet the selectivity challenge, Grasselli and Callahan [50] considered the active site isolation as a basic approach. Active site isolation is a model based on the idea that the selective oxidation requires smaller amounts of oxygen than total oxidation. Accordingly, the limitation of the oxygen availability around the active site determines a decrease of the selectivity toward total oxidation in favor of selective oxidation [51]. The original model developed for the U-Sb-O catalyst [52, 53] showed that the dissolution of a redox active component (uranium oxide) in a redox stable matrix (antimony oxide) at an optimum dilution led to an increased selectivity for acrolein in the selective oxidation of propene.

Another approach considered for the increase of the selectivity in the partial oxidation was the decrease of the mobility of the lattice oxygen. A high mobility of the lattice oxygen is one of the key features of metal oxides used as total oxidation catalysts [54].

Taking these into consideration and based on the above presented results we decided to investigate the effect of surface-phosphating ceria, on one hand, and of doping ceria with phosphorus, on the other hand, on the selectivity of ODH of propane. The results obtained were published in Ref. [55]. The physico-chemical characteristics of the catalysts are resumed in Table I.4. Note that the phosphorus contents were much lower than for the phosphated-ceria samples previously studied.

Table I.4. Specific surface areas and chemical compositions of the catalysts.

Catalyst	BET surface area (m^2/g)	P/(P+Ce) (%)		P/Ce (%)		Elemental composition from EDX (at. %)		
		nominal	from EDX	from EDX	from XPS	P	Ce	O
CeO_2	25.7	-	-	0	0	0	34.64	65.36
0.01P@CeO_2	25.3	-	-	-	< 3.0	< LD [a]	33.68	66.32
0.1P@CeO_2	21.1	-	1.25	1.27	25.5	0.43	33.86	65.71
0.3P@CeO_2	19.9	-	2.19	2.24	-	0.81	36.20	62.99
0.9P@CeO_2	16.9	-	6.44	6.89	76.1	2.16	31.37	66.47
0.5P-CeO_2	32.1	0.5	0.47	0.47	< 8.0	0.17	35.82	64.01
1P-CeO_2	42.5	1	0.86	0.87	-	0.33	37.60	62.07
2P-CeO_2	24.1	2	1.70	1.73	16.9	0.57	32.89	66.54
4P-CeO_2	31.7	4	3.85	4.00	30.4	1.24	31.00	67.76

[a] Limit of Detection.

The catalytic performances of the prepared catalysts in the oxydehydrogenation of propane are resumed in Fig. I.5. For the surface-phosphated samples (Fig. I.5.a) the selectivity to propene increased with the increase of the phosphorus content reaching a plateau for phosphorus contents higher than 0.8 at. % (0.3P@CeO_2 catalyst). Thus, for the 0.3P@CeO_2 and 0.9P@CeO_2 catalysts, in which the $CePO_4$ phase becomes detectable by Raman spectroscopy [55], the selectivity for ODH remained almost unchanged but was more than double compared with pure ceria. It is worth noting that the increase in ODH selectivity was achieved mainly at the expense of total oxidation selectivity. At the same time, the addition of phosphorus to ceria led to a decrease of the catalytic activity, but the further increase of its content led to an increase of the catalytic activity that passes through a maximum for a phosphorus content of 0.8 at. % (0.3P@CeO_2 catalyst). These results may suggest that, indeed, for surface-phosphated samples, the active and selective sites for ODH are Ce^{4+} cations in interaction with phosphorus, as it was also suggested previously. Once the amount of phosphate groups in the surface and subsurface region of ceria is high enough, $CePO_4$ begins to nucleate, and adding more phosphorus leads to growth of the $CePO_4$ crystals as it was shown by Efstathiou et al. [56]. Taking into consideration

that the interaction of Ce^{4+} cations with phosphate groups is the cause of reduced oxygen mobility and reduced oxygen storage capacity [56], the correlation between the increased selectivity and phosphorus content may thus be explained. On the other hand, the selectivity for ODH in the case of the surface phosphated samples does not pass through a maximum value at a certain phosphorus content, as would be expected for a catalyst fully obeying the site isolation principle [51]. This suggests that the Ce^{4+} species isolation takes place only at a low phosphorus content while for phosphorus contents higher than 0.8 at. % (when $CePO_4$ begins to nucleate) new catalytic sites selective for ODH reaction were formed. It is noteworthy that $CePO_4$ containing Ce^{4+} species as an impurity has also been shown to be a selective catalyst for ODH of isobutane [48]. It is worth noting that the surface-phosphated catalysts preserved their catalytic activity under the reaction conditions for the 40 h of on-stream reaction suggesting their high stability.

For the bulk-phosphated solids an increase in the ODH selectivity can also be observed with the increase of phosphorus content, mainly at the expense of total oxidation selectivity (Fig. I.5.b). However, the increase is smaller than that observed for the surface-phosphated samples, probably because of the lower surface concentration of Ce^{4+} cations in interaction with phosphorus. These data suggest that this interaction provide the selective catalytic sites and are in line with both the surface chemical analysis and the DRIFT spectra [55]. As in the case of surface-phosphated ceria, the catalytic activity decreased by adding phosphorus to ceria, but a further increase of the phosphorus content led to an increase of the activity/selectivity confirming that indeed the association of Ce^{4+} cations with phosphorus corresponds to the active sites.

A different behavior has been observed for the 4P-CeO_2 catalyst, i.e. the catalyst with the highest quantity of phosphorus in the bulk-phosphated series. At both reaction temperatures, an oscillating behavior was observed. High conversions corresponded to high total oxidation selectivity, while low conversions to high ODH selectivity. This effect could be justified by the formation of coke deposits on the surface of the catalyst, which grow until they are burned off by the gas phase oxygen, producing CO_2 and giving rise to the observed increase in total oxidation selectivity. The accumulation of coke deposits on the catalyst are likely caused by a decrease in lattice oxygen mobility due to the presence of phosphorus [56] in a higher quantity. The lowered lattice oxygen mobility would determine a slow reoxidation of the catalytic sites, thus leading to adsorbed hydrocarbonate species.

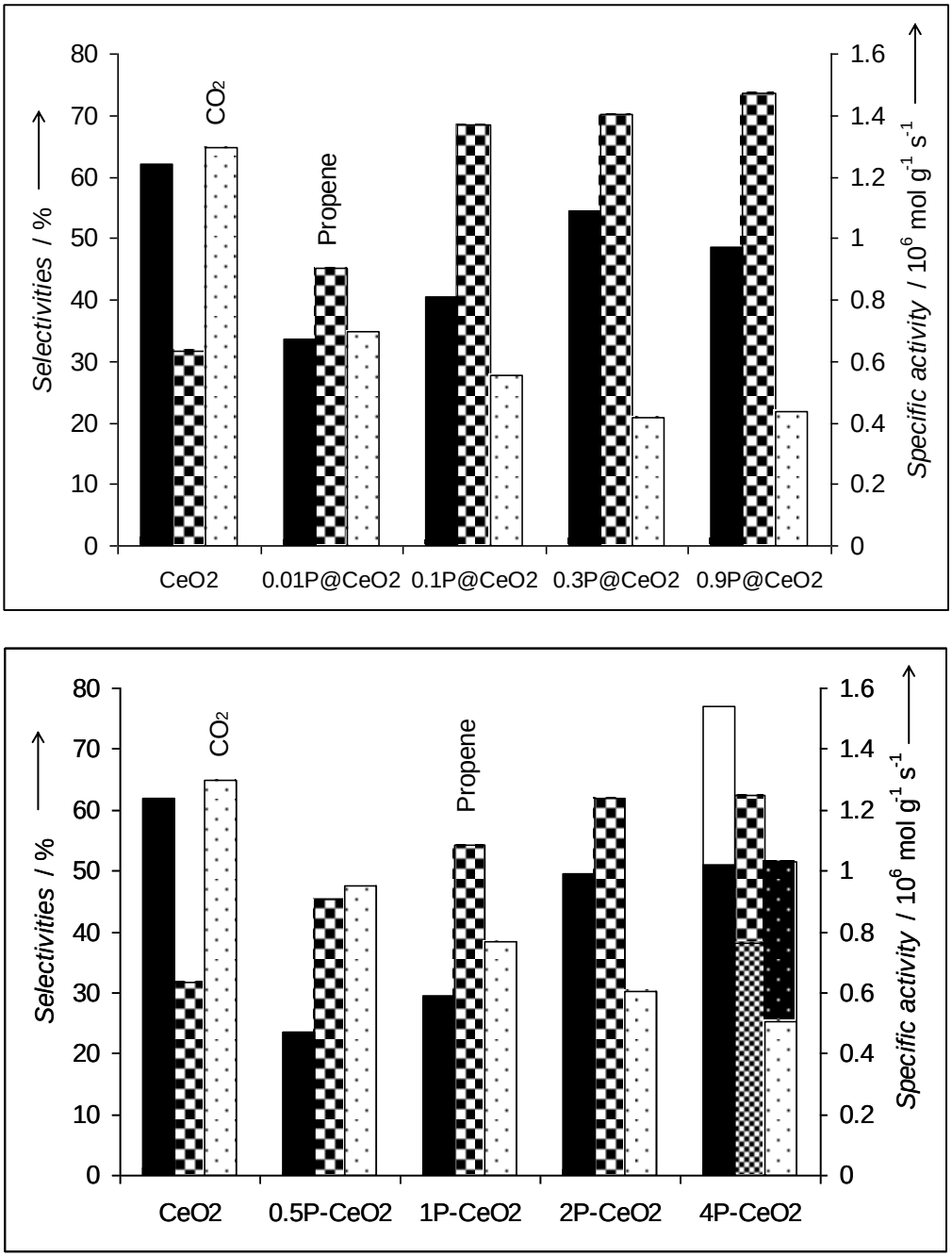

Figure I.5. Effect of phosphorus content on the catalytic properties of (a) surface-phosphated and (b) bulk-phosphated ceria catalysts for the reaction of propane at 600 °C, air to propane molar ratio = 2.5 and VHSV of 9000 h^{-1}.

It is worth noting that the selectivity vs. conversion data (not shown here) suggested that, for CeO_2 the total oxidation product (carbon dioxide) was formed by both direct oxidation of

propane and further oxidation of propene while for the phosphated samples carbon dioxide was formed rather by further oxidation of propene than by direct oxidation of propane [55].

In conclusion, adding phosphorus to ceria and increasing its content produces an increase in propane ODH selectivity at the expense of total oxidation selectivity for both surface-phosphated and bulk-phosphated ceria catalysts. The deactivation of the ceria catalyst and the formation of active sites selective for ODH consisting in Ce^{4+} cations in interaction with phosphorus are the main causes for the observed increase in ODH selectivity. The isolation of Ce^{4+} species takes place only at low phosphorus content while at high content, $CePO_4$ starts to nucleate and new catalytic sites selective for ODH reaction were formed. In the case of the bulk-phosphated ceria the increase in the selectivity was smaller than in the case of the surface phosphated samples, most likely due to a lower surface concentration of Ce^{4+} cations in interaction with phosphorus. This was most probably associated to the decrease of the lattice oxygen mobility.

I.2. NEW MIXED OXIDE-BASED CATALYSTS FOR PROPANE OXIDATIVE DEHYDROGENATION

I.2.1. Oxidative dehydrogenation of propane over LnMgAlO (Ln = Ce, Sm, Dy, Yb) mixed oxides catalysts

Heterogeneous catalysts for the oxidative dehydrogenation of propane typically contain vanadium and molybdenum as the critical elements [57-65]. Nevertheless, among other oxide systems, those containing rare-earth oxides are also reported as active and selective [66-68]. It has been shown that γ-Al_2O_3-supported rare-earth (Y, Dy, Tb, Yb, Ce, Tm, Ho and Pr) oxides are reactive in propane oxidative dehydrogenation, but propene selectivities were relatively low, namely under 40 % [66]. Taking into consideration the electron-donating character of the olefinic species, it was of interest to investigate whether the propene selectivity could be enhanced by increasing the catalyst basicity. It is well known that the LDH-derived Mg-containing mixed oxides exhibit a high amount of strong basic O^{2-} sites [69], their use as catalysts in the ODH reaction being expected to improve the ODH selectivity. For this reason we prepared Mg-Al mixed oxide-supported rare-earth oxides from layered double hydroxide (LDH) precursors and we studied their catalytic properties in the oxidative dehydrogenation of propane. The obtained results were published in Ref. [70].

Poorly crystallized layered hydrotalcite-type structures, as generally observed for multicationic LDH, were detected on all the LnMgAl-LDH precursors. Poorly crystallized CeO_2, $Sm(OH)_3$ and Dy_2O_3 were also detected in Ce-, Sm- and DyMgAl-LDH, respectively. The samples calcined at 750 °C exhibited, in all cases, diffraction lines corresponding to the MgAlO mixed oxide phase with the periclase-like structure and lines corresponding to CeO_2, Sm_2O_3, Dy_2O_3 and Yb_2O_3 phases for Ce-, Sm-, Dy- and Yb-Mg-Al-O mixed oxides, respectively. The physico-chemical characteristics of the mixed oxides catalysts are resumed in Table I.5.

The conversion of propane and the product selectivities as a function of reaction temperature are depicted in Fig. I.6. The blank tests have shown that the non-catalytic oxidative conversion of propane is not significant in our testing conditions (Fig I.6.a). For all the catalysts

the conversion increased with increasing the reaction temperature while the propene selectivity decreased to the benefit of CO_x for Ce-based system and of cracking products for the other systems. Note that the Yb-based system was not active at temperatures lower than 500 °C.

Table I.5. Physico-chemical characteristics of the catalysts.

Catalyst	Specific surface area (m^2/g)	Ln content by EDX (% at. with respect to cations)	Total basicity by CO_2-TPD (mmol CO_2/g)	H_2 consumption by TPR (mol H_2/mol Ln)
Ce-Mg-Al-O	157	5.6	1.63	0.13
Sm-Mg-Al-O	160	5.2	2.18	0.12
Dy-Mg-Al-O	102	5.1	2.52	0.18
Yb-Mg-Al-O	142	5.6	1.96	0.19

For the reaction at 500°C the catalytic activity followed the order: Dy > Sm ≥ Ce > Yb. The differences in conversions indicate the influence of the metallic properties on the rate-determining hydrogen abstraction by the catalysts [66]. In the case of Ce-Mg-Al-O system, the sum of the selectivities of CO_x and CH_4 was not equal to that of ethylene, as was the case with the other systems, but much higher within all the range of temperatures studied. This suggests that for Ce-based system, total oxidation products (CO_x) were formed not only from C1 species resulting from the cracking of propane, but also by the direct oxidation of propane or by further oxidation of propene. This was not the case for Sm-, Dy and Yb-Mg-Al-O catalysts. Note that the selectivity vs. conversion data (not shown here) confirmed that, among the catalysts studied, the parallel reaction of propane leading to carbon oxides is specific only for Ce-based system. It has also been shown that the oxidative dehydrogenation selectivity followed the order: Dy > Sm > Yb > Ce.

A linear correlation between the catalyst CO_2-TPD basicity and the propene selectivity was observed as shown in Fig. I.7 both for the reaction at 500 and 550 °C. The direct relationship found between surface basicity and propene selectivity can be accounted for by the electron-donating character of the olefinic species and the consequent easier desorption from a more basic

surface, thus preventing further overoxidation into carbon oxides. Interestingly, the most selective catalysts proved to be the most active as well.

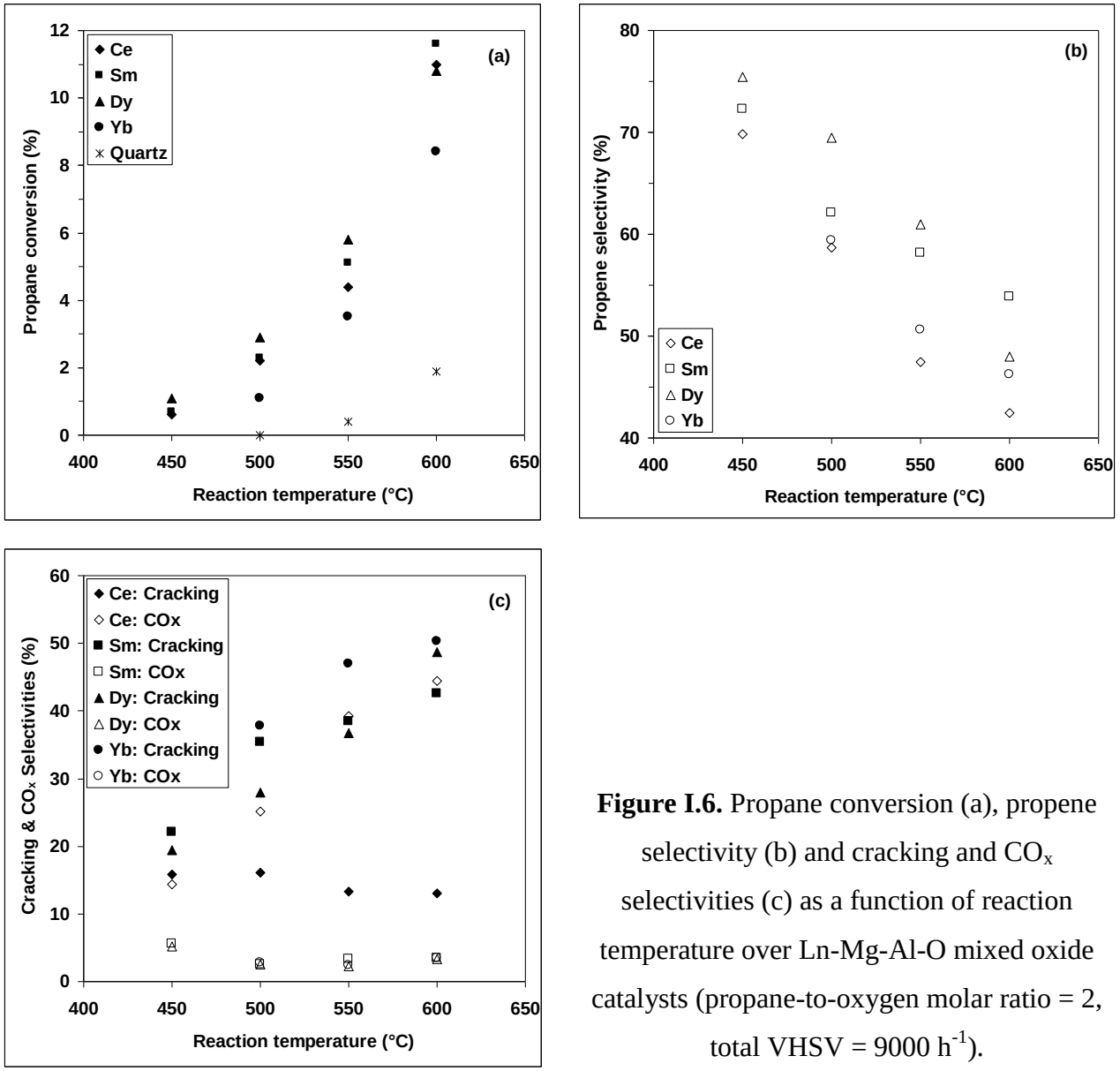

Figure I.6. Propane conversion (a), propene selectivity (b) and cracking and CO_x selectivities (c) as a function of reaction temperature over Ln-Mg-Al-O mixed oxide catalysts (propane-to-oxygen molar ratio = 2, total VHSV = 9000 h^{-1}).

It is noteworthy that the Mg-Al mixed oxide-supported rare-earth oxides studied in this work exhibit better performance in terms of selectivity to propene than the γ-Al_2O_3-supported rare-earth oxides in Ref. [66], confirming the expected effect of magnesium.

Finally, we note that no correlation between the H_2-TPR reducibility of the rare-earth cation and the catalytic performances was observed, suggesting that the surface-adsorbed oxygen

but not lattice oxygen species are involved in the reaction. A similar result was obtained by Al-Zahrani et al. [66] for γ-Al_2O_3-supported rare-earth oxide catalysts by estimating the lattice oxygen reactivity from the reduction potential of the cation.

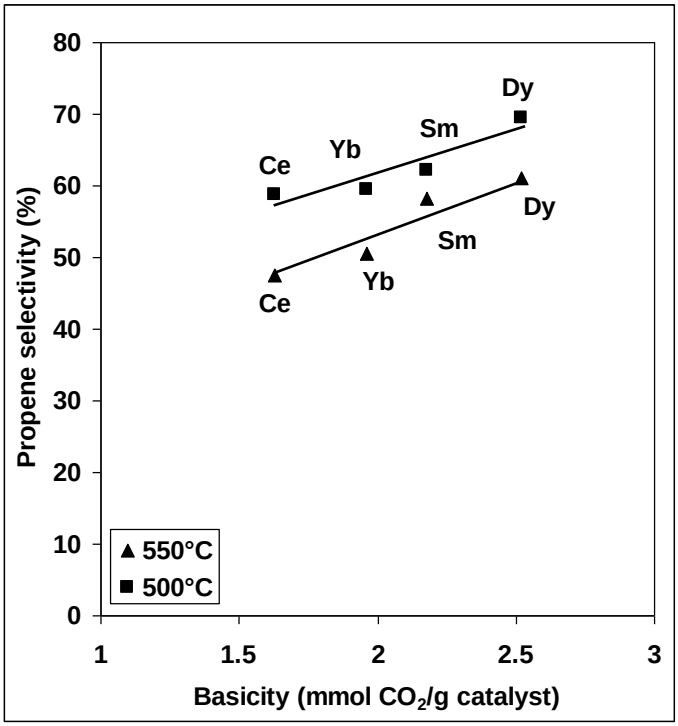

Figure I.7. Propene selectivity versus the catalyst basicity for the reaction at 500 and 550 °C over the studied catalysts.

In conclusion, the Ln-Mg-Al-O mixed oxides catalysts derived from LDH precursors are relatively good catalysts for the ODH of propane. The best yields in propene were obtained with Dy- and Sm-Mg-Al-O systems, Dy-based catalyst being the most selective one. A linear correlation between the catalyst basicity and the propene selectivity was observed. The LDH-derived catalysts exhibit better performance in terms of selectivity to propene than the γ-Al_2O_3-supported rare-earth oxides. It seems that the surface-adsorbed oxygen but not lattice oxygen species are involved in the reaction over Ln-Mg-Al-O mixed oxides catalysts.

I.2.2. Oxidative dehydrogenation of propane over transition metal-containing mixed oxides catalysts derived from LDH precursors

The catalytic oxidative dehydrogenation (ODH) of propane into propene has been widely investigated as an alternative to the most largely used pyrolysis processes. A wide variety of catalytic systems has been proposed for this reaction, the most studied being based on vanadium [57, 58, 71-80] or molybdenum [61, 64, 81-87]. Though scarcely studied, other transition metal-based catalytic materials could exhibit comparable catalytic efficiencies [66, 88-95]. Thus, Al-Zahrani et al. [66] showed that Cr, Mn, Zr or Ni oxides supported on γ-Al_2O_3 were reactive in this reaction. The Cr-Al-O mixed oxide led to the highest propene yield (~ 9 %) at 450 °C and was more active and selective than a Mo-Al-O mixed oxide catalyst studied as a reference. Jibril et al. [88] studied Kieselguhr-supported transition metal oxides (metal cations being Cr, Mn, Co, Ni, V and Mo) and showed that Mn- and Co-based catalysts exhibited the maximum propene yields: ~ 5 % and ~ 4 %, respectively, for the reaction at 500 °C. Ge et al. [89] investigated lithium salts-promoted Portland cement-supported MnO_x catalysts and showed that they give more than 60 % alkane conversion and 80 % olefins selectivity at 650 °C for ODH of ethane and propane to ethylene and propylene, respectively. Jalowiecki-Duhamel et al. [90] studied Ce-M-O mixed oxides (M = Ni, Cu, Co, Cr, or Zn) and showed that Ce-Ni-O was the most efficient catalyst yielding 5.4 % of propene at 375 °C. Wang et al. [91] studied the ODH of ethane and propane over LiCl-promoted NiO/sulfated zirconia catalysts. They were very active and selective in both reactions leading to 73.5 % ethylene yield at 650 °C and 10.4 % propylene yield at 600 °C, respectively. More recently, Wu et al. [92] showed that TiO_2-doped nickel oxide yielded 12 % propene from propane at 300 °C. A Co (7.6 wt. %)/TiO_2 supported catalyst has been found active in the ODH of ethane with an ethylene yield of 13.2 % at 550 °C [93]. CoH-containing BEA, MFI, MOR and FER zeolites have been found active for the ODH of ethane and propane, the best alkene yields of ~ 3 % being obtained in both cases with Co-BEA catalyst. Their activity has been influenced by the zeolite topology and decreased following the order: Co-BEA > Co-MFI >> Co-MOR > Co-FER [94]. Cobalt incorporated into the framework of MCM-41-like silicas has been reported to be active and selective for the ODH of isobutane into isobutene, even though methacrolein and other oxygenates were also formed in noticeable quantities [95]. The best isobutene yield obtained with Co-MCM-41 was 3.3 % for the reaction at 525 °C. It has been

shown that the active and selective sites in Co-MCM-41 were Co^{2+} species with a unique tetrahedral coordination.

On the other hand, it is well known [69] that the mixed oxides obtained by thermal decomposition of LDHs show high surface area and metal dispersion, small crystallite size and good stability against sintering, properties which are usually required for high-temperature oxidation catalysts. Moreover, as the adsorbed alkenes are subjected to further transformation into carbon oxides negatively affecting the ODH selectivity and the LDH-derived Mg-containing mixed oxides exhibit a high amount of strong basic O^{2-} sites [69], their use as catalysts in the ODH reaction is expected to favor the desorption of alkenes, species with an electron-donating character, and, consequently, to improve the ODH selectivity. It must be pointed out that mixed oxides derived from LDH precursors and containing vanadium have already been studied as catalysts for the oxidative dehydrogenation of light alkanes [96-101]. VMgAlO mixed oxides [100, 101] were indeed characterized by catalytic performances comparable or better than that of reference VMgO catalysts [102, 103] in the oxidative dehydrogenation of propane.

These results reveal the strong potentialities of transition metal-containing mixed oxides derived from LDH precursors as oxidation catalysts and led us to study a series of MMgAlO mixed oxides (M = Mn, Fe, Co, Ni, Cu and Zn) in the oxidative dehydrogenation of propane. Our work has been published in Ref. [104].

A well crystallized LDH structure has been evidenced for MgAl-LDH precursor. Less crystallized structures, as often observed for multicationic LDH, were detected on all MMgAl-LDH samples. Silver and palladium cations cannot be introduced in the brucite-like layers or only in minor amounts regarding Pd [105], so in addition to the LDH phase, crystallized Ag_2O and poorly crystallized PdO phases were observed for AgMgAl-LDH and PdMgAl-LDH samples, respectively. For all MMgAlO mixed oxides calcined at 750 °C the well known MgAlO mixed oxide phase with the periclase-like structure has been observed. The periclase-like phase alone was observed in the case of CoMgAlO, NiMgAlO and CuMgAlO samples. Reflections corresponding to the $MnAl_2O_4$ and $ZnAl_2O_4$ phases were also observed for MnMgAlO and ZnMgAlO catalysts, respectively. In the case of FeMgAlO catalyst, the broad and weakly intense reflections can correspond both to Fe_2O_3 and $FeAl_2O_4$ phases whose peaks were superimposed. PdO phase was observed in the case of PdMgAlO. In the case of AgMgAlO sample metallic silver was clearly evidenced in agreement with the total decomposition of bulk Ag_2O above

300°C [106]. The physico-chemical characteristics of the mixed oxide catalysts are resumed in Table I.6.

Table I.6. Physico-chemical characteristics of the mixed oxide catalysts.

Catalyst	Surface area ($m^2 g^{-1}$)	Transition metal content (% at. with respect to cations)		Chemical composition (% at.) by EDX [a]			H_2 consumption by TPR (μmol g^{-1})
		theor.	EDX	M	Mg	Al	
MgAlO	188	-	-	-	22.23	6.71	-
MnMgAlO	134	5.0	6.1	2.00	22.62	8.13	76.5
FeMgAlO	172	5.0	6.8	1.99	19.50	7.70	70.4
CoMgAlO	167	5.0	7.5	1.97	17.22	7.03	82.8
NiMgAlO	161	5.0	6.3	1.83	19.47	7.99	100.5
CuMgAlO	157	5.0	6.7	1.74	18.32	5.95	276.0
ZnMgAlO	144	5.0	6.5	2.14	22.74	8.15	1.6
AgMgAlO	137	5.0	6.6	1.73	18.78	5.68	12.0
PdMgAlO	151	5.0	4.0	1.05	18.70	6.69	-

[a] Oxygen in balance.

The conversion of propane and the product selectivities as a function of the reaction temperature obtained with the different MMgAlO (M = Mn, Fe, Co, Ni, Cu and Zn) catalysts were presented in Table I.7. We have previously shown that the contribution of the homogeneous reaction is negligible in these reaction conditions [70]. For all the catalysts the conversion increased with the reaction temperature. We noted that MgAlO was not active below 500 °C. Propene selectivity behaved differently depending on the nature of the catalyst. It went through a maximum at 500 and 550 °C for MnMgAlO and FeMgAlO, respectively, whereas it decreased continuously in the temperature range from 450 to 600 °C for CoMgAlO, NiMgAlO, CuMgAlO and ZnMgAlO catalysts. It is noteworthy that this decrease for propene selectivity occurred to the benefit of CO_x for CuMgAlO and of cracking products for CoMgAlO, NiMgAlO and ZnMgAlO. MgAlO was, on one hand, less active than the transition metal-containing catalysts.

Table I.7. Catalytic performances of the MMgAlO catalysts in the oxidative dehydrogenation of propane.[a]

Catalyst	Reaction temperature (°C)	Propane conversion (%)	Selectivities (%)			Specific rate (10^6 mol g^{-1} s^{-1})	E_{act} (kJ mol^{-1})
			Propene	Cracking products	Carbon oxides		
MnMgAlO	450	2.7	73.4	5.5	21.1	0.93	53.6
	500	4.6	83.3	8.6	8.1	1.58	
	550	7.1	75.9	14.7	9.4	2.44	
	600	12.9	70.3	19.9	9.8	4.44	
FeMgAlO	450	0.9	36.0	12.8	51.2	0.38	75.3
	500	1.9	47.8	25.1	27.1	0.79	
	550	3.7	53.6	33.7	12.7	1.54	
	600	7.9	47.4	43.2	9.4	3.30	
CoMgAlO	450	1.5	92.5	3.0	4.5	0.54	82.0
	500	3.1	90.3	5.7	4.0	1.12	
	550	7.2	82.0	14.4	3.6	2.60	
	600	15.4	67.5	29.5	3.0	5.56	
NiMgAlO	450	1.0	86.4	7.5	6.1	0.39	88.3
	500	2.1	79.6	15.7	4.7	0.82	
	550	5.2	70.8	25.6	3.6	2.03	
	600	12.4	66.3	30.8	2.9	4.83	
CuMgAlO	450	2.5	26.1	13.9	60.0	0.80	51.5
	500	4.3	21.6	16.2	62.2	1.38	
	550	6.8	18.4	16.6	65.0	2.18	
	600	11.0	11.1	17.2	71.7	3.53	
ZnMgAlO	450	0.6	76.7	11.8	11.5	0.26	95.8
	500	1.7	73.6	14.7	11.7	0.72	
	550	3.6	67.9	17.8	14.3	1.52	
	600	9.8	64.0	29.4	6.6	4.15	
MgAlO	500	0.8	10.8	2.9	86.3	0.34	127.2
	550	2.9	20.5	12.8	66.7	1.24	
	600	7.7	25.6	28.3	46.1	3.31	

[a] Reaction conditions: total VHSV = 9000 h^{-1}; propane-to-oxygen molar ratio = 2.

On the other hand, it showed an increase of propene and cracking products selectivities at the expense of CO_x selectivity as the reaction temperature increased. The highest propene yields were obtained in all cases above 550 °C where the catalysts can be ranked in the order: CoMgAlO > MnMgAlO > NiMgAlO > ZnMgAlO > FeMgAlO > CuMgAlO. It must be pointed out that in all cases the sum of selectivities of CO_x and CH_4 was higher than the selectivity of ethylene in the temperature range studied, the highest values being observed for CuMgAlO. This suggests that the total oxidation products (CO_x) were formed not only from C1 species resulting from the cracking of propane, but also by the direct oxidation of propane or by further oxidation of propene. This is in line with the activity of these catalysts in the short-chain hydrocarbon combustion in an excess of air reported elsewhere [104]. It is worth noting that the selectivity vs. conversion data for MnMgAlO, CoMgAlO and NiMgAlO catalysts, leading to the highest propene yields, showed that the total oxidation products (CO_x) were formed rather by oxidation of propene than by direct oxidation of propane, the oxidative dehydrogenation ability of the catalysts following the order: CoMgAlO > MnMgAlO > NiMgAlO.

We noted that no close correlation could be observed between the reducibility and the catalytic behaviour of the samples suggesting that the reducibility is not the only determining parameter.

In conclusion, during the oxidative dehydrogenation of propane performed within the temperature range 450 – 600 °C, the propene selectivity passed through a maximum for MnMgAlO and FeMgAlO catalysts. For CuMgAlO it decreased continuously to the benefit of CO_x and for CoMgAlO, NiMgAlO and ZnMgAlO it also decreased to the benefit of cracking products. Considering the propene yield, the catalysts can be ranked in the order: CoMgAlO > MnMgAlO > NiMgAlO > ZnMgAlO > FeMgAlO > CuMgAlO. We suggested that total oxidation products observed (CO_x) during the oxidative dehydrogenation were formed not only from C1 species resulting from the cracking of propane, but also by oxidation of propene owing to the activity of these catalysts in this reaction. No close correlation between the H_2-TPR reducibility of the catalysts and their performances in the oxidative dehydrogenation of propane into propene could be observed.

I.2.3. Oxidative dehydrogenation of propane over cobalt-containing mixed oxides obtained from LDH precursors

We showed in the previous section that MMgAlO mixed oxides (M = Mn, Fe, Co, Ni, Cu and Zn) obtained from layered double hydroxide (LDH) precursors were active and selective for ODH of propane, the best propene yields being obtained with CoMgAlO catalyst. Here we resume the study of CoMgAlO mixed oxides with different cobalt contents (1 – 20 at. %) as catalysts for ODH of propane, which has been published in Ref. [107].

All the Co(x)MgAl-LDH precursors exhibited the LDH structure. As the nominal Co content was increased the crystallinity decreased but no Co-containing phase was detected suggesting that multicationic brucite-like layers containing Co, Mg and Al cations were formed. In all the Co(x)MgAlO samples calcined at 750 °C the well known Mg(Al)O mixed oxide phase with the periclase-like structure was detected. For Co loadings higher than 7 %, diffraction peaks ascribed to $CoAl_2O_4$ and/or Co_3O_4 spinel phases were observed. The physico-chemical characteristics of the Co(x)MgAlO catalysts are resumed in Table I.8.

Table I.8. Specific surface areas, chemical compositions and TPR data obtained with the Co(x)MgAlO catalysts.

Catalyst	Surface area ($m^2 g^{-1}$)	Co content (% at. with respect to cations)		Chemical composition by EDX (% at.) [a]			Total H_2 consumption by TPR	
		theor.	EDX	Co	Mg	Al	μmol g^{-1}	mol H_2/mol Co
MgAlO	188	-	-	-	22.23	6.71	-	-
Co(1)MgAlO	122	1.0	1.3	0.44	25.72	7.28	16.7	0.07
Co(3)MgAlO	81	3.0	3.5	1.21	26.53	6.92	-	-
Co(5)MgAlO	167	5.0	7.5	1.97	17.22	7.03	82.8	0.08
Co(7)MgAlO	109	7.0	9.1	3.13	23.75	7.48	-	-
Co(10)MgAlO	114	10.0	12.7	4.16	21.35	7.32	267.0	0.13
Co(20)MgAlO	114	20.0	22.4	7.66	18.71	7.74	633.3	0.18

[a] Oxygen in balance.

The conversion of propane and the product selectivities as a function of the reaction temperature obtained with the different Co(x)MgAlO catalysts were presented in Table I.9. We have shown that the contribution of the homogeneous reaction is negligible in these reaction conditions: the propane conversion in the absence of a catalyst was lower than 2 % for the reaction at 600 °C [70]. For all the catalysts the conversion increased with the reaction temperature. We noted that MgAlO was not active below 500 °C. Propene selectivity decreased continuously in the temperature range from 450 to 600 °C for all the cobalt-containing catalysts, probably due to the increase in the conversion, a well known fact in the ODH of light alkanes. At the same time, the selectivity for cracking products (ethene and methane) increased in all cases, as expected, with the reaction temperature. It is noteworthy that the observed decrease of selectivity for propene with the reaction temperature occurred mainly at the benefit of cracking products for Co(1)MgAlO, Co(3)MgAlO, Co(5)MgAlO and Co(7)MgAlO samples and of CO_x for Co(10)MgAlO and Co(20)MgAlO samples. Moreover, the Co(10)MgAlO and Co(20)MgAlO samples gave much larger quantities of CO_x within all the temperature range studied. This is not surprising if one considers that, on one hand, a higher number of active centers will increase the probability of further oxidation of propene [95] and, on the other hand, the Co_3O_4 spinel phase, active for short-chain alkanes combustion [108, 109], has been clearly evidenced by XRD and Raman spectroscopy in Co(10)MgAlO and Co(20)MgAlO samples [107].

In all the temperature range studied, the activity decreased by decreasing the cobalt content in the catalyst in line with the decreased reducibility suggested in the H_2-TPR experiments. We have indeed shown that both the maximum reduction peak was shifted towards higher temperatures and that the H_2/Co molar ratio decreased as the cobalt content decreased [107]. Moreover, a correlation between the specific rate of propane transformation at 600 °C over the different Co-containing catalysts and the corresponding total hydrogen consumption in TPR experiments (Fig. I.8) has been observed. This suggests that the same CoO_x species are involved in both the catalytic reaction and the reduction.

Note that the observed increase of selectivity toward propene with the reaction temperature for the MgAlO support is an unusual behavior for the ODH reaction performed over oxide-based catalyst, although it has been reported in some studies but at low conversions [66, 110, 111]. The highest propene yields were obtained in all cases above 550 °C.

Table I.9. Conversions and selectivities obtained in the ODH of propane with the Co(x)MgAlO catalysts.[a]

Catalyst	Reaction temperature (°C)	Propane conversion (%)	Selectivities (%)			Specific rate (10^6 mol g^{-1} s^{-1})	E_{act} (kJ mol^{-1})
			Propene	Cracking products	Carbon oxides		
Co(1)MgAlO	450	1.8	96.4	2.1	1.5	0.62	57.7
	500	3.2	90.8	8.3	0.9	1.10	
	550	5.1	79.8	18.2	2.0	1.75	
	600	9.7	70.5	27.9	1.6	3.33	
Co(3)MgAlO	450	1.9	96.6	0.9	2.5	0.79	59.5
	500	3.7	93.1	2.5	4.4	1.54	
	550	6.6	81.9	13.3	4.8	2.75	
	600	10.3	70.0	25.5	4.5	4.30	
Co(5)MgAlO	450	1.5	92.5	3.0	4.5	0.54	82.0
	500	3.1	90.3	5.7	4.0	1.12	
	550	7.2	82.0	14.4	3.6	2.60	
	600	15.4	67.5	29.5	3.0	5.56	
Co(7)MgAlO	450	3.0	92.6	5.1	2.3	1.17	58.3
	500	5.2	86.4	10.3	3.3	2.03	
	550	9.3	72.1	20.5	7.4	3.62	
	600	15.8	52.2	35.7	12.1	6.16	
Co(10)MgAlO	450	3.1	68.4	1.3	30.3	1.21	76.6 / 25.0[b]
	500	6.9	59.5	5.2	35.3	2.69	
	550	14.6	47.4	14.7	37.9	5.69	
	600	18.0	35.8	25.0	39.2	7.02	
Co(20)MgAlO	450	6.4	63.4	1.5	35.1	2.49	93.5 / 24.3[b]
	500	17.5	50.3	4.4	45.3	6.82	
	550	21.7	36.3	10.7	53.0	8.46	
	600	27.0	24.1	17.5	58.4	10.52	
MgAlO	500	0.8	10.8	2.9	86.3	0.34	127.2
	550	2.9	20.5	12.8	66.7	1.24	
	600	7.7	25.6	28.3	46.1	3.31	

[a] Reaction conditions: total VHSV = 9000 h^{-1}; propane-to-oxygen molar ratio = 2.

[b] For the reaction at high temperatures.

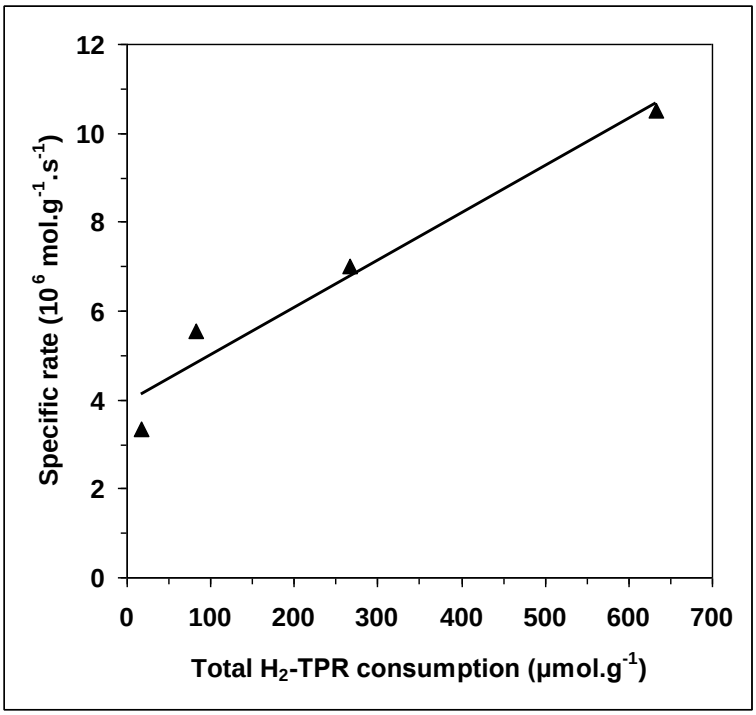

Figure I.8. Specific rate of propane transformation at 600 °C, VHSV = 9000 h^{-1} and propane-to-oxygen molar ratio = 2, versus total hydrogen consumption in TPR experiments.

The evolution of the propane conversion and propene selectivity as well as of the propene yield as a function of the cobalt content in the catalyst for the reaction temperatures of 550 °C and 600 °C was depicted in Fig. I.9. For both reaction temperatures considered, the propane conversion continuously increased with the cobalt content in the catalyst while the propene selectivity remained almost constant for cobalt contents up to 7.5 at. % (Co(5)MgAlO sample) then it decreased for higher cobalt contents. For the reaction at 600 °C the propene yield passed through a maximum of ~ 10 % for cobalt contents between 7.5 and 9.1 at. %, that is for Co(5)MgAlO and Co(7)MgAlO samples. For the reaction at 550 °C the propene yield increased continuously up to ~ 7 % for 9.1 at. % cobalt content (Co(7)MgAlO sample) and remained almost constant for higher contents. It can be underlined that the highest propene yield was reached at higher temperature (600 °C) below 7 at. % Co content and at lower temperature (550 °C) above this Co content. Interestingly, as observed by Raman and photoluminescence spectroscopies [107], the amount of well-dispersed cobalt species with tetrahedral coordination reached a maximum for Co(7)MgAlO, suggesting that these species play a main role in the ODH of propane.

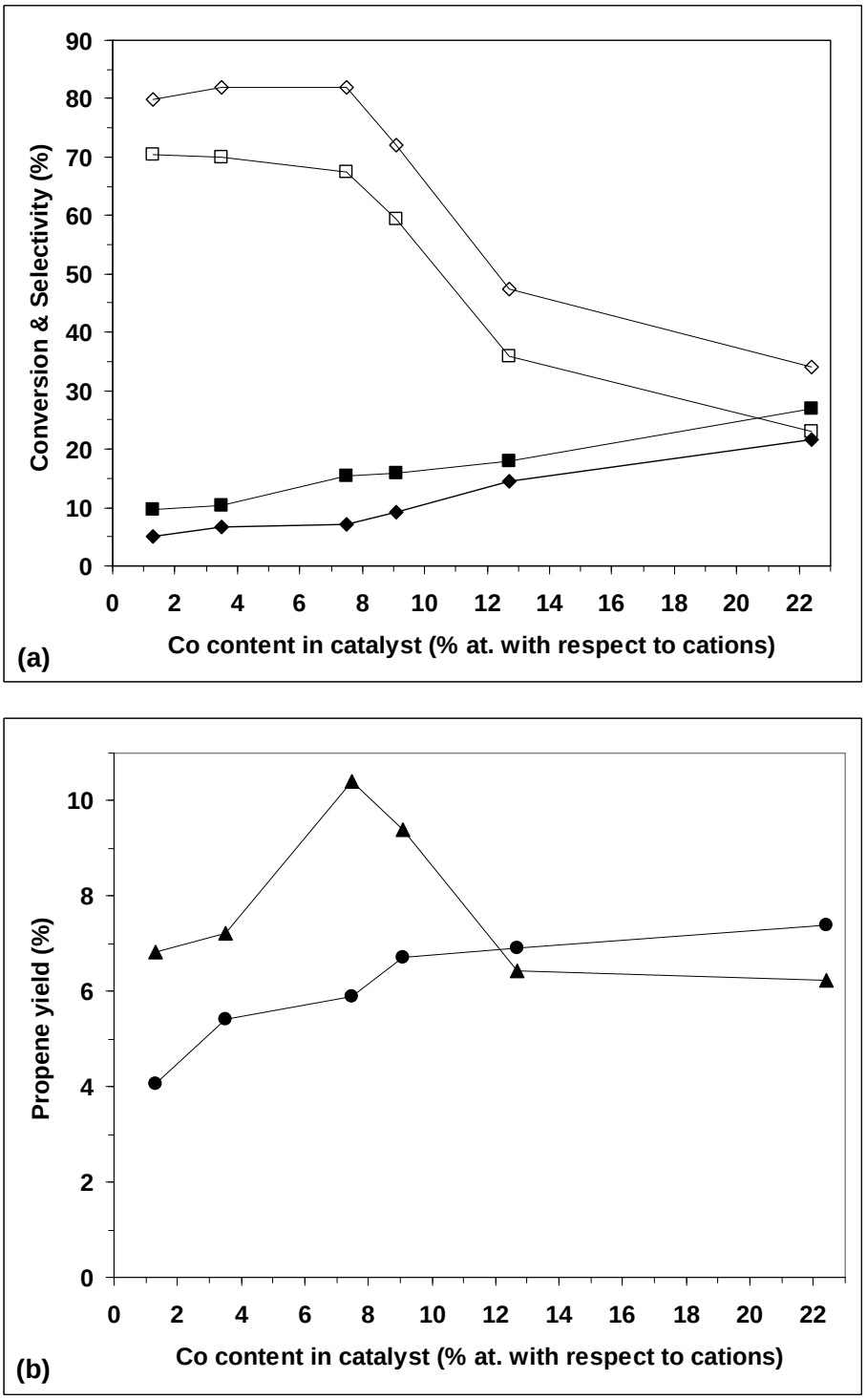

Figure I.9. The effect of the Co content in catalyst (a) on the propane conversion (◆, ■) and propene selectivity (◇, □) for the reaction at 550 (◆, ◇) and 600 °C (■, □) and (b) on the propene yield for the reaction at 550 (●) and 600 °C (▲) (VHSV = 9000 h^{-1} and propane-to-oxygen molar ratio = 2).

This type of cobalt species with tetrahedral coordination has already been found to be active and selective for the ODH of isobutane on Co-MCM-41 catalysts [95]. It is noteworthy that compared with other cobalt-containing catalysts reported in the open literature [88, 94], the CoMgAlO catalysts studied in this work gave much higher propene yields.

It must also be pointed out that in all cases the selectivity for CO_x and CH_4 was higher than that for ethylene in the temperature range studied, the highest values being observed for Co(10)MgAlO and Co(20)MgAlO. This suggests that the total oxidation products (CO_x) were formed, not only from C1 species resulting from the cracking of propane, but also by the direct oxidation of propane or by further oxidation of propene. This is in line with the already reported combustion activity of cobalt-based catalysts in an excess of air [108, 112].

In conclusion, high surface area CoMgAlO mixed oxide catalysts with different cobalt contents (1 – 20 at. %) were prepared by calcination of LDH precursors at 750 °C. Beside a CoMgAlO mixed oxide phase exhibiting the periclase-like structure, Co-containing phases with the spinel structure were also observed for higher Co contents. One of these highly dispersed spinel-like phase reached a maximum amount in the Co(7)MgAlO sample. The catalytic activity in the ODH reaction of propane increased with the cobalt content in the catalyst in agreement with their increase of reducibility, and the highest propene selectivities were obtained at lower cobalt content. For all the CoMgAlO catalysts, the conversion increased with the reaction temperature, while the propene selectivity decreased continuously to the benefit of CO_x for the catalysts with higher cobalt contents and of the cracking products for the catalysts with lower cobalt contents. The well-dispersed cobalt species with tetrahedral coordination played a main role in the ODH reaction of propane into propene while the spinel Co_3O_4 phase appeared responsible for the large quantities of CO_x observed at higher cobalt contents. The highest propene yields (~ 10 %) were obtained with Co(5)MgAlO and Co(7)MgAlO catalysts at 600 °C.

II. CATALYTIC TOTAL OXIDATION OF LIGHT ALKANES

Volatile organic compounds (VOCs) emitted during many industrial processes and transport activities contribute significantly to the atmospheric pollution [1]. One of the most effective and economically attractive methods of their neutralization is the catalytic total oxidation to carbon dioxide and water [2]. Light alkanes are amongst the most prevalent environmental VOCs emissions due to their use as transportation fuels as well as being essential feedstocks for chemicals production [3]. Although alkane oxidation leads to CO_2, another greenhouse gas, this can be readily absorbed whereas alkanes cannot. On the other hand, the difficulty in destroying light alkanes by catalytic total oxidation, since they are very difficult to activate, makes them excellent model compounds to test the efficiency of catalysts for VOCs combustion, as the catalytic combustion of most organic compounds would be ensured if light alkanes are quantitatively abated.

Seventy-five percent of the catalysts used for VOCs destruction are precious metal catalysts, generally supposed to be more active than metal oxide catalysts [4]. Nevertheless they have some disadvantages like high sintering rates, volatility, poisoning in presence of water or sulfur compounds and high price [5]. Metal oxides have not these disadvantages and can furthermore be more easily prepared, which makes them promising substitution catalysts [6]. Moreover, it was recently shown [4] that metal oxides can compete with noble metals in terms of catalytic performances. Therefore, in recent years, my research work was directed towards the design of catalytic materials based on transition-metal oxides to replace noble metal catalysts for VOCs abatement.

II.1. Total oxidation of methane over $BaTiO_3$ and $PbTiO_3$ perovskite catalysts

Perovskites are extensively studied as catalysts for the total oxidation of methane in particular due to their thermal, chemical and structural stability and in many cases improved catalytic activity [7, 8]. Furthermore, their dispersion on supports may lead to increased exposed surface areas [9]. To our knowledge, none of the $BaTiO_3$ and $PbTiO_3$ perovskites had ever been studied before as catalysts for the total oxidation of methane. This is why we decided to study unsupported and γ-Al_2O_3-supported $BaTiO_3$ and $PbTiO_3$ perovskites as catalysts for this reaction. Our work has been published in Ref. [10].

The physico-chemical characteristics of the catalysts studied are summarized in Table II.1. Note that for $BaTiO_3$ and $PbTiO_3$ samples the XRD analysis indicated only the formation of perovskite phases with tetragonal symmetry. After dispersion on γ-Al_2O_3, Ba and Pb titanates maintained their structural integrity.

Table 1. Textural properties and surface Ti/M atomic ratios of the catalysts (M = Pb or Ba).

Sample	BET surface area (m^2/g)	Average pore diameter (nm)	Pore volume (cm^3/g)	XPS surface Ti/M atomic ratio
γ-Al_2O_3	191.0	05.1	0.350	-
$BaTiO_3$	000.4	60.2	0.006	1.1
$BaTiO_3/Al_2O_3$	193.0	04.6	0.350	-
$PbTiO_3$	000.5	15.1	0.002	0.5
$PbTiO_3/Al_2O_3$	175.0	06.4	0.270	-

The catalytic activities in methane total oxidation of unsupported and supported perovskites as well as of the alumina support have been determined in the temperature range of 550-800 °C. The only reaction product detected on unsupported and supported perovskites was CO_2, while with γ-Al_2O_3 support a significant amount of CO was found in the products in line with what was reported in Ref. [11]. As clearly shown by the values of T_{50} (temperature corresponding to 50 % conversion) and of the specific reaction rate in Table II.2, unsupported

$PbTiO_3$ perovskite was more active than $BaTiO_3$, the last being, surprisingly, less active than alumina. In terms of the specific activity, both perovskites seem to be less active than alumina. This may be due to the very high surface area of alumina compared to unsupported perovskites. On the other hand, both supported catalysts are more active than the corresponding unsupported perovskites, both in terms of T_{50} values and of specific reaction rates. Moreover, an important increase in the reaction rate per unit mass of active component was observed after dispersion of the perovskite phase: 25 times for $BaTiO_3/\gamma\text{-}Al_2O_3$ and 30 times for $PbTiO_3/\gamma\text{-}Al_2O_3$ compared with the unsupported perovskite phases. At the same time, a decrease of the apparent activation energy was observed for the supported catalysts, more significant for $BaTiO_3$ perovskite (Table II.2). These observations suggest that dispersion of perovskites on $\gamma\text{-}Al_2O_3$ results in an interaction of the active component with the alumina support, responsible for the observed increase of the catalytic activity.

Table II.2. Catalytic performances of the catalysts in methane combustion.[a]

Catalyst	T_{50} (°C)	E_a (kcal/mol)	Reaction rate at 700°C (10^6 mol/g·s)	Reaction rate over perovskite phase at 700°C (10^6 mol/g·s)
$\gamma\text{-}Al_2O_3$	719	29.7	5.57	-
$BaTiO_3$	744	38.1	1.95	1.95
$BaTiO_3/Al_2O_3$	708	27.4	7.69	47.78
$PbTiO_3$	697	31.1	3.94	3.94
$PbTiO_3/Al_2O_3$	678	29.1	11.25	118.98

[a] Reaction conditions: 5 % vol. CH_4 in air, total VHSV = 16000 h^{-1}.

Note that the specific activity of the supported perovskite phase (the active component) in the supported catalyst, a, was calculated from the difference between the overall specific activity of the supported catalyst, a_1, and the specific activity of alumina support, a_0, as follows:

$a = (a_1 - 0.95a_0)/0{,}05$

where 0.95 and 0.05 are factors corresponding to the alumina and perovskite content in the supported catalyst, respectively.

In conclusion, the $BaTiO_3$ and $PbTiO_3$ catalysts, single perovskite phases with an important surface enrichment in lead for $PbTiO_3$, exhibit good activity in methane catalytic combustion, $BaTiO_3$ being less active than $PbTiO_3$. Dispersion of perovskites on γ-Al_2O_3 results in an increase of the catalytic activity due to the interaction between the active component and alumina support.

II.2. Transition metal-containing mixed oxides catalysts derived from LDH precursors for short-chain alkanes total oxidation

Only few studies concerned the transition metal-containing mixed oxides derived from layered double hydroxide (LDH) precursors although recognized as very promising combustion catalysts due to their high specific surface areas, thermal stabilities and tunable acid-base properties [12-18]. Kovanda et al. [14] showed that such Mn-Co containing-mixed oxides were active in the total oxidation of ethanol, while Dula et al. [15] showed that Mn-containing ones were active in the combustion of toluene. Methane [16, 17] and propane [18] total oxidation was also successfully performed with such Co- or Cu-containing mixed oxides. These promising results led us to study a series of MMgAlO mixed oxides (M = Mn, Fe, Co, Ni, Cu, Zn, Ag and Pd) in the total oxidation reaction of short-chain hydrocarbons. For the sake of comparison, the total oxidation activity of these catalysts was compared to that of a reference PdMgAlO catalyst. The obtained results have been published in Ref. [19].

The physico-chemical characteristics of the mixed oxide catalysts were resumed in Table I.6. The catalytic activities in methane total oxidation performed in the temperature range from 300 to 730 °C and 1 % vol. CH_4 in air (VHSV = 20000 h^{-1}), are shown in Fig. II.1, where the methane conversions were plotted as a function of the reaction temperature. For the blank experiment performed to establish the eventual influence of the quartz chips filling the dead volumes of the reactor, the reaction temperature has been raised up to 780 °C. One can note that methane ignites above 710 °C, therefore at a temperature ca. 150 °C higher than on MgAlO and FeMgAlO, the less active catalysts. The noble metal-containing catalyst PdMgAlO presented the highest activity with total conversion being reached below 500 °C. Among the non-noble metal-containing catalysts, CuMgAlO was the most active, total conversion being achieved at 585 °C. The activity of the different catalysts ranged as follows: MgAlO ≈ FeMgAlO < NiMgAlO < ZnMgAlO < MnMgAlO < CoMgAlO < AgMgAlO < CuMgAlO < PdMgAlO. This was confirmed by comparison of the temperatures, noted T_{10}, T_{50} and T_{90}, corresponding to 10, 50 and 90 % methane conversions of the different catalysts (Table II.3). The specific reaction rate of the non-noble metal-containing catalysts at 550 °C presented in Table II.3 followed the order already reported. The methane light-off temperatures estimated for the non-noble metal-containing catalysts were well consistent with the specific combustion rates.

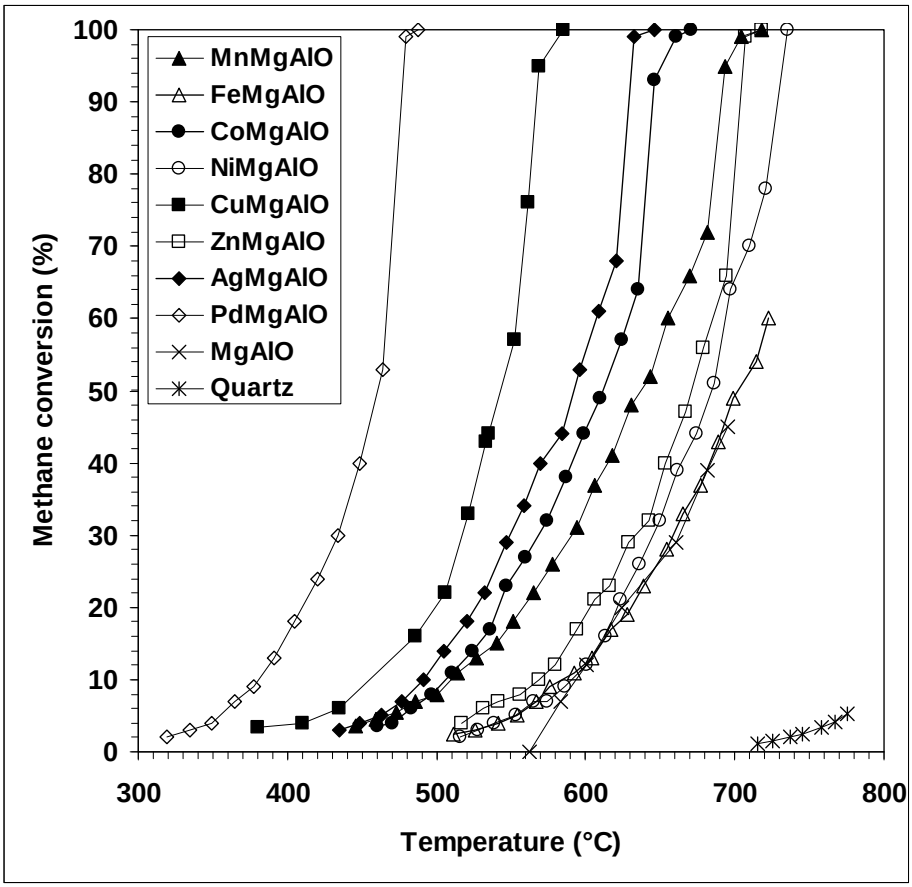

Figure II.1. CH_4 conversion as a function of the reaction temperature for the MMgAlO catalysts (1 % vol. CH_4 in air, total VHSV = 20000 h^{-1}).

The apparent activation energies (E_{act}) on the different catalysts have been calculated and are presented in Table II.3. They were in the range from 75 to 116 kJ mol^{-1} and in agreement with those reported for methane catalytic combustion over transition-metal oxide based catalysts [16, 20]. These values are specific for kinetic regimes free of mass transport limitations [21]. The apparent activation energy was significantly higher for the reaction on quartz (218 kJ mol^{-1}) and close to previous results [16, 21].

It is noteworthy that the most active non-noble metal-containing catalysts showed H_2-TPR consumption below 350 °C [19]. This suggested that highly reducible metal oxide species played an important role in the catalytic combustion of methane over these catalysts. This was obvious regarding CuMgAlO which exhibited the highest H_2-TPR consumption below 350 °C and was the most active.

Table II.3. Catalytic performances in methane total oxidation of MMgAlO catalysts.[a]

Catalyst	T_{10} (°C)	T_{50} (°C)	T_{90} (°C)	Specific rate [b] (10^7 mol g^{-1} s^{-1})	E_{act} (kJ mol^{-1})
PdMgAlO	380	460	477	-	83.3
CuMgAlO	456	543	565	14.1	95.4
AgMgAlO	491	592	629	8.5	91.7
CoMgAlO	505	612	645	5.5	93.7
MnMgAlO	510	637	691	5.2	74.9
ZnMgAlO	569	671	703	2.2	99.6
NiMgAlO	590	684	729	1.2	116.3
FeMgAlO	585	702	-	1.2	100.9

[a] Reaction conditions: 1 % vol. CH_4 in air, total VHSV = 20000 h^{-1}.
[b] At 550 °C.

Despite its high catalytic activity, the Pd-containing catalyst was characterized by a low stability for methane combustion [3]. This was confirmed comparing the activities of CuMgAlO and PdMgAlO at 560 °C and 470 °C, respectively, in the reaction with 1 % CH_4 in air for 20 h (Fig. II.2). CuMgAlO catalyst displayed a very good stability, while the conversion decreased from 60 % to 45 % for PdMgAlO, operating at a reaction temperature lower by 90 °C.

The most active CuMgAlO catalyst was also tested in the total oxidation of ethane, propane and propene. The characteristic activity data T_{10}, T_{50}, T_{90}, the specific activity at 450 °C and the apparent activation energy were reported in Table II.4. Carbon dioxide was the only product observed in all cases. According to the higher reactivity of light alkenes than alkanes, and the enhanced oxidability of alkanes with the number of carbon [22], the following increase in light-off temperature was observed: $C_3H_6 < C_3H_8 < C_2H_6 < CH_4$. The specific activity for the reaction at 450 °C decreased in the following range: $C_3H_6 > C_3H_8 > C_2H_6 > CH_4$. The apparent activation energy decreased from methane to ethane and propane as the strength of the C–H bond that must be broken to activate the alkane molecule decreased as well [23]. The great decrease of the apparent activation energy occurring above 350 °C for the oxidation of propene accounted for the mass transport limitation.

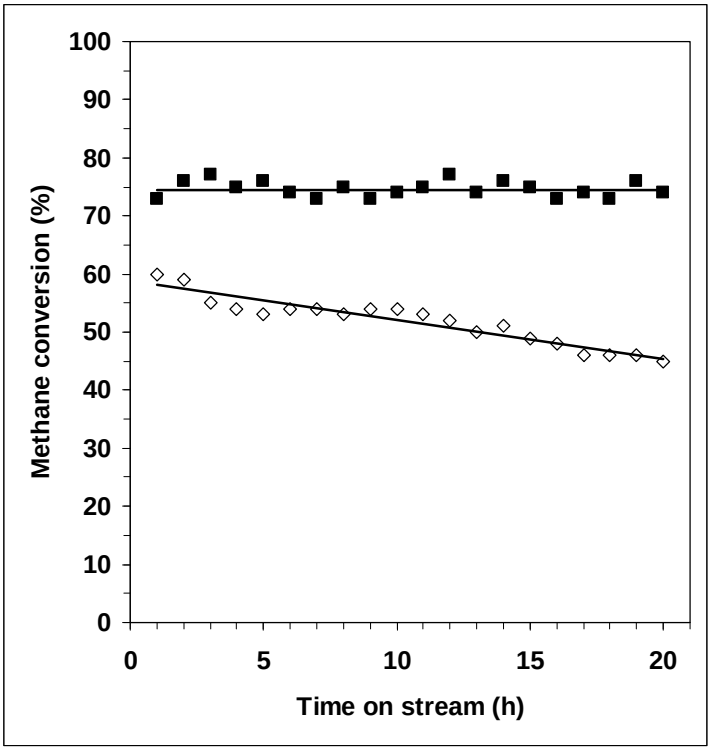

Figure II.2. Effect of time on stream on the catalytic properties of CuMgAlO at 560 °C (■) and of PdMgAlO at 470 °C (◇) (1 % vol. CH_4 in air, total VHSV = 20000 h^{-1}).

Table II.4. Catalytic performances of CuMgAlO catalyst in short-chain hydrocarbon total oxidation.[a]

Hydrocarbon	T_{10} (°C)	T_{50} (°C)	T_{90} (°C)	Specific rate [b] (10^7 mol g^{-1} s^{-1})	E_{act} (kJ/mol)
propene	288	338	411	24.4	89.6 / 11.7 [c]
propane	380	438	498	14.8	84.9
ethane	423	498	554	4.6	87.5
methane	456	543	565	2.3	95.4

[a] Reaction conditions: 1 % vol. CH_4 in air, total VHSV = 20000 h^{-1}.

[b] At 450 °C.

[c] For the reaction at temperatures higher than 350 °C.

In conclusion, the Pd-based catalyst was the most active for the complete oxidation of methane, total conversion being achieved at 488 °C. Among the non-noble metal-containing

catalysts the sequence of activity followed the order: MgAlO ≈ FeMgAlO < NiMgAlO < ZnMgAlO < MnMgAlO < CoMgAlO < AgMgAlO < CuMgAlO showing that highly reducible cationic species play an important role in the catalytic combustion of methane. Total conversion with the most active CuMgAlO catalyst was achieved at 585 °C. It is highly stable, while for PdMgAlO conversion decreased from 60 to 45 % after 20 h of reaction at 470 °C. The CuMgAlO mixed oxide catalyst was also able to perform the complete oxidation of other short-chain hydrocarbons, i.e. ethane, propane and propene.

II.3. Total oxidation of methane over Cu-based mixed oxides obtained from LDH precursors

A number of studies related to the total oxidation of methane on Cu based catalysts were published up to now [17, 20, 24-28], alumina being used as support for copper oxide in most cases. All these studies show that copper based systems are very active catalysts for methane total oxidation, the nature of the support and the Cu loading being important factors determining the catalytic performances. On the other hand, it has recently been shown [29] that adding magnesia to $CuO/\gamma\text{-}Al_2O_3$ enhances the activity of carbon monoxide oxidation.

We showed in the previous chapter that among MMgAlO mixed oxides (M = Mn, Fe, Co, Ni, Cu, Zn and Ag) obtained from layered double hydroxide (LDH) precursors the CuMgAlO was the most active catalyst in methane total oxidation. Thus, here we resume the study of CuMgAlO mixed oxides with different copper contents (1 – 20 at. %) as catalysts for the total oxidation of methane, which has been published in Ref. [30].

Physico-chemical characteristics of the catalysts are resumed in Table II.5. Note that the XRD analysis of the LDH precursors showed the presence of the LDH phase with low crystallinity as generally observed for multicationic LDH. For the samples with copper contents higher than 7 %, we noted the presence of CuO tenorite. The formation of copper-side phases is often observed in the case of copper-containing hydrotalcites due to the Jahn-Teller effect in the Cu^{2+} ions [31]. The Mg-Al mixed oxide phase with the periclase-like structure was detected in the mixed oxide catalysts after calcination at 750°C. CuO with a higher crystallinity than in the LDH precursor and copper aluminate were also detected for Cu loadings higher than 7 %. The average crystallite size of CuO increases from 18 to 35 nm, while that of $CuAl_2O_4$ remains constant at ca. 10 nm when the copper content in the catalyst increases from 10 to 20 %. At lower loadings, Cu can form a solid solution with Mg and Al, or give well dispersed CuO crystallites not detected by XRD. The XRD patterns of the catalysts recorded after the catalytic test showed no modifications even after the long-term runs.

The catalytic activities in methane total oxidation are resumed in Table II.6. As clearly shown by the values of T_{50} and T_{90} (temperature corresponding to 50 % and 90 % conversion, respectively), and of the specific reaction rate, MgAlO was the less active, while both Cu(10)MgAlO and Cu(20)MgAlO gave the highest activity with total conversion being achieved

at temperatures lower than 525 °C. Nevertheless, we note that the temperature at which the reaction starts (T_{onset}) on Cu(20)MgAlO is 50 °C higher than on Cu(10)MgAlO. Taking into account that VOCs catalytic combustion process requires the heating of great amounts of air up to the reaction temperature, a difference of 50 °C becomes significant.

Table II.5. Physico-chemical characteristics of the catalysts.

Catalyst	Specific surface area (m^2g^{-1})	Copper content (% at. with respect to cations)		Chemical composition (% at.) by EDX [a]			Total H_2 consumption (mol H_2/mol Cu)
		theor.	by EDX	Cu	Mg	Al	
MgAlO	188	-	-	-	-	-	-
Cu(1)MgAlO	163 (161)[b]	01.0	01.1	0.27	18.94	5.75	0.76
Cu(3)MgAlO	155	03.0	-	-	-	-	-
Cu(5)MgAlO	157	05.0	06.7	1.74	18.32	5.95	0.29
Cu(7)MgAlO	163	07.0	-	-	-	-	-
Cu(10)MgAlO	169 (163)[c]	10.0	12.3	3.26	17.05	6.04	0.20
Cu(20)MgAlO	114 (108)[c]	20.0	22.9	6.36	14.97	6.46	0.22

[a] Oxygen in balance.

[b] After the catalytic test.

[c] After the long-term runs.

Table II.6. Catalytic performances in methane total oxidation of CuMgAlO catalysts.

Catalyst	T_{50} (°C)	T_{90} (°C)	Specific rate (510°C) (10^7.mol/g.s)	E_{act} (kcal/mol)
Cu(1)MgAlO	626	658	00.3	31.1
Cu(3)MgAlO	568	588	05.7	26.6
Cu(5)MgAlO	543	565	06.6	22.8
Cu(7)MgAlO	522	560	12.2	21.1
Cu(10)MgAlO	482	519	18.4	15.8
Cu(20)MgAlO	490	504	21.9	21.8

For the Cu-containing samples the activity increased with the Cu content up to 10 % and remained constant above this content, *i.e.* for Cu(20)MgAlO. This behavior suggested that the activity of bulk CuO is substantially lower than that of highly dispersed CuO, as already shown in the literature [26, 28]. The activity ranges as follows: Cu(20)MgAlO ≈ Cu(10)MgAlO > Cu(7)MgAlO > Cu(5)MgAlO > Cu(3)MgAlO > Cu(1)MgAlO > MgAlO. However, when the methane conversion per unit mass of copper (mol methane converted per g Cu per second) is considered (Fig. II.3), the order of activity is somewhat modified: Cu(10)MgAlO > Cu(5)MgAlO > Cu(20)MgAlO > Cu(1)MgAlO. This sequence suggests that the Cu(10)MgAlO sample displays the optimum dispersion of the copper-containing species in the MgAlO matrix. A similar behavior has already been observed for supported Cu catalysts [24, 28]. This decrease of specific activity observed for Cu(20)MgAlO catalyst can be assigned to the CuO average crystallite size. It is worth noting that the results obtained with the best catalysts are comparable or even better than those reported up to now in the literature with CuO based catalysts.

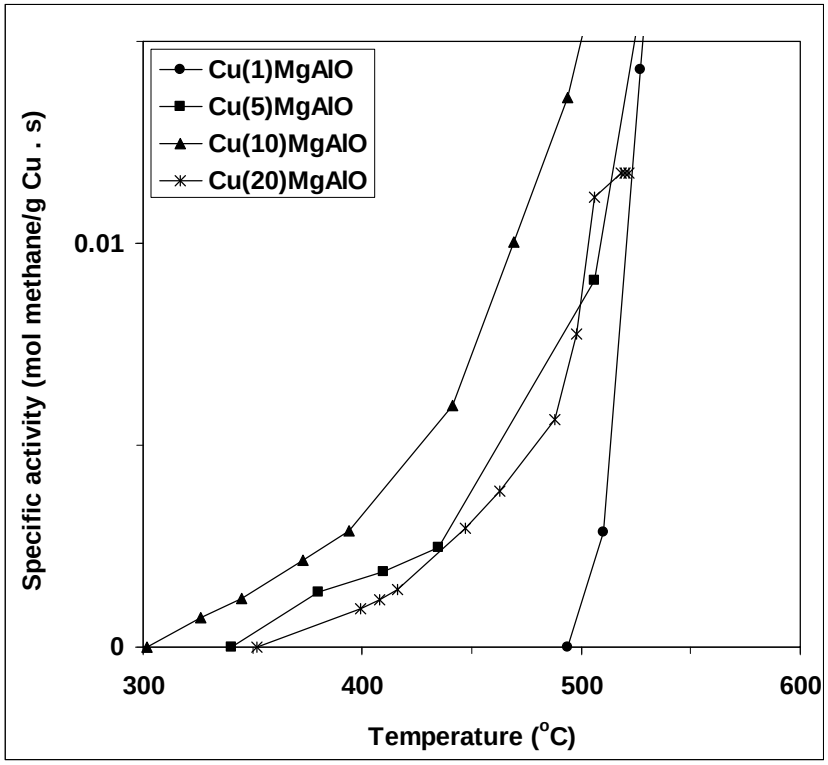

Figure II.3. Specific activity per unit mass of copper as a function of the reaction temperature for Cu(1)MgAlO, Cu(5)MgAlO, Cu(10)MgAlO and Cu(20)MgAlO catalysts (1 % vol. CH_4 in air, total VHSV = 20000 h^{-1}).

The apparent activation energies (E_{act}) on the different catalysts have been calculated being presented in Table II.6. In contrast with CuO supported on alumina where E_{act} does not depend on the CuO loading [25, 28], the E_{act} on Cu-Mg-Al-O catalysts decreased when the copper content increased up to 10 % (Cu(10)MgAlO sample), being then higher for Cu(20)MgAlO sample. This evolution means that the nature of the active site changes with the Cu content, in agreement with the H_2-TPR data [30]. The most efficient catalyst is Cu(10)MgAlO, in line with the observed variation of the specific catalytic activity. On the other hand, the values obtained for the E_{act} were in agreement with those measured for methane catalytic combustion over supported CuO catalysts [20, 32]. These values show that the kinetic of the reaction is chemically controlled.

It is interesting to note that a linear correlation was observed between the H_2 consumption below 400 °C and the specific activity of the catalysts (Fig. II.4). Such correlation was not found for the H_2 consumption at higher temperature suggesting that only the highly reducible copper species were catalytically active.

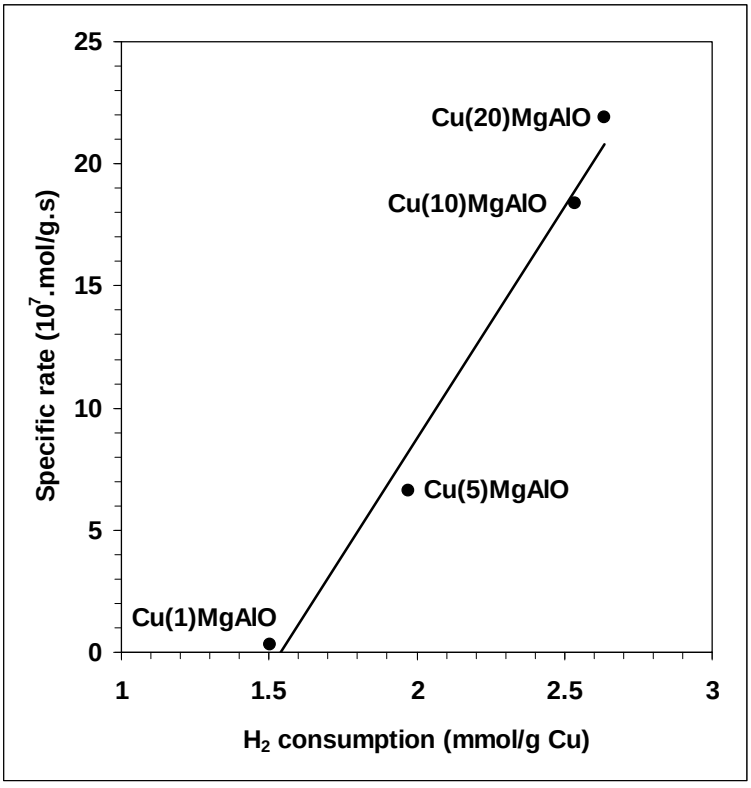

Figure II.4. Specific activity of the catalysts versus H_2 consumption below 400 °C.

It is worth noting that both Cu(10)MgAlO and Cu(20)MgAlO catalysts display a very good stability as shown in Fig. II.5.

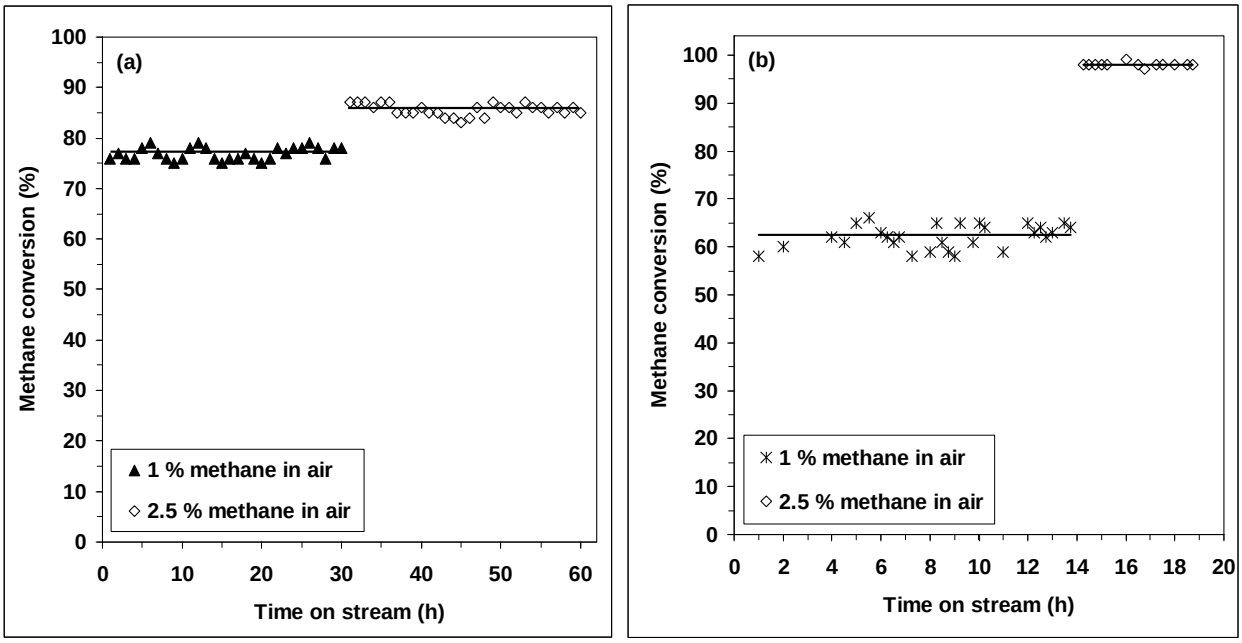

Figure II.5. Effect of time on stream on the catalytic properties of (a) Cu(10)MgAlO at 515 °C with 1 % CH_4 in air then at 555 °C with 2.5 % CH_4 in air and (b) Cu(20)MgAlO at 495 °C with 1 % CH_4 then at 590 °C with 2.5 % CH_4 in air (total VHSV = 20000 h^{-1} in all cases).

In conclusion, the Cu-free MgAlO mixed oxide was the less active, while both Cu(10)MgAlO and Cu(20)MgAlO gave the highest activity, allowing total conversion of methane at temperatures lower than 525°C. For the Cu-containing samples the activity increased with the Cu content up to 10 %. Above this content the influence becomes negligible in terms of methane conversion, but the Cu(10)MgAlO sample showed the best specific activity per unit mass of copper. Under all the experimental conditions investigated, no CO could be detected at the exhaust. The Cu-Mg-Al mixed oxide catalysts showed a good stability during the catalytic test.

II.4. Co and Ni ferrospinels as catalysts for propane total oxidation

Up to now, there are no studies investigating spinel ferrites as catalysts for light alkanes total oxidation although they were shown to be effective catalysts for the total oxidation of VOCs [33-35] as well as for CO oxidation [36]. We resume here a study of Co and Ni ferrospinels, prepared by coprecipitation or by mechano-chemical method, used for the first time as catalysts for total oxidation of propane. It has been published in Ref. [37].

The physico-chemical characteristics of the ferrospinel catalysts are resumed in Table II.7. For all the solids, the crystallized ferrospinel structure was observed. For $CoFe_2O_4$ samples, a tiny amount of α-Fe_2O_3 phase was also noted.

Table II.7. Physico-chemical characteristics of the ferrospinel catalysts.

Sample	Mass % by EDX	BET surface area (m^2/g)	Pore volume (cm^3/g)	Average pore size (nm)	H_2 consumption by TPR (mol H_2/mol ferrite)
Ni ferrite-M1[b]	Ni: 33.8 (34.5)[a] Fe: 66.2 (65.5)	53.8 (51.2)	0.32	20.8	2.07
Co ferrite-M1[b]	Co: 34.1 (34.5) Fe: 65.9 (65.5)	20.5 (21.1)	0.16	27.4	2.02
Co ferrite-M2[c]	Co: 34.4 (34.5) Fe: 65.6 (65.5)	08.4 (8.1)	0.07	29.4	2.13

[a] Theoretical mass % in parentheses.

[b] Prepared by coprecipitation.

[c] Prepared by mechano-chemical method.

The catalytic activities of the prepared ferrospinels in propane total oxidation are resumed in Table II.8. As clearly shown by the values of T_{10} (temperature corresponding to 10 % conversion), T_{50} (temperature corresponding to 50 % conversion), T_{90} (temperature corresponding to 90 % conversion) and of the specific reaction rate, Co ferrite-M1 was the most active catalyst giving total conversion at temperatures as low as 400°C, the sequence of activity following the order: Co ferrite-M1 > Ni ferrite-M1 > Co ferrite-M2. It has already been shown

that Co-containing catalysts are more active than Ni-containing ones in methane combustion [38]. We noted that the catalyst prepared by the mechano-chemical method (Co ferrite-M2) was less active than that prepared by coprecipitation (Co ferrite-M1) probably due to the lower specific surface area of the former.

Table II.8. Catalytic performances in propane total oxidation of ferrospinels catalysts.[a]

Catalyst	T_{10} (°C)	T_{50} (°C)	T_{90} (°C)	Specific rate (10^7.mol/g.s)		E_{act}
				320°C	350°C	(kcal/mol)
Ni ferrite-M1	330	370	415	1.3	2.4	15.8
Co ferrite-M1	310	335	360	1.7	8.6	39.6
Co ferrite-M2	380	450	490	0.5	0.9	21.5

[a] Reaction conditions: 2 vol % propane in air, total VHSV = 6000 h^{-1}.

The apparent activation energies (E_{act}) corresponding to propane transformation on the different catalysts have been calculated from the Arrhenius plots obtained from the experimental data up to 60 % conversion. The differences observed between the activation energies suggest that the nature of the catalytic site differs from one ferrite to the other. On the other hand, if one takes into consideration the catalytic activities observed it is clear that the surface density of the active sites also differs from one ferrite to the other. The values obtained for the activation energies fall within the usual range measured for propane total oxidation over oxide-based catalysts working within the chemical regime [39, 40]. These values suggest that the kinetic regime is chemical, i.e. the rate determining step is the surface chemical reaction.

The stability of Co ferrite catalysts was studied and the obtained results can be observed in Fig. II.6, where the propane conversions in terms of the time on stream for Co ferrite-M1 at 340 °C and Co ferrite-M2 at 480 °C are shown. No deactivation was observed in any of the samples after 24 h, in line with the observation that the physico-structural characteristics of the catalysts did not change after the catalytic tests. Both Co-ferrite catalysts display a good stability, at least for the reaction conditions and the reaction time chosen.

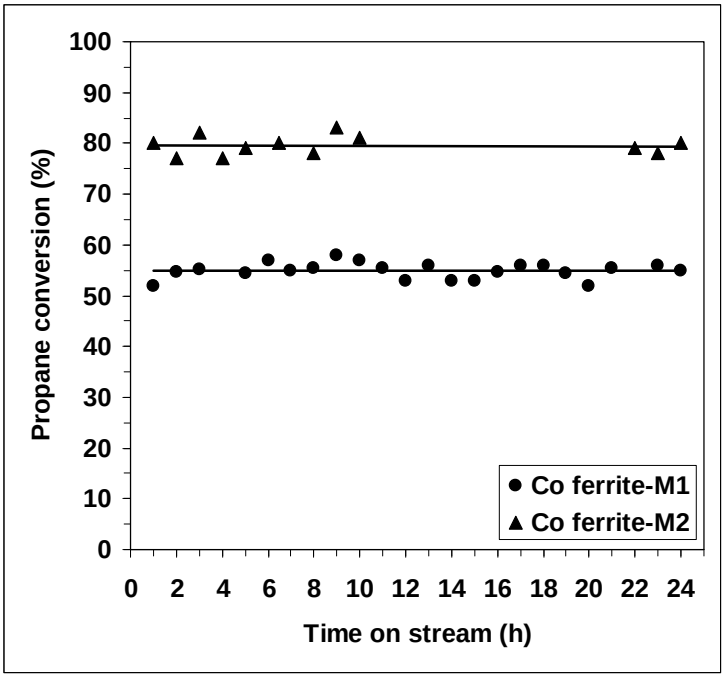

Figure II.6. Effect of time on stream on the catalytic properties of Co ferrite-M1 at 340 °C and Co ferrite-M2 at 480 °C (2 % vol. propane in air, total VHSV = 6000 h^{-1}).

In conclusion, high surface area ferrospinels of nickel and cobalt were prepared and their catalytic properties for the catalytic total oxidation of propane were for the first time investigated. Co ferrite was more active than Ni ferrite prepared using the same method, Co ferrite-M1 being the most active among the tested catalysts giving total conversion at temperatures as low as 400°C. The physico-chemical characteristics of the Co ferrite and its catalytic properties are determined by the method used for the catalyst preparation. The ferrospinel catalysts showed a good stability during the catalytic test. In all the experimental conditions tested, no CO could be detected at the exhaust.

III. CHARACTERIZATION OF OXIDATION CATALYSTS BY ELECTRICAL CONDUCTIVITY MEASUREMENTS

Electrical conductivity measurements carried out on oxides used as catalysts in oxidation reactions involving redox processes between reactants and catalysts can provide information on the nature of surface structure defects, the existence of oxidizing species (ionosorbed oxygen species, active surface anions) and the nature of the oxidic phase involved in catalytic reactions as described in Ref. [1].

The electrical conductivity σ of an oxide catalyst can be expressed by the formula:

$$\sigma = \frac{1}{R} \cdot \frac{t}{S} \tag{1}$$

where R is the electrical resistance and t/S is the geometrical factor including the thickness t of the catalyst pellet and the cross sectional area S of the circular platinum electrodes having the catalyst pellet in between.

To compare the electrical conductivities of the oxide samples, it is required that they have similar textures and identical surface states. This requirement is easily fulfilled if all the samples have similar textures. Indeed, the electrical conductivity of semiconducting oxide powders can be written as:

$$\sigma = A \cdot n \tag{2}$$

where *n* is the concentration of the main charge carriers and *A* is a coefficient of proportionality which includes the mobility of the main charge carriers and the elementary charge of the electron and depends on the compression of the powder and on the number and quality of contact points between particles [1]. If the samples are compressed at the same pressure and have similar BET surface areas and the electrical measurements are standardized, *A* can be considered as identical for all the samples under identical conditions. Thus, the electrical behavior of these catalysts will generally be a function of the temperature, whose influence can be followed in the same range as that of catalysis, of the oxygen pressure and of the nature of the gas phase in contact with the solid. Consequently, electrical conductivity measurements can constitute a useful tool to characterize oxidation catalysts [1].

This technique was largely used in catalysis [2-13], some of the most interesting results obtained being resumed below. Thus, Herrmann et al. [4] established the p-type character of the V-P-O catalysts used for the partial oxidation of *n*-butane to maleic anhydride and clearly evidenced the redox mechanism involved with the initial hydrogen abstraction from *n*-butane by O^- species from surface V^{4+}–O^- pairs. Using the same technique, a change in the nature of the semiconductivity that passes from p-type under air to n-type under *n*-butane – air reaction mixture was evidenced for Ti and Zr pyrophosphates used as catalysts for the oxydehydrogenation of *n*-butane, and a reaction mechanism involving surface O^- species was proposed [5, 6]. The same reaction was studied over promoted and unpromoted nickel molybdates and by using the electrical conductivity measurements the n-type character of the solids and the role of the promoter have been established and a redox-type reaction mechanism has been proposed [7, 8]. In the case of Mo-V-M-O (M = Zn, Ni, Cu, Sb) oxides, catalysts for isobutane oxydehydrogenation, it has been shown that they were of n-type or of p-type as a function of their composition and redox-type reaction mechanisms have been proposed. Moreover, a correlation between the electrical conductivity and the catalytic activity was found for both n-type and p-type series suggesting that the rate of electronic transfer is a key factor determining the catalytic activity [10]. Millet et al. [11] studied by electrical conductivity measurements V-Sb-(Fe)-O catalysts which are active in the ammoxidation of propane, and found that an increased concentration of cationic vacancies and isolated V^{4+} species, due to the introduction of increasing amounts of Fe in the lattice, led to a proportionally higher activity. Supported oxide-based catalysts, such as V_2O_5-WO_3/TiO_2 used in selective catalytic reduction (SCR) deNO_x reaction, have also been studied by means of electric conductivity measurements [12]. It has been shown that the SCR deNO_x reaction over V_2O_5-WO_3/TiO_2 catalyst is a redox process assisted by acidic sites necessary for the dissociative chemisorption of ammonia. Finally, this technique was used for the characterization of TiO_2-based photocatalysts, the detrimental effect of Cr-doping TiO_2 being recently explained by an electron-hole recombination [13]. We also applied the electrical conductivity measurements to the characterization of the oxide-based catalysts studied in both oxidative dehydrogenation and total oxidation of light alkanes, the results obtained being presented in this chapter.

III.1. Study by electrical conductivity measurements of semiconductive and redox properties of ceria and phosphated ceria catalysts

Up to now there are several studies concerning the use of ceria and CeO_2-containing materials as catalysts or catalysts' supports, a book being already devoted to this topic [14]. Also, several studies concerning the electrical properties of pure and doped ceria have already been performed and reviewed in Refs. [14, 15]. The electrical properties of these materials are mainly associated to the presence of oxygen vacancies also recognized to play a key role in the catalytic activity by improving the lattice oxygen mobility and lability, and, for the noble metals supported on ceria-based materials, by favoring the electronic transfer from the support to the noble metal [16].

For better understanding the catalytic behavior of ceria and phosphated ceria in oxidative dehydrogenation of isobutane described in Chapter I, their DC-electrical conductivity was studied as a function of the temperature, the air pressure, the nature of different gaseous reactant atmospheres and the reaction mixture. Reaction mechanisms for the transformation of isobutane over these catalysts have been proposed and a correlation between their semiconductive and catalytic properties has been established. The results obtained have been published in Ref. [17] and are presented below. Note that the common reference state for σ determination has been chosen under air at atmospheric pressure and at 490 °C or 610 °C. At these temperatures, which are in the range used in the catalytic reactions, most of the ionically adsorbed species such as H_3O^+, HO^- which would produce an additional surface conductivity are eliminated. The solid was initially heated from room temperature to the desired temperature at a heating rate of 5 °C/min.

First, the electrical conductivities of the ceria and phosphated ceria samples have been measured as a function of temperature to determine the activation energy of conduction E_c, under air at atmospheric pressure, in the temperature range from 400 to 660 °C. Linear variations of the semi-log plots [$\log\sigma = f(1/T)$] were observed showing that all the compounds behaved as semiconductors whose electrical conductivities varied exponentially with temperature according to the typical activation law:

$$\sigma = \sigma_0 \cdot \exp\left(-\frac{E_c}{RT}\right) \qquad (3)$$

where σ_0 is the preexponential factor. The slopes of the semi-log plots enabled one to calculate

the E_c values presented in Table III.1. It can be observed that the activation energy of conduction decreased by adding phosphorus to ceria and by increasing its content. It is noteworthy that the electrical conductivity of the samples increased following the order: CeO_2 < 1.1P/CeO_2 < 2.2P/CeO_2. This means, according to Eq. (2), that the concentration of charge carriers increased by adding phosphorus to ceria and by increasing its content.

Table III.1. Electrical characteristics of ceria and phosphated ceria samples.

Catalyst	E_c [a] (kJ.mol^{-1})	Exponent *n* [b]
CeO_2	139.8	4
1.1P/CeO_2	80.9	20
2.2P/CeO_2	59.6	-

[a] Activation energy of conduction.
[b] From Eq. (4)

According to the Heckelsberg criterion [18], as the electrical conductivity was lower under air than under nitrogen within all the temperature range considered, the CeO_2 and 1.1P/CeO_2 samples have a n-type semiconductor character. The 2.2P/CeO_2 sample could be an intrinsic semiconductor as the electrical conductivity under air was practically equal to that under nitrogen.

Fig. III.1 shows the variations of σ as a function of oxygen pressure at 490 °C in a log–log plot. It clearly appeared that CeO_2 and 1.1P/CeO_2 samples were of the n-type under oxygen since $\partial\sigma/\partial P_{O_2} < 0$, while no dependence of σ on the oxygen pressure was observed for 2.2P/CeO_2 sample.

It is generally assumed that the electrical conductivity σ of n-type oxides varies as a function of partial pressure of oxygen P_{O_2} and temperature T, according to the equation:

$$\sigma\left(P_{O_2}, T\right) = C \cdot P_{O_2}^{-1/n} \cdot \exp\left(-\frac{\Delta H_c}{RT}\right) \qquad (4)$$

where ΔH_c represents the enthalpy of conduction and C is a constant which only depends on various characteristics of the sample (charge and mobility of the charge carriers, number of contact points between grains etc.) [1]. The value of the exponent *n* can be indicative of the nature of the defects in the solid, which generate charge carriers.

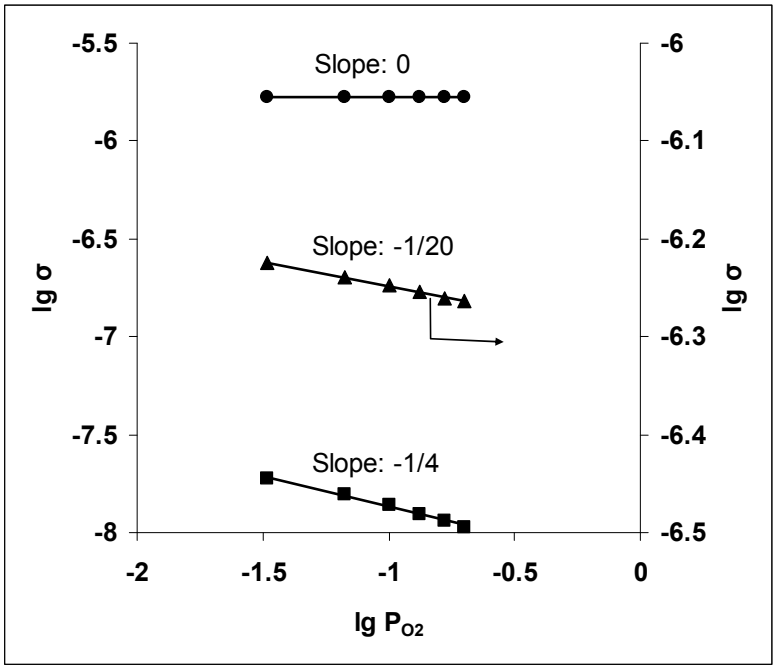

Figure III.1. Variation of σ as a function of the oxygen pressure for CeO_2 (■), 1.1P/CeO_2 (▲) and 2.2P/CeO_2 (●) at 490 °C (P_{O_2} in atm; σ in ohm^{-1}.cm^{-1}).

The values of the exponent *n* calculated for the different solids from the slopes of the log–log plots in Fig. III.1, are presented in Table III.1. From these values, only CeO_2 behaved according to a simple conduction model with *n* equal to 4. Such a value corresponds to the formation of singly ionized anionic vacancies according to the equations:

$$O_O^{\times} \leftrightarrows \tfrac{1}{2}O_{2(g)} + V_O^{\times} \tag{5}$$

$$V_O^{\times} \leftrightarrows V_O^{\bullet} + e' \tag{6}$$

where $O_O^{\times}$ represents an oxygen anion of the solid in regular lattice points, $V_O^{\times}$ a filled anionic vacancy, $V_O^{\bullet}$ a singly ionized anionic vacancy and e' a quasi-free electron.

The mass action law applied to Eqs. (5) and (6) gives:

$$K_5 = P_{O_2}^{1/2}[V_O^{\times}] \tag{7}$$

$$K_6 = [V_O^{\bullet}][e']/[V_O^{\times}] \tag{8}$$

The electroneutrality condition

$$[e'] = [V_O^{\bullet}] \tag{9}$$

combined with the mass action law yields:

$$\sigma \propto [e'] = (K_5 K_6)^{1/2} P_{O_2}^{-1/4} \quad (10)$$

In the case of CeO_2 sample the log–log plot of σ as a function of P_{O_2} in air gives a descending straight line whose slope is indeed equal to –1/4 (Fig. III.1). In addition, constants K_5 and K_6 follow the van't Hoff's law as a function of temperature:

$$K_5 = (K_5)_0 \exp(-\Delta H_5/RT) \quad (11)$$

$$K_6 = (K_6)_0 \exp(-\Delta H_6/RT) \quad (12)$$

where ΔH_5 and ΔH_6 are the enthalpies of reactions (5) and (6). Combining Eqs. (10), (11) and (12), one gets:

$$\sigma \propto [e'] = [(K_5)_0 (K_6)_0]^{1/2} \exp\left[-\frac{\Delta H_5 + \Delta H_6}{2RT}\right] P_{O_2}^{-1/4} \quad (13)$$

Generally, the ionization energy of the first electron ΔH_6 can be neglected with respect to the formation enthalpy of anionic vacancies ΔH_5. Consequently, for CeO_2 the heat of formation of anionic vacancies is equal to $2E_c$, that is 279.6 kJ.mol^{-1} (per mole of vacancies). This enthalpy value is lower than that already reported for ceria (396 kJ.mol^{-1}) [15] or other n-type oxide such as titania (342.7 kJ.mol^{-1}) [19], but higher than that of tin oxide (226.0 kJ.mol^{-1}) [20] and gives information about the lability of surface lattice oxygen anions able to react with isobutane. Under our experimental conditions, CeO_2 was active, as a n-type semiconductor, for the reaction of isobutane but gave high quantities of carbon oxides (see Table I.3) suggesting a high reactivity of the surface lattice oxygen anions in line with the relatively low enthalpy of formation of anionic vacancies observed.

The case study of the two phosphated ceria samples was more complex. Thus, for the 1.1P/CeO_2 sample the value of *n* was equal to 20 being significantly higher than 4 or 6 that respectively correspond to the formation of singly or doubly ionized vacancies. Such a phenomenon could be explained by a more complex model involving two different sources of electrons, one of them being independent of the partial pressure of oxygen:

$$\sigma = \sigma_1 + \sigma_2 \quad (14)$$

with $\sigma_1 = A(K_5 K_6)^{1/2} P_{O_2}^{-1/4}$ and σ_2 independent of the partial pressure of oxygen P_{O_2}. Such a model has already been proposed for TiO_2 and related compounds [21] and vanadium antimonate based catalysts [11]. In the present case, a linear relationship was obtained when plotting the total

conductivity σ as a function of $P_{O_2}^{-1/4}$ confirming the existence of a source of conduction electrons whose nature was independent of oxygen pressure. Moreover, the *y*-intercept representing the conductivity σ_2 at the temperature concerned, it was possible to separate the two contributions. Thus, σ_2 being equal to $4.54 \cdot 10^{-7}$ $ohm^{-1}.cm^{-1}$, σ_1 was calculated by subtracting σ_2 from σ according to Eq. (14) and was represented as a function of the oxygen pressure in a log–log plot. The obtained plot exhibited the expected –1/4 slope confirming, thus, the model proposed.

In the case of $2.2P/CeO_2$ sample, the variation of σ with P_{O2}, displayed in Fig. III.1, shows that the electrical conductivity is practically independent of the oxygen pressure. This could lead to the conclusion that this material is rather an intrinsic semiconductor ($\partial\sigma/\partial P_{O_2} = 0$) as also suggested by the Heckelsberg criterion. If that were the case, the theory would imply that the band-gap energy E_G should be equal to twice the activation energy of conduction E_c ($E_G = 2E_c$). Consequently, E_G should be equal to 119.2 $kJ.mol^{-1}$, that is 1.24 eV. However, the band-gap energy determined from the UV spectrum of $2.2P/CeO_2$ sample was equal to 3.2 eV. This value is quite different from that calculated, and the solid cannot be considered an intrinsic semiconductor under our conditions but an extrinsic one with sources of electrical charge carriers independent of oxygen pressure.

The observed increase of the electrical conductivity of the samples caused by adding phosphorus to ceria and by increasing its content must be related to the $P–CeO_2$ interaction and could be explained taking into consideration a partial dissolution of P(V) in the lattice of ceria occurring via the substitution of P(V) to Ce(IV) ions in the surface and subsurface lattice positions of ceria. It is noteworthy that it has already been shown that P(V) ions can enter the fluorite CeO_2 structure by the substitution of Ce(IV) with P(V) [22]. This causes a doping effect according to the valence induction law of Verwey [23]. Each dissolved P(V) species shares four electrons with four O^{2-} neighbor anions, whereas the fifth electron is delocalized around the P(V) impurity as represented in Fig. III.2.

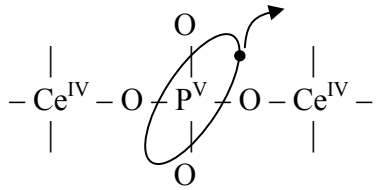

Figure III.2. Doping of ceria by P(V) dissolved species.

The P(V) impurities are associated with donor levels between the conduction band and the valence band of ceria. A small energy is sufficient to ionize this donor level and to enable the fifth electron to reach the conduction band. This explains the observed decrease of the activation energy of conduction E_c (Table III.1) under air caused by adding phosphorus to ceria and by increasing its content. Moreover, these substitution defects can be associated to the source of conduction electrons whose nature is independent of oxygen pressure evidenced in the phosphated ceria samples. On the other hand, the introduction of a higher valence cation, such as P(V), not only increases the substitution defects responsible for the increase of the charge carriers concentration but also reduces the vacancy population according to the reactions (15) and, to a lesser extent, (16):

$$P_2O_5 + V_O^{\bullet} \leftrightarrows 2P_{Ce}^{\bullet} + 5O_O^{\times} + e' \quad (15)$$

$$P_2O_5 + V_O^{\bullet\bullet} \leftrightarrows 2P_{Ce}^{\bullet} + 5O_O^{\times} \quad (16)$$

In that way we can explain the weakened dependence of the electrical conductivity on the oxygen pressure for 1.1P/CeO_2 and 2.2P/CeO_2 samples. Moreover, the consumption of oxygen vacancies results in lower surface lattice oxygen mobility and reactivity, in line with the hydrogen temperature-programmed reduction (H_2-TPR) data (see Fig. I.4), explaining the observed decrease of the catalytic activity of the studied catalysts in the order CeO_2 > 1.1P/CeO_2 > 2.2P/CeO_2 for the reaction at 490°C. The observed increase of the isobutene selectivity following the order CeO_2 < 1.1P/CeO_2 < 2.2P/CeO_2, can also be correlated with the decrease of the lattice oxygen mobility and lability suggested by the weakened dependence of the electrical conductivity on the oxygen pressure observed by adding phosphorus to ceria and by increasing its content.

To get information on the solids under conditions as close as possible to those of catalysis, the electrical conductivity measurements were performed at a temperature within the reaction temperature range during sequential periods under air, under nitrogen, under isobutane-air mixture (reaction mixture with an air-to-isobutane molar ratio equal to 2.5) and under isobutane-nitrogen mixture (nitrogen-to-isobutane molar ratio equal to 2.5). The results obtained at 490 °C are displayed in Fig. III.3.

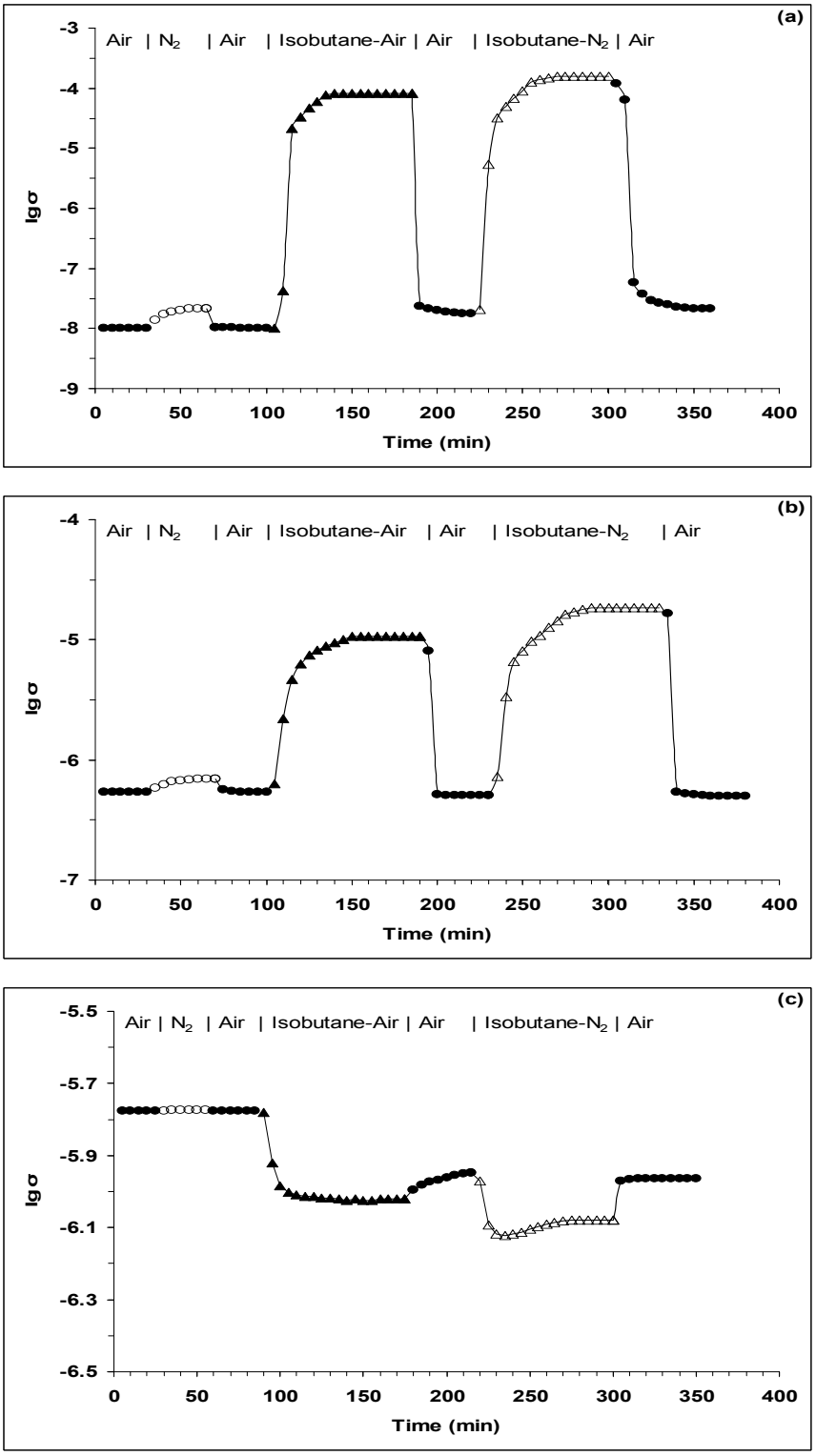

Figure III.3. Variation of the electrical conductivity under sequential exposures to air (●), N_2 (○), i-C_4H_{10} – air mixture (reaction mixture) (▲) and i-C_4H_{10} – N_2 mixture (△) for CeO_2 (a), 1.1P/CeO_2 (b) and 2.2P/CeO_2 (c) at 490 °C (σ in $ohm^{-1}.cm^{-1}$).

The solids were heated from room temperature to 490 °C, at a heating rate of 5 °C/min in air flow at atmospheric pressure. After reaching the steady state under the air flow, nitrogen was introduced over the samples. As expected, the electrical conductivity increased for CeO_2 and 1.1P/CeO_2 samples and remained constant for 2.2P/CeO_2, confirming again the n-type character of CeO_2 and 1.1P/CeO_2 samples according to the Heckelsberg criterion. Then, air was again introduced over the samples and, after reaching the steady state, an isobutane-air mixture (reaction mixture) was passed over the samples. In the case of CeO_2, the electrical conductivity immediately increased abruptly by 4 orders of magnitude. The same increase of the electrical conductivity was observed for 1.1P/CeO_2, but within less than 2 orders of magnitude so that it becomes lower than that of CeO_2. These behaviors correspond to the n-type semiconductive character, since, for oxide semiconductors, the n-type criterion is $\partial\sigma/\partial P_{O_2} < 0$ or, considering isobutane as a reductant, $\partial\sigma/\partial P_{i\text{-}C_4H_{10}} > 0$. Surprisingly, for 2.2P/CeO_2 sample the electrical conductivity slightly decreased under the isobutane-air flow. This behavior corresponds rather to the p-type character, since, for oxide semiconductors, the p-type criterion is $\partial\sigma/\partial P_{O_2} > 0$ or, considering isobutane as a reductant, $\partial\sigma/\partial P_{i\text{-}C_4H_{10}} < 0$.

After reaching the steady state under the isobutane-air flow, air was again introduced over the samples. The electrical conductivity decreased immediately and reached a plateau for CeO_2 and 1.1P/CeO_2 samples confirming the n-type character of both solids. In the case of 2.2P/CeO_2 sample the electrical conductivity slightly increased, but the plateau corresponding to the new steady state under air was not the same as before the isobutane-air mixture sequence, suggesting a new state of the solid that obviously corresponds to a reduced oxide.

After reaching the steady state under the air flow, the isobutane-nitrogen mixture was introduced in contact with the samples and then, after reaching the steady state under this mixture, the air sequence was repeated for observing the reversibility of the phenomena. Again, an important increase of the electric conductivity was observed for CeO_2 and 1.1P/CeO_2 samples corresponding to their n-type semiconductive character. Under air their electrical conductivities decreased immediately and reached a plateau confirming the reversibility of the phenomena observed. For the 2.2P/CeO_2 sample, the electrical conductivity slightly decreased under the isobutane-nitrogen flow suggesting again a p-type character for this sample. Under air, the electrical conductivity of the 2.2P/CeO_2 sample increased and reached a plateau identical to that

reached after the isobutane-air sequence, but different from that corresponding to the initial state suggesting an irreversible reduction of the solid.

The reversible redox process observed in the case of the CeO_2 and $1.1P/CeO_2$ samples during successive sequences under isobutane-air mixture or isobutane-nitrogen mixture and air can be explained as follows. Isobutane is oxidized by reaction with surface lattice oxygen anions, thus partially reducing the surface. The increase of σ can be ascribed to the creation of anionic vacancies, $V_O^{\times}$, by reduction of the solid by isobutane:

$$O_O^{\times} + \text{i-}C_4H_{10} \rightarrow \text{i-}C_4H_8 + H_2O + V_O^{\times} \quad (17)$$

followed by the spontaneous ionization of the anionic vacancies according to the following equations:

$$V_O^{\times} \leftrightarrows V_O^{\bullet} + e' \quad (18)$$

$$V_O^{\bullet} \leftrightarrows V_O^{\bullet\bullet} + e' \quad (19)$$

where $O_O^{\times}$ represents an oxygen anion of the solid in regular lattice points (O^{2-}), $V_O^{\times}$ a filled anionic vacancy, $V_O^{\bullet}$ a singly ionized anionic vacancy and $V_O^{\bullet\bullet}$ a doubly ionized anionic vacancy.

The release of free electrons into the conduction band of the solid accounts for the observed increase in electrical conductivity. The subsequent introduction of air over the samples restores the initial value of σ indicating the refilling of the previously created anionic vacancies by dissociation of oxygen and capture of free electrons according to the reactions:

$$1/2O_2 + V_O^{\bullet} + e' \leftrightarrows O_O^{\times} \quad (20)$$

$$1/2O_2 + V_O^{\bullet\bullet} + 2e' \leftrightarrows O_O^{\times} \quad (21)$$

This behavior is in agreement with a Mars – van Krevelen type mechanism [24]. Note that, in our case, the reactions (19) and (21) involving doubly ionized anionic vacancies are negligible as suggested by the variation of the electrical conductivity as a function of oxygen partial pressure.

The case of $2.2P/CeO_2$ sample is more complex. It seems to behave as a p-type semiconductor with positive holes, $h^{\bullet}$, as the main charge carriers under the reaction conditions. For confirming this behavior and for explaining the inverse order of activity observed at temperatures higher than 570 °C, that is $2.2P/CeO_2 > 1.1P/CeO_2 > CeO_2$, electrical conductivity measurements were performed with $2.2P/CeO_2$ at 610 °C during sequential periods under air,

under nitrogen, under isobutane-air mixture and under isobutane-nitrogen mixture, the results obtained being presented in Fig. III.4.

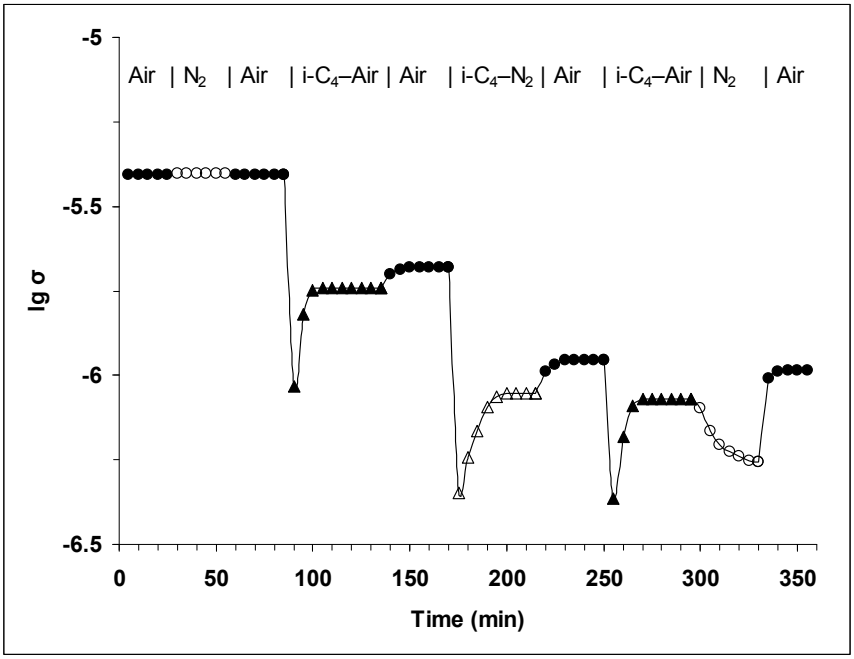

Figure III.4. Variation of the electrical conductivity under sequential exposures to air (●), nitrogen (○), isobutane – air mixture (reaction mixture) (▲) and isobutane – nitrogen mixture (△) for 2.2P/CeO_2 at 610 °C (σ in $ohm^{-1}.cm^{-1}$).

It can be observed that, as expected, the electrical conductivity of the solid remained almost constant during air-nitrogen-air sequential periods. When the air flow was replaced by the isobutane-air mixture (reaction mixture), the electrical conductivity firstly decreased abruptly and then increased to reach the plateau corresponding to the steady state. This corresponds to the combination of two opposite phenomena, an initial reduction by isobutane followed by a kind of reoxidation of the surface region as already observed for vanadium pyrophosphate under *n*-butane [4] and confirms the p-type behavior of the 2.2P/CeO_2 catalyst under the isobutane-air mixture. After reaching the steady state under the isobutane-air flow, a new sequence of air was introduced over the 2.2P/CeO_2 sample. The electrical conductivity slightly increased to reach a plateau which is different from that observed under air before the isobutane-air mixture sequence suggesting a new state of the solid that obviously corresponds to a reduced oxide. After reaching the new steady state under the air flow, a sequence of isobutane-nitrogen mixture was introduced

over the sample. The electrical conductivity firstly decreased abruptly and then increased slowly to reach the plateau corresponding to the steady state. This confirms the p-type character of the $2.2P/CeO_2$ catalyst in the presence of isobutane. When air was again introduced over the sample, the electrical conductivity increased immediately and reached a plateau corresponding to a new σ value different from the previous value under air suggesting that the solid was further and irreversibly reduced by the isobutane-nitrogen mixture. The air was replaced by a new isobutane-air flow when the solid was again reduced, then a sequence of nitrogen was admitted over the sample. One can observe that the electrical conductivity decreased to reach the plateau corresponding to the new steady state under nitrogen. When air was finally introduced over the sample, the electrical conductivity increased and reached a plateau that did not correspond to the fully oxidized initial solid but was similar to the value observed during the last sequence under air suggesting a redox behavior of the $2.2P/CeO_2$ catalyst. It is noteworthy that for the reduced solid, the electrical conductivity under nitrogen was lower than that under air. This confirms that, according to Heckelsberg criterion, it behaves as a p-type semiconductor.

The results obtained with $2.2P/CeO_2$ catalyst showed that it behaves as an extrinsic semiconductor with sources of electrical charge carriers independent of oxygen pressure under air but became a p-type semiconductor under the reaction mixture (isobutane-air). Such a phenomenon can only be explained by a change in the structure of the solid, at least in the surface region [11]. The existence of such an irreversible change was supported by the fact that after the first reduction, the solid underwent redox cycles that were not completely reversible and remained characteristic of a p-type semiconductor. For explaining this behavior we have to consider the $2.2P/CeO_2$ catalyst as a mixture of two conducting phases, CeO_2 and $CePO_4$, as evidenced by XRD [25]. It is well known that in a mixture of two conducting oxides, the overall conductivity of the sample becomes governed by the more conducting component above a certain percentage, called the percolation threshold [12]. In our case, the $CePO_4$ is rather a surface phase as expected taking into consideration the method of preparation used for the phosphated samples and as confirmed by the XPS analysis [25]. For confirming that the surface $CePO_4$ phase was responsible for the electrical conductivity behavior of the $2.2P/CeO_2$ sample under sequences of reactants, electrical conductivity measurements of $CePO_4$ (Alfa Aesar) were performed at 610 °C during sequential periods under air, isobutane-air mixture, nitrogen and isobutane-nitrogen mixture [17]. Its behavior was very similar to that of the $2.2P/CeO_2$ catalyst. This confirms that

the electrical conductivity behavior of the 2.2P/CeO_2 catalyst was mainly determined by the cerium (III) phosphate phase evidenced on its surface. Moreover, the activation energy of conduction E_c under air at atmospheric pressure, determined for $CePO_4$ sample from the semi-log plot [$\log\sigma = f(1/T)$] in the temperature range from 400 to 660°C, was equal to 0.65 eV. This value is strongly similar to that obtained for the 2.2P/CeO_2 sample, i.e. 0.62 eV, suggesting that the charge carrier formation needs similar energies in the two samples [26]. Consequently, the p-type conductivity observed for the 2.2P/CeO_2 catalyst after reduction during the sequence under isobutane-air mixture flow could be explained considering only the contribution of the surface cerium (III) phosphate phase to the overall electrical conductivity of the 2.2P/CeO_2 sample and regarding this phase as a Ce(IV)-doped $CePO_4$. Note that, it has already been shown that a ceria-doped $CePO_4$ catalyst was active and selective in isobutane oxydehydrogenation reaction [27]. In this case, the following electrochemical equilibrium can be assumed:

$$Ce^{4+} \leftrightarrows Ce^{3+} + h^{\bullet} \quad (22)$$

If one considers that from the chemical point of view, a positive hole corresponds to an electron vacancy in the valence band of lattice $O_O^{\times}$ anions, i. e. the "chemical site" of a positive hole corresponds in fact to a lattice $O_O^{\bullet}$ anion [4], according to the reaction:

$$O_O^{\times} + h^{\bullet} \leftrightarrows O_O^{\bullet} \quad (23)$$

the transformation of isobutane into isobutene over 2.2P/CeO_2 catalyst can be written:

$$i\text{-}C_4H_{10} + O_O^{\bullet} \rightarrow i\text{-}C_4H_9^{\bullet} + (HO^-)^{\bullet} \quad (24)$$

$$i\text{-}C_4H_9^{\bullet} + O_O^{\bullet} \rightarrow i\text{-}C_4H_8 + (HO^-)^{\bullet} \quad (25)$$

Water elimination generates oxygen vacancies, according to the reaction:

$$2\,(HO^-)^{\bullet} \leftrightarrows H_2O_{(g)} + O_O^{\times} + V_O^{\bullet\bullet} \quad (26)$$

These vacancies must be filled in by gaseous oxygen in order to reoxidize the solid:

$$1/2\,O_{2(g)} + V_O^{\bullet\bullet} \rightarrow O_O^{\times} + 2\,h^{\bullet} \quad (27)$$

This suggests that the overall reaction mechanism on 2.2P/CeO_2 catalyst can also be assimilated to a Mars – van Krevelen type mechanism [24], but in this case the oxydehydrogenation reaction involves surface lattice O^- species ($O_O^{\bullet}$), whereas for CeO_2 surface lattice O^{2-} anions ($O_O^{\times}$) are involved. The O^- species are known to be quite active species for alkanes' oxidation [4], explaining the highest activity observed for 2.2P/CeO_2 catalyst at 610 °C.

The weak variations of the electrical conductivity observed in that case suggest a low concentration of O^- species on the surface in line with the high isobutene selectivity measured during the catalytic process (see Table I.3). If the O^- species were too numerous on the surface, they might promote isobutane combustion rather than oxydehydrogenation.

The equilibrium (22) responsible for the generation of the positive holes obviously involves the low reducible Ce(IV) species interacting with the phosphate phase evidenced by H_2-TPR experiments [25]. Taking it into consideration, one could explain the lowest activity of the 2.2P/CeO_2 catalyst in the series studied at low temperature as well as its highest activity at high temperatures where the low reducible Ce(IV) species are more easily reduced.

1.1P/CeO_2 catalyst has an intermediate behavior between CeO_2 and 2.2P/CeO_2: it can also be considered as a mixture of two phases, CeO_2 and $CePO_4$, as evidenced by XRD, but the overall electrical conductivity is governed by the ceria phase. On the other hand, this solid contains a small, but nevertheless significant concentration of low reducible Ce(IV) species interacting with the phosphate phase as evidenced in H_2-TPR experiments [25]. Consequently, it is reasonable to consider that, in this case, the reaction mechanism involves mainly surface lattice O^{2-} anions but a mechanism involving surface lattice O^- species especially at high temperatures cannot be excluded.

In conclusion, it has been established that pure ceria as well as the two surface-phosphated ceria, 1.1P/CeO_2 and 2.2P/CeO_2, were n-type semiconductors under air. Their electrical conductivity increased while their activation energy of conduction decreased following the order CeO_2 < 1.1P/CeO_2 < 2.2P/CeO_2 suggesting the formation of substitution defects of Ce(IV) with P(V) in the phosphated ceria samples. Under isobutane – nitrogen mixture or under isobutane – air mixture, CeO_2 and 1.1P/CeO_2 remained n-type semiconductors whereas 2.2P/CeO_2 became p-type semiconductor, its electrical conductivity behavior being governed by the $CePO_4$ phase.

For the 2.2P/CeO_2 catalyst the oxydehydrogenation reaction involves surface lattice O^- species, whereas for CeO_2 surface lattice O^{2-} anions are involved. For the 1.1P/CeO_2 catalyst the reaction mechanism involves mainly surface lattice O^{2-} anions but a mechanism involving surface lattice O^- species, especially at high temperatures, must be considered. These results explained the difference in catalytic performances encountered on the three solids as well as the compensation effect in catalysis evidenced. In all cases the overall reaction mechanism can be assimilated to a Mars and van Krevelen mechanism.

III.2. Study of the catalytic activity – semiconductive properties relationship for $BaTiO_3$ and $PbTiO_3$ perovskites

For better understanding the catalytic behavior of $BaTiO_3$ and $PbTiO_3$ perovskites in the total oxidation of methane described in Chapter II, their DC-electrical conductivity was studied as a function of the temperature, the air pressure, the nature of different gaseous reactant atmospheres and the reaction mixture. A reaction mechanism for the transformation of methane over barium and lead perovskite catalysts has been proposed and a correlation between their semiconductive and catalytic properties has been established. The results obtained have been published in Ref. [28] and are presented below. Note that the common reference state for σ determination has been chosen under nitrogen or under air at atmospheric pressure and at 690 °C. At this temperature, which is in the catalytic reaction temperature range, the ionically adsorbed species such as H_3O^+, HO^- which would produce an additional surface conductivity are eliminated.

The electrical conductivities of the perovskites were first measured as a function of temperature to determine the activation energy of conduction E_c, under air at atmospheric pressure, in the temperature range from 500 to 700 °C. The slopes of the semi-log plots [$\log\sigma = f(1/T)$] enabled one to calculate the E_c values: 85.8 $kJ.mol^{-1}$ (0.89 eV) and 104.9 $kJ.mol^{-1}$ (1.09 eV) for $BaTiO_3$ and $PbTiO_3$, respectively. We have also shown that, according to the Heckelsberg criterion [18], both perovskites have a p-type semiconductor character [28].

It is noteworthy that the electric conductivity of $PbTiO_3$ was with *ca*. 3 orders of magnitude higher than that of $BaTiO_3$. This means, according to Eq. (2), that the concentration of charge carriers, i.e. positive holes, was 1000 times higher for $PbTiO_3$ than for $BaTiO_3$.

The electrical conductivity σ of $BaTiO_3$ and $PbTiO_3$ perovskites was measured under air at 690 °C as a function of oxygen pressure. In both cases it was observed that the conductivity varied linearly with the oxygen pressure (Fig. III.5). Moreover, it is confirmed that they are both of the p-type under air atmosphere since $\partial\sigma/\partial P_{O_2} > 0$. The slopes of the log–log plots of σ as a function of P_{O_2} in air for $BaTiO_3$ and $PbTiO_3$ were close to +1/6 and +1/4, respectively.

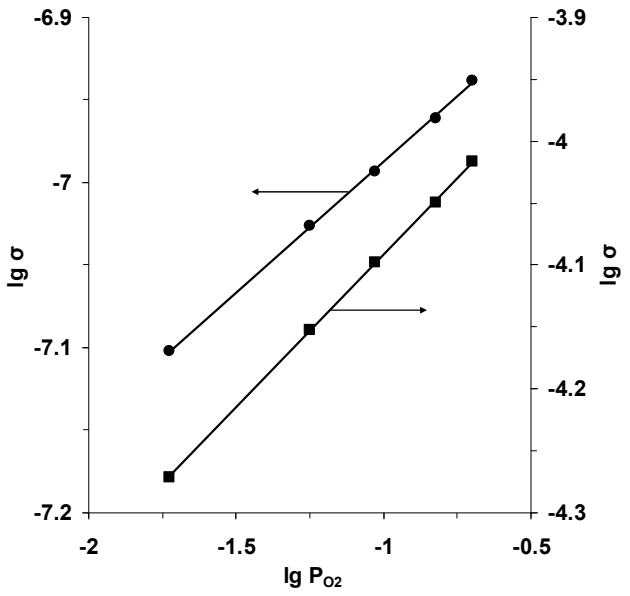

Figure III.5. Variation of σ as function of the oxygen pressure for $BaTiO_3$ (●) and $PbTiO_3$ (■) (P_{O_2} in atm; σ in $ohm^{-1}.cm^{-1}$).

It is well known [1] that, in the case of a p-type semiconductor σ varies with T and P_{O_2} according to the general equation

$$\sigma = \sigma_0 \exp(-E_c/RT)\ P_{O_2}^{+1/p} \qquad (28)$$

Depending upon the value of *p*, the mode of conduction can be related to a special type of structure defects acting as hole sources.

The model that could explain the p-type character of $MTiO_3$ perovskites, M = Ba and Pb, corresponds to the formation of cationic vacancies involving the following equilibrium:

$$1/2\ O_{2\ (g)} \leftrightarrows O_O^{\times} + V_M^{\times} \qquad (29)$$

where $O_O^{\times}$ denotes the neutral oxygen with respect to the lattice on the regular oxygen sites in the solid and $V_M^{\times}$ denotes the cationic vacancy, neutral acceptor level trapped by to positive holes. With increasing temperature, the acceptor levels can be successively ionized by receiving electrons from the valence band of the solid according to the following equations:

$$V_M^{\times} \leftrightarrows V_M^{'} + h^{\bullet} \qquad (30)$$

$$V_M^{'} \leftrightarrows V_M^{''} + h^{\bullet} \qquad (31)$$

where $V_M^{'}$ and $V_M^{''}$ represent singly and doubly ionized cationic vacancies, respectively, and $h^{\bullet}$

represents a positive hole.

When the equilibrium (30) is dominant, the following chemical total equation can be written:

$$1/2\ O_{2\ (g)} \leftrightarrows\ O_O^{\times} + V_M^{'} + h^{\bullet} \tag{32}$$

The mass action law applied to Eq. (32) gives:

$$K_7 = \frac{[V_M^{'}][h^{\bullet}]}{P_{O_2}^{1/2}} \tag{33}$$

and the electroneutrality condition implies:

$$[V_M^{'}] = [h^{\bullet}] \tag{34}$$

The combination of Eqs. (33) and (34) yields:

$$\sigma \propto [h^{\bullet}] = K_7^{1/2} P_{O_2}^{1/4} \tag{35}$$

In the case of $PbTiO_3$ the log–log plot of σ as a function of P_{O_2} in air gives an ascending straight line whose slope was indeed equal to +1/4 (Fig. III.5). In addition, the constant K_7 follows the van't Hoff's law as a function of temperature:

$$K_7 = (K_7)_0 \cdot \exp(-\Delta H_7/RT) \tag{36}$$

ΔH_7 being the enthalpy of the reaction (32).

Combining Eqs. (35) and (36), one gets:

$$\sigma \propto [h^{\bullet}] = [(K_7)_0]^{1/2} \cdot \exp(-\Delta H_7/2RT) \cdot P_{O_2}{}^{1/4} \tag{37}$$

Since the solid is a semiconductor, i.e. having a conductivity varying exponentially with temperature according to Eq. (28), there results from Eqs. (28) and (37), the identity:

$$\Delta H_7 = 2 \cdot E_c \tag{38}$$

Since E_c is 104.9 $kJ.mol^{-1}$ for $PbTiO_3$ perovskite, this means that the enthalpy of formation ΔH_7 of singly ionized cationic vacancies $V_{Pb}^{'}$ is equal to:

$$\Delta H_7 = 2 \cdot E_c = 209.8\ kJ.mol^{-1}.$$

When the equilibrium (31) is dominant, the following chemical total equation can be written:

$$1/2\ O_{2\ (g)} \leftrightarrows\ O_O^{\times} + V_M^{''} + 2h^{\bullet} \tag{39}$$

The mass action law applied to Eq. (39) gives:

$$K_{14} = \frac{[V_M^{''}][h^{\bullet}]^2}{P_{O_2}^{1/2}} \quad (40)$$

and the electroneutrality condition implies:

$$2[V_M^{''}] = [h^{\bullet}] \quad (41)$$

The combination of Eqs. (40) and (41) yields:

$$\sigma \propto [h^{\bullet}] = (2K_{14})^{1/3} P_{O_2}^{1/6} \quad (42)$$

Actually, for $BaTiO_3$ the log–log plot of σ as a function of P_{O_2} gives an ascending straight line whose slope was close to +1/6 (Fig. III.5). In addition, constant K_{14} follows the van't Hoff's law as a function of temperature:

$$K_{14} = (K_{14})_0 \cdot \exp(-\Delta H_{14}/RT) \quad (43)$$

ΔH_{14} being the enthalpy of the reaction (39).

Combining Eqs. (42) and (43), one gets:

$$\sigma \propto [h^{\bullet}] = [2(K_{14})_0]^{1/3} \cdot \exp(-\Delta H_{14}/3RT) \cdot P_{O_2}^{1/6} \quad (44)$$

Since the solid has a conductivity varying exponentially with temperature according to Eq. (28), there results from Eqs. (28) and (44), the identity:

$$\Delta H_{14} = 3 \cdot E_c \quad (45)$$

Since E_c is 85.8 kJ.mol^{-1} for $BaTiO_3$ perovskite, this means that the enthalpy of formation ΔH_{14} of doubly ionized cationic vacancies $V_{Ba}^{''}$ is equal to:

$$\Delta H_{14} = 3 \cdot E_c = 257.4 \text{ kJ.mol}^{-1}.$$

Note that, as expected, the enthalpy of formation ΔH_{14} of doubly ionized cationic vacancies in $BaTiO_3$ was higher than the enthalpy of formation ΔH_7 of singly ionized cationic vacancies in $PbTiO_3$.

To get information on the solids under conditions as close as possible to those of catalysis, the electrical conductivity measurements were performed at a temperature within the reaction temperature range during sequential periods under nitrogen, under 5 % methane in nitrogen, under air and under 5 % methane in air (reaction mixture) or 10 % methane in air.

The solids were heated from room temperature to 690 °C, at a heating rate of 5 °C/min in nitrogen flow at atmospheric pressure. After reaching the steady state under the nitrogen flow, a 5 % methane in nitrogen mixture was introduced over the samples (Fig. III.6). Surprisingly, an

important increase of the electric conductivity was observed for $BaTiO_3$ perovskite that corresponds to the n-type semiconductive character, since, for oxide semiconductors, the n-type criterion is $\partial\sigma/\partial P_{O_2} < 0$ or, considering methane as a reductant, $\partial\sigma/\partial P_{CH_4} > 0$. For $PbTiO_3$ perovskite, the electrical conductivity strongly decreases initially probably due to the rapid consumption of positive holes (whose concentration is 1000 times higher than for $BaTiO_3$) from the p-type solid, and then increases to reach the plateau corresponding to the steady state under the methane-nitrogen mixture, as in the case of $BaTiO_3$ sample. It is noteworthy that the n-type electrical conductivity of the $PbTiO_3$ sample was with *ca*. 1.5 orders of magnitude higher than that of the $BaTiO_3$ sample. This means, according to Eq. (2), that the concentration of charge carriers, i.e. quasi-free electrons, e', was 10 to 100 times higher for $PbTiO_3$ than for $BaTiO_3$.

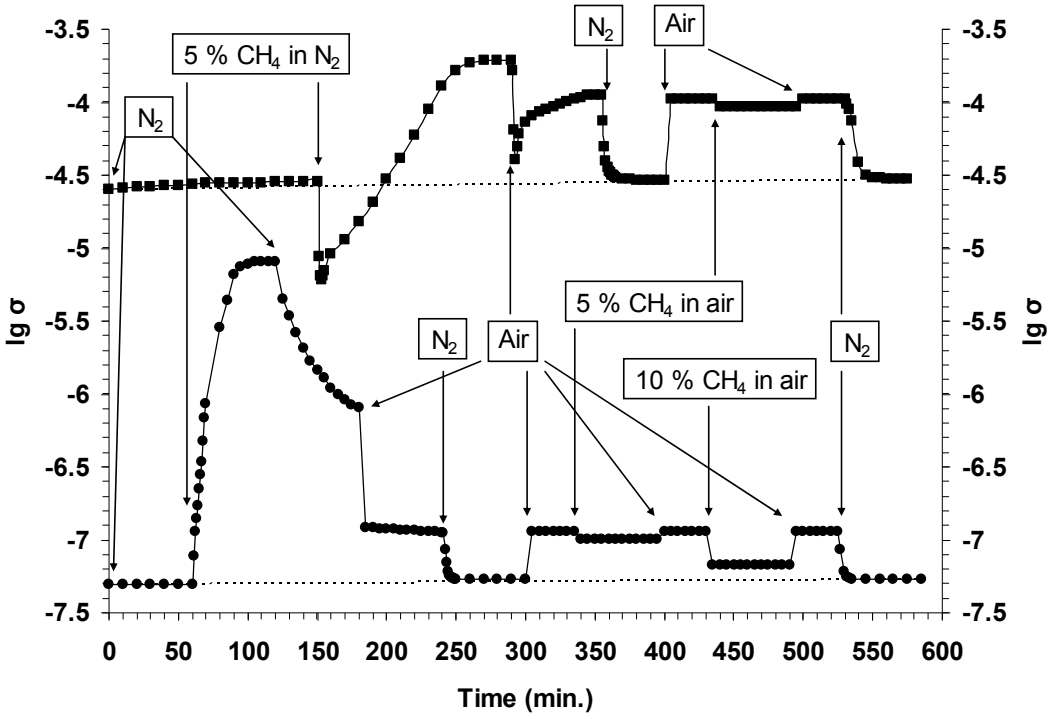

Figure III.6. Variations of the electrical conductivity under sequential exposures to nitrogen, methane – nitrogen mixture, air and methane – air mixture (reaction mixture) for $BaTiO_3$ (●) and $PbTiO_3$ (■) at 690 °C (σ in $ohm^{-1}.cm^{-1}$).

The introduction of methane-nitrogen mixture in contact with the solid changed the nature of the semiconductivity of both solids, passing from p-type to n-type conduction. Such a

phenomenon can be ascribed to the formation of free electrons. They can arise from the creation of anionic vacancies, $V_O^{\times}$, by reduction of the solid by methane:

$$2\,O_O^{\times} + CH_4 \rightarrow CO_2 + 2H_2O + 2\,V_O^{\times} \qquad (46)$$

followed by the ionization of the anionic vacancies according to the Eqs. (18) and (19).

After reaching the steady state under the methane-nitrogen flow, a sequence of nitrogen was introduced over $BaTiO_3$ perovskite. One can observe that the plateau corresponding to the new steady state under nitrogen is not the same as before the methane-nitrogen mixture sequence (Fig. III.6) suggesting a new state of the solid that obviously corresponds to a reduced oxide. When air was introduced over the sample, the electrical conductivity decreased immediately and reached a plateau. This behavior confirmed the n-type character of the solid when contacted with the methane-nitrogen mixture.

When air was introduced over the $PbTiO_3$ sample, the electrical conductivity first decreased immediately and then increased to reach the plateau corresponding to the steady state under air (Fig. III.6). The initial decrease corresponds to the re-oxidation of the solid. After that, the formation of positive holes takes place.

After reaching the steady state under the air flow, the nitrogen was again introduced in contact with the samples. In both cases the electrical conductivity regained the initial value under nitrogen, confirming the reversibility of the phenomena observed.

After the nitrogen sequence, the air flow was again introduced over the samples. As expected, the electrical conductivity increased in both cases to reach the plateau corresponding to steady state under air. This behavior confirms the p-type conductivity of both perovskites under air.

After reaching the steady state under the air flow, the reaction mixture (5 % methane in air) was introduced in contact with the samples and then, after reaching the steady state under the reaction mixture, the air sequence was repeated for observing the reversibility of the phenomena. When the nitrogen was finally introduced in contact with the samples, the electrical conductivity regained the initial value for both samples, confirming again the reversibility of the phenomena observed.

When the reaction mixture was introduced over the samples, the electric conductivity decreased slightly, for both samples. The same behavior, but more pronounced, was observed when 10 % of methane in air mixture was introduced over $BaTiO_3$ sample. These results suggest

that methane in the reaction mixture transforms by consuming the positive holes evidenced in the solids under air and it can be proposed that the initial activation step of the methane is a C-H bond cleavage via the attack by a positive hole:

$$CH_4 + h^{\bullet} \rightarrow CH_3^{\bullet} + H^{+} \quad (47)$$

If one considers that the "chemical site" of a positive hole corresponds in fact to a lattice $O_O^{\bullet}$ anion, according to the reaction (23), the initial activation step of the methane may be written:

$$CH_4 + O_O^{\bullet} \rightarrow CH_3^{\bullet} + (HO^{-})^{\bullet} \quad (48)$$

where $O_O^{\bullet}$ represents rather a superficial lattice than a bulk lattice species.

The methyl radical formed is trapped on the Ti^{4+} Lewis acid sites before being further transformed. Water elimination generates oxygen vacancies, according to the reaction (26).

Carbon dioxide formation also involves positive holes consumption and generates oxygen vacancies, according to the simplified reactions:

$$C + 2\ O_O^{\bullet} + 2\,h^{\bullet} \leftrightarrows CO_{2(g)} + 2\ V_O^{\bullet\bullet} \quad (49)$$

or

$$C + 2\ O_O^{\times} + 4\,h^{\bullet} \leftrightarrows CO_{2(g)} + 2\ V_O^{\bullet\bullet} \quad (50)$$

where, for simplicity, we considered a carbon atom, C, instead of CH_x species.

Because of the low concentration of methane in air, when the solids are under the reaction mixture, we did not observe an important reduction of the solid as under methane-nitrogen mixture flow. On the other hand, the formation of oxygen vacancies proposed is in line with the observed reduction of the solid under methane-nitrogen mixture flow. These vacancies must be filled in by gaseous oxygen in order to reoxidize the solid according to Eq. (27). This suggests that the overall reaction mechanism on Ba and Pb titanates can be assimilated to a Mars and van Krevelen mechanism [24].

The higher catalytic activity of $PbTiO_3$ catalyst compared to $BaTiO_3$ can be explained taking into consideration that the concentration of the positive holes $h^{\bullet}$, i. e. $O_O^{\bullet}$ species involved in the initial activation step of the methane, is 1000 times higher for the former.

In conclusion, both titanates were p-type semiconductors under air but became n-type semiconductors when contacted with methane. The comparison of $BaTiO_3$ and $PbTiO_3$ indicated

that in the case of $PbTiO_3$ the electrical conductivity σ was approximately 3 orders of magnitude higher as p-type semiconductors and approximately 1.5 orders of magnitude higher as n-type semiconductors.

Because under the catalytic reaction conditions they have a p-type character, the activation mechanism of methane on both perovskites could be based upon the formation of methyl radicals on lattice $O_O^{\bullet}$ species, which are oxidizing species strong enough to attack alkanes' C–H bonds. The concentration of the lattice $O_O^{\bullet}$ species, that are the chemical sites of the positive holes, was 1000 times higher for $PbTiO_3$ than for $BaTiO_3$, explaining why $PbTiO_3$ perovskite was more active than $BaTiO_3$ for methane total oxidation. The overall reaction mechanism on Ba and Pb titanates can be assimilated to a Mars and van Krevelen mechanism.

III.3. Study by electrical conductivity measurements of redox properties of vanadium antimonate and mixed vanadium and iron antimonate

Vanadium antimonates are known to be efficient catalysts for the ammoxidation of propane [29-32]. It is commonly admitted that the active phase of these catalysts is the $VSbO_4$ phase. Its structure is derived from TiO_2 rutile-type, with two Ti^{4+} cations formally substituted by one V and Sb cation with however a cation deficiency [33]. This cation deficiency has been shown to be related to the presence of V^{4+}, leading to the formula $V^{4+}_{0.64}V^{3+}_{0.28}Sb^{5+}_{0.92}[]_{0.16}O_4$ where [] stands for cationic vacancy [34].

It has been shown that iron could substitute to vanadium and that a continuous solid solution was formed in the $VSbO_4$–$FeSbO_4$ system [35]. At low loading, iron appeared to substitute V^{4+} with a resulting charge discrepancy balanced by oxygen vacancies. Simultaneously, cationic vacancies remained present in the solid with even a small increase of their content so that a maximum of both types of vacancies was observed between 10 and 20 % of iron substitution. Such modification generated very active sites for propane activation but more selective to form propene than acrylonitrile. Iron loading higher than 60 % induced the disappearance of V^{4+} and cationic vacancies, as well as the substitution of V^{3+} by Fe^{3+} in the lattice structure. It decreased the activity but increased the selectivity to acrylonitrile.

In order to understand the catalytic properties of the vanadium antimonate and to specify the reasons of the changes in the catalytic properties observed with the substitution of vanadium by iron, we have characterized by electrical conductivity measurements, the redox properties of pure vanadium and iron antimonates and of a mixed vanadium-iron antimonate. The vanadium-iron antimonate was chosen with a stoichiometry corresponding to 10 % of vanadium substitution, in the range that led to the highest increase in catalytic activity. This was my first work after the PhD thesis. It was published in Ref. [11] and resumed below.

The variations of log σ versus reciprocal temperature under oxygen at atmospheric pressure between 420 and 480 °C were linear suggesting that all the compounds behaved as semiconductors whose electrical conductivities varied exponentially with temperature according to the typical activation law expressed by the Eq. (3). The activation energies of conduction have been calculated for the different solids and found to be quite similar (Table III.2).

Table III.2. The activation energy of conduction (E_c) and *n* exponent of Eq. (4) for the different solids.

Catalyst	E_c (kJ.mol^{-1})	Exponent *n*
VSb	61.0	9.5
10FeVSb	65.1	8.0
FeSb	72.6	4.5

The isotherms of the electrical conductivity as a function of the oxygen partial pressure were studied at 480 °C. Fig. III.7 shows the variations of σ as a function of P_{O_2} in a log–log plot. It clearly appeared that all the solids were of the n-type under oxygen since $\partial\sigma/\partial P_{O_2} < 0$. For $FeSbO_4$ this result confirmed that previously obtained by Tianshu and Hing, who had already determined its semi-conduction type [36].

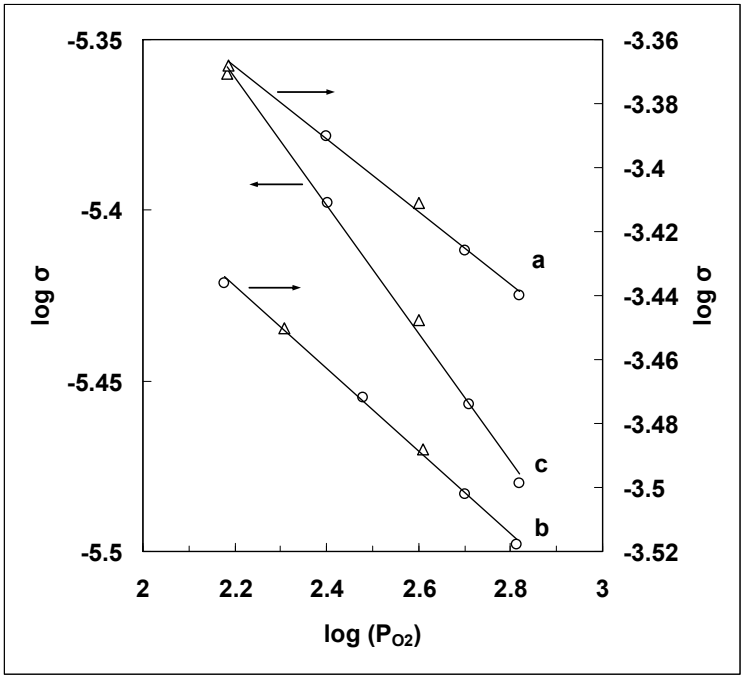

Figure III.7. Plots of log σ = f(logP_{O_2}) for VSb (a), 10FeVSb (b) and FeSb (c) at 480 °C (△ – under increasing oxygen pressure, ○ – under decreasing oxygen pressure).

It is generally assumed that the electrical conductivity σ of oxides varies as a function of the partial pressure P_{O_2} and temperature T, according to the Eq. (4). The values of exponent *n*,

indicative of the nature of the solid defects which generate charge carriers, calculated for the different solids are presented in Table III.2. From these values, only FeSb behaved according to a simple conduction model with *n* approximately equal to 4. Such a value corresponds to the formation of singly ionized anionic vacancies according to the equations (5) and (6). In this case Eq. (13) allowed us to calculate the enthalpy of formation of anionic vacancies for FeSb sample which was equal to 145.2 $kJ.mol^{-1}$ (per mole of vacancies). This enthalpy could appear substantially smaller than that observed for other n-type oxides [19, 20]. However, this low value could be responsible for a higher lability of surface lattice anions able to react with the mixture (propene + ammonia) in the ammoxidation of propene into acrylonitrile. Under our experimental conditions, $FeSbO_4$ was efficient, as an n-type semiconductor, for propene ammoxidation but not for that of propane [35].

The case study of the two vanadium containing antimonates was more complex. The *n* values calculated for these compounds were significantly higher than 4 or 6 that respectively correspond to the formation of singly or doubly ionized vacancies. Such a phenomenon could be explained by a more complex model involving two different sources of electrons, one being independent of the partial pressure of oxygen while the other one is related to the defects connected to it such as anionic vacancies according to Eq. (14). Indeed, a linear relationship was obtained when plotting σ as a function of $P_{O_2}^{-1/4}$ for VSb and FeVSb samples confirming the existence of a source of conduction electrons whose nature was independent of oxygen pressure.

The results of the *in situ* electrical conductivity measurements under subsequent gaseous atmospheres are presented in Fig. III.8. When propane was introduced into the cell, immediately the electrical conductivity of the three solids increased abruptly. Propane reduced the catalyst, which behaved as a typical n-type semiconductor. After reaching the steady state under propane, the cell was evacuated and replaced by pure oxygen. For 10FeVSb and FeSb compounds, the electrical conductivity decreased as anticipated for n-type semiconductors. By contrast, for VSb sample the electrical conductivity slightly increased. This appeared more clearly when σ was directly plotted as a function of the sequence duration [11]. Such phenomena were reproducible and appeared also under the propane-oxygen sequences. The results obtained on VSb showed that it was an n-type semiconductor but that after reduction it behaved as a p-type semiconductor. Such a phenomenon can only be explained by a change in the structure of the compound, at least in the surface region.

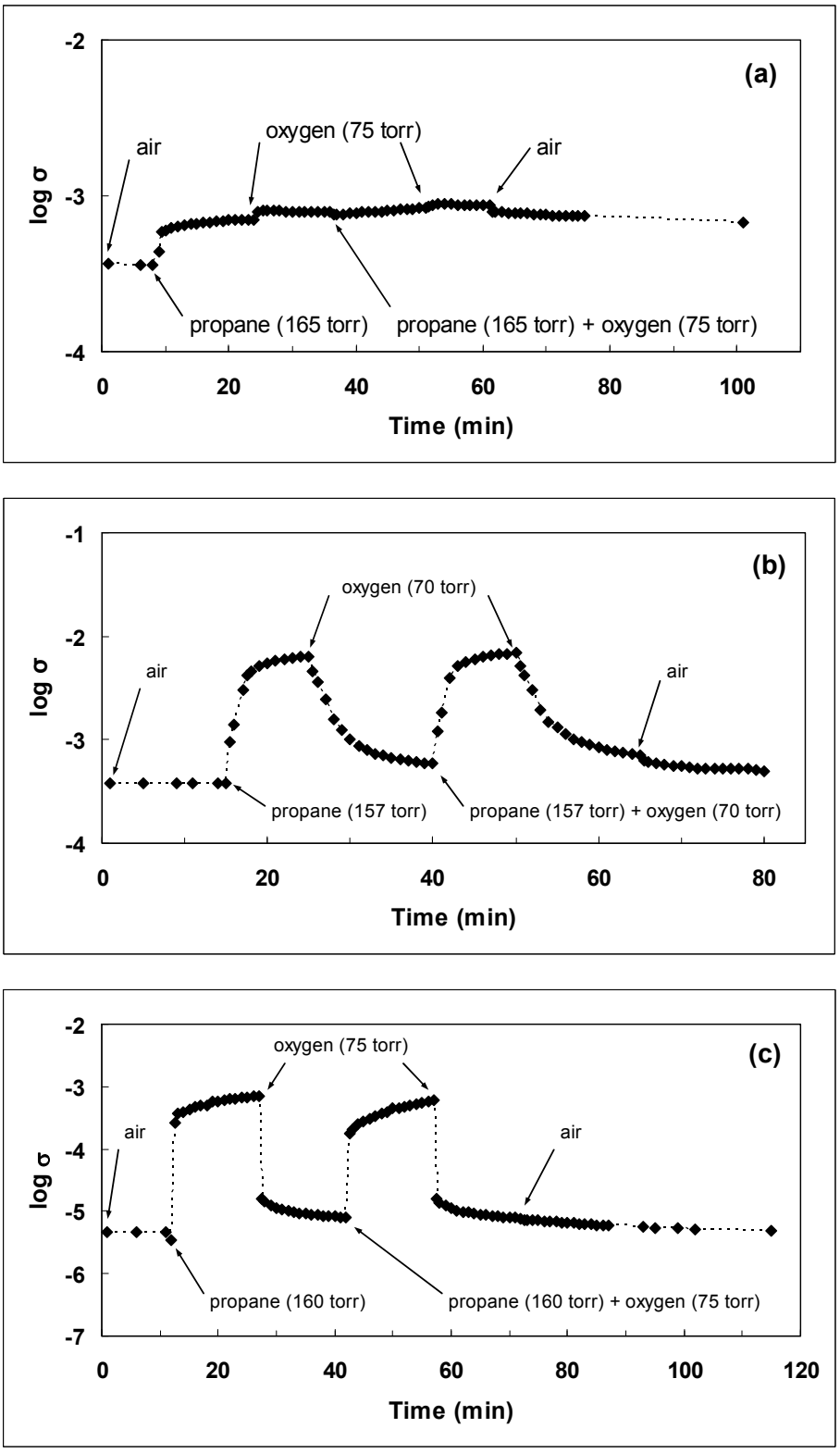

Figure III.8. Variations of the electrical conductivity at 480 °C under sequential exposures to air, propane, oxygen and propane-oxygen reaction mixture for VSb (a), 10FeVSb (b) and FeSb (c).

The existence of such irreversible change was supported by the fact that after the first reduction, the VSb sample underwent redox cycles that were not reversible and remained characteristic of a p-type semiconductor. Because this change should be limited to the surface of the solid, it was not observed by X-ray diffraction. However, XPS analyses indicated that the surface composition changed during the electrical conductivity measurement as well as during the catalytic test with an apparent surface enrichment in antimony oxide [11]. It can be assumed that the increase of electrical conductivity under propane was related to that of the free electrons concentration originating from the creation of ionized anionic vacancies. Propane removed the surface lattice oxygen of the oxide phase and created anionic vacancies according to the reaction:

$$x C_3H_8 + V^{4+}_{0.64} V^{3+}_{0.28} Sb^{5+}_{0.92} []_{0.16} O_4 \leftrightarrows V^{4+}_{0.64-2x} V^{3+}_{0.28+2x} Sb^{5+}_{0.92} []_{0.16} O_{4-x} + x C_3H_6 + x H_2O \qquad (51)$$

The solid formed containing both cationic and anionic vacancies should not be stable and a phase transformation should occur leading to a vanadium antimonate richer in vanadium and supporting an antimony oxide partially coating the surface. This interpretation can be supported by the fact that such a composition can be obtained when the vanadium antimonate was prepared with a heat treatment under nitrogen [37]. Such a behavior of vanadium antimonate means that it contained after reduction only cationic vacancies and mainly vanadium with its lower oxidation state (V^{3+}), typical of a p-type semiconductor such as NiO [38]. It could be noted that the same segregation was already observed in SnSbO system [39].

It was shown that at a low substitution level ($x < 0.4$ in $Fe_xV_{1-x}SbO_4$), Fe^{3+} substituted to V^{4+} in the cationic deficient structure of vanadium antimonate leading to a structure with both cationic and anionic vacancies [35]. For the 10FeVSb sample, the calculated stoichiometry corresponded to: $Fe^{3+}_{0.09} V^{3+}_{0.32} V^{4+}_{0.52} []_{0.18} Sb^{5+}_{0.94} O_{3.95}$. The substitution of vanadium by iron allowed the stabilization of the reduced compound with a structure presenting both cationic and anionic vacancies without phase transformation [35]. Such stabilization effect induced by iron had previously been observed in FeSnSbO system [40]. The solid then always behaved as an n-type semiconductor under oxygen and during the following redox cycle under catalytic propane–oxygen mixtures. The fact that the electrical conductivity cycles were not exactly reversible could account for a slight transformation of the surface as shown by XPS measurements [11]. Both types of semiconductivity may co-exist and account for the behavior of the 10FeVSb catalyst.

For FeSb sample the results obtained were typical of a pure n-type semiconductor behavior.

Because of the p-type character of the VSb catalyst, the same activation mechanism of propane as that already postulated by Aika and Lundsford [41] has been proposed. It is based upon the formation of hydrocarbon radicals initiated by positive holes, $h^{\bullet}$, related to the presence of cationic vacancies. These positive holes correspond to electron vacancies in the valence band of lattice $O_O^{\times}$ anions that can be filled by electrons hopping from neighboring anion leading to the equivalent equation (23). Propane activation could proceed with a C–H bond cleavage via the attack by a hole

$$C_3H_8 + h^{\bullet} \rightarrow C_3H_7^{\bullet} + H^{+} \quad (52)$$

The chemical support of a hole being an $O_O^{\bullet}$ species, Eq. (52) can also be written as

$$C_3H_8 + O_O^{\bullet} \rightarrow C_3H_7^{\bullet} + (HO^{-})^{\bullet} \quad (53)$$

The radical formed would undergo a second hydrogen abstraction according to a similar mechanism leading to propene. It could be outlined that such a process is similar to that encountered in the oxidation of *n*-butane on $(VO)_2P_2O_7$ [4] or on TiP_2O_7 [5] which are p-type semiconductors.

In 10FeVSb catalyst, the presence of Fe^{3+} allowed the stabilization of the compound with more anionic vacancies in reducing conditions and limits the formation of surface antimony oxide as shown from electrical conductivity measurements with mostly a n-type semiconductor behavior under propane. In this case the activation of propane would be related to the presence of isolated V species, which have been proposed to be the most active species [42] and that should correspond to the V^{4+}–O^{-} already suggested as activation site by Grasselli [43] and Andersson et al. [44]. It is difficult to know if the concomitant presence of anionic vacancies may play a role or not. The increase in selectivity to propene detrimental to that in acrylonitrile or CO_2 may be explained by the absence of antimony oxide at the surface of the active phase, which has been shown to be responsible for the selective synthesis of acrylonitrile from intermediate propene [45], or by the presence of the anionic vacancies that limits the number of active oxygen species available for the further transformation of the propene or intermediate formed. The presence of these anionic vacancies in catalytic conditions was clearly demonstrated by the electrical conductivity measurements data and the n-type semiconductivity observed.

In conclusion, it was established the n-type semiconductor character of $VSbO_4$ under air, which is considered as the active phase in the selective ammoxidation of propane. However, it

has been observed that $VSbO_4$ behaved as a p-type semiconductor under propane or under oxygen-propane mixture. This could be explained by a surface transformation with the formation of antimony oxide and a rutile phase richer in vanadium. Such transformation could account for the surface antimony enrichment observed by XPS.

$VSbO_4$ with vanadium partially substituted by iron as well as $FeSbO_4$, appeared also as n-type semiconductors under air. They kept the same type of conductivity under propane or propane-oxygen mixture. In the case of the mixed vanadium and iron antimonate, the absence of a total reversibility of the electrical conductivity supported a partial modification of the surface with a small increase in antimony surface content.

Because $VSbO_4$ transforms under catalytic reaction conditions with the appearance of a p-type character, the activation mechanism of propane on $VSbO_4$ could be based upon the formation of hydrocarbon radicals on $O_O^{\bullet}$, i.e. O^- species, which are oxidizing species strong enough to attack alkanes C–H bonds. Although that when Fe substituted partially V the n-type of semiconductivity was kept, the same type of activation could be carried but it would be related to the presence of isolated V species.

IV. CATALYTIC VALORIZATION OF LIGHT ALCOHOLS

IV.1. Ethanol conversion over MMgAlO (M = Pd, Ag, Mn, Fe, Cu, Sm, Yb) mixed oxide catalysts derived from LDH precursors

The catalytic transformation of ethanol into higher added value products has been investigated for more than 3 decades [1-5]. Mixed oxides catalysts have been widely used allowing either the dehydrogenation of ethanol into acetaldehyde followed by the condensation into acetals or higher alcohols, or its dehydration toward ethylene depending on the balance between acid and basic functions [6-9].

The synthesis of diethylacetal (1,1-diethoxyethane) from ethanol alone has been scarcely reported. It generally involves ethanol and acetaldehyde as starting materials [10, 11]. The diethylacetal is known to be a good additive to diesel fuel blends [12, 13], as well as an important starting chemical for the perfume industry and the synthesis of polyacetal resins [14, 15].

On the other hand, the conversion of ethanol into 1-butanol is of particular industrial interest. 1-butanol is indeed a crucial building block for acrylic acid and acrylic esters and is widely used as a solvent or as an additive to gasoline [7, 16-18]. The potential use of bioethanol as a raw material could also allow obtaining convenience products coming from renewable resources widely available throughout the world. Therefore, the Guerbet reaction, which corresponds to the catalytic transformation of alcohols into higher alcohols, attracts more and more interest. Several studies of this reaction in liquid phase have shown that a basic catalyst is needed along with hydrogenating functions [19-22]. Several homogeneous or heterogeneous catalytic systems have been tested and usually associate basic catalysts with transition metals such as Ni, Ru or Rh [5, 19-25]. However, the production of 1-butanol from ethanol over mixed oxides catalysts has seldom been investigated [4, 5].

Thus, we studied the conversion of ethanol over M-Mg-Al (with M= Pd, Ag, Mn, Fe, Cu, Sm, Yb) oxide based catalysts obtained from LDH precursors. We investigated particularly the nature of the added cation in order to modify the equilibrium between acid and basic function, thus modulating the catalytic performances. This work has been done during my post-doc stay in

the Laboratory of Advanced Materials for Catalysis and Health from the Institute Charles Gerhardt of Montpellier, France, and has been published in Ref. [26].

The physico-chemical characteristics of the mixed oxide catalysts calcined at 550 °C are resumed in Table IV.1.

Table IV.1. The physico-chemical characteristics of the catalysts.

Catalyst	Surface area (m^2g^{-1})	Pore volume (cm^3g^{-1})	Phases identified by XRD	Total basicity (mmol CO_2 g^{-1})	Total acidity (mmol NH_3 g^{-1})
Pd5MgAlO	187 (189)[a]	0.20	Mg(Al)O; PdO	1.94	1.74
Ag5MgAlO	166	0.23	Mg(Al)O; Ag_2O	1.62	2.34
Mn5MgAlO	167 (163)	0.22	Mg(Al)O	1.36	3.37
Fe5MgAlO	213	0.25	Mg(Al)O; $FeAl_2O_4$	1.60	3.51
Cu5MgAlO	180	0.23	Mg(Al)O	1.58	2.30
Sm5MgAlO	187 (187)	0.39	Mg(Al)O; Sm_2O_3	1.97	1.51
Yb5MgAlO	183	0.74	Mg(Al)O; Yb_2O_3	1.68	1.54

[a] After the catalytic test.

The seven M5MgAlO catalysts were evaluated in ethanol conversion performed in a steel autoclave under autogenic pressure and stirring, the obtained results being presented in Table IV.2. It can be observed that the ethanol conversion varied between 0.3 % for Fe based catalyst and 4.1 % for Cu based catalyst. Obviously, the catalytic activity depends on the acido-basic properties of the catalysts related to the nature of the metal M. In all cases butanol was the main reaction product. Cu and Pd-based catalysts were the most active, but the former gave both butanol and 1,1-diethoxyethane as main products, while the later was quite selective to butanol. Note that they have similar concentrations of strong basic sites, but Cu5MgAlO has a higher concentration of strong acid sites as well as a higher total acidity. Sm5MgAlO is also highly selective to butanol which is in agreement with its similar total concentration and distribution of basic sites of different strength than Pd5MgAlO. However, Sm5MgAlO is less active than Pd5MgAlO, suggesting that the equilibrium between basic and acid sites is better achieved in this later sample. The same conversion was reached with Yb5MgAlO and Sm5MgAlO but the former

was less selective to butanol according, as previously suggested for the other samples, to its lower basic character. Fe5MgAlO and Mn5MgAlO which were amongst the most acid catalysts, were poorly active and highly selective to 1,1-diethoxyethane and acetaldehyde. Ag5MgAlO which has the lowest concentration of strong basic sites gave the lowest selectivity to butanol and a high selectivity to ethyl acetate. These results confirmed that the equilibrium between the acid and basic functions of the mixed oxides determine the activity and the selectivity in the conversion reaction of ethanol. The selectivity for *n*-butanol increased when the number of strong basic sites increased. This suggests that acetaldehyde self-condensation, catalyzed by the basic sites, would be the rate determining step of the transformation of ethanol into butanol. The acid properties of the catalysts play an important role in the formation of the other products.

Table IV.2. Ethanol conversion and product selectivities over M5MgAlO catalytic systems. Reaction conditions: 200 °C, 5 h.

Catalyst	Conv (%)	Selectivities[a] (%)							
		Acetal C6	Acetal C8	Ethanal	Butanal	Crotonal	Butanol	EA	DET
Pd5MgAlO	3.8	2.5	1.0	12.3	7.0	-	72.7	4.0	0.6
Ag5MgAlO	1.6	7.5	1.3	17.5	5.6	3.3	38.8	25.9	-
Mn5MgAlO	0.7	6.9	5.0	21.0	4.1	6.8	53.3	2.9	-
Fe5MgAlO	0.3	26.7	2.4	21.7	-	7.1	39.2	2.7	-
Cu5MgAlO	4.1	35.9	5.1	9.9	1.7	0.2	40.3	6.9	-
Sm5MgAlO	1.3	6.6	1.2	15.1	4.0	3.6	66.3	3.1	-
Yb5MgAlO	1.2	15.1	3.7	19.1	2.7	2.3	53.0	4.1	-

[a] Acetal C6: 1,1-diethoxyethane; Acetal C8: 1,1-diethoxybutane; Ethanal: acetaldehyde; Butanal: butyraldehyde; Crotonal: crotonaldehyde; EA: ethyl acetate; DET: diethyl ether.

A reaction scheme can be proposed for the reaction of ethanol on MMgAlO (M = Pd, Ag, Mn, Fe, Cu, Sm, Yb) catalysts in agreement with the nature of sites involved and the nature of the products obtained (Fig. IV.1). After the first step of ethanol dehydrogenation into acetaldehyde, two main pathways lead to: (i) 1-butanol by hydrogenation of butyraldehyde formed by self-condensation of acetaldehyde and (ii) 1,1-diethoxyethane by cross-condensation of ethanol and acetaldehyde.

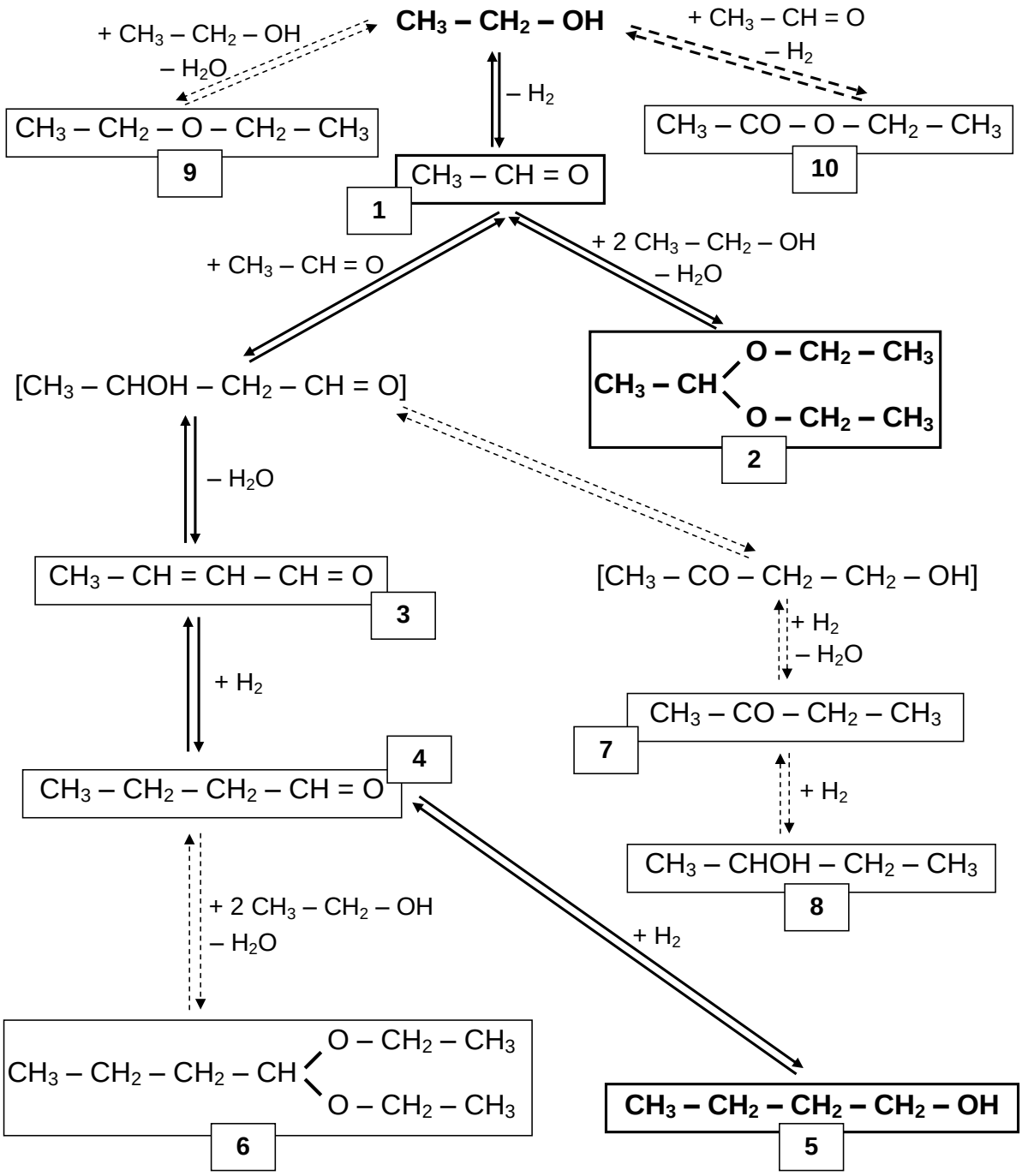

Figure IV.1. Reaction scheme for ethanol transformation on M-MgAlO catalysts. The observed products are presented in a frame. The continuous line arrows show the two main pathways leading to the two main products: 1-butanol and 1,1-diethoxyethane. The dotted line arrows show the secondary pathways of the ethanol reaction. 1 – acetaldehyde; 2 – 1,1-diethoxyethane; 3 – crotonaldehyde; 4 – butyraldehyde; 5 – 1-butanol; 6 – 1,1-diethoxybutane; 7 – methyl ethyl ketone; 8 – 2-butanol; 9 – diethyl ether; 10 – ethyl acetate.

The Pd based catalyst being the most selective for butanol, was more extensively studied. Firstly, we checked the stability of Pd5MgAlO catalyst and we have shown that the conversion and the product distribution remained strictly the same for three successive reactions, suggesting that the catalytic properties are stable at least during three successive reactions.

When the reaction temperature was increased in the range from 200 to 260 °C, the ethanol conversion increased from ~ 4 % to 17 %. At the same time, the selectivity for butanol increased up to 81 % at the expense of acetaldehyde and butyraldehyde.

When the reaction time was varied from 2 h to 100 h, the ethanol conversion increased from 2.1 % to 13.2 % and the selectivity for butanol increased from 65 % to 81.5 % still at the expense of acetaldehyde and butyraldehyde.

It is well-known that, in the case of mixed oxides obtained from LDH precursors, water can have a specific influence [27, 28]. Thus, it can influence the structure of the catalysts due to the well known memory effect of the Mg(Al)O mixed oxide obtained from LDH precursor. Presence of water is also able to modify the nature of the active sites from Lewis to Brønsted type. Therefore the influence of the addition of water to ethanol was investigated with the most active Pd5MgAlO catalyst. As reported in Table IV.3, only a slight decrease of conversion was observed whereas selectivities to acetals, acetaldehyde and butyraldehyde were increased at the expense of that to butanol.

Table IV.3. Effect of water addition to the reactant on the catalytic properties of the Pd-based catalyst. Reaction temperature: 200 °C. Reaction time: 5 h.

Reaction conditions	Conv	Selectivities[a] (%)						
	(%)	Acetal C6	Acetal C8	Ethanal	Butanal	Butanol	EA	DET
with pure ethanol	3.8	2.5	1.0	12.3	7.0	72.7	4.0	0.6
with ethanol 96 %	3.0	9.5	7.6	18.5	11.4	48.2	4.9	-

[a] Acetal C6: 1,1-diethoxyethane; Acetal C8: 1,1-diethoxybutane; Ethanal: acetaldehyde; Butanal: butyraldehyde; EA: ethyl acetate; DET: diethyl ether.

In conclusion, ethanol conversion into butanol was performed over MMgAlO mixed oxide catalysts (M = Pd, Ag, Mn, Fe, Cu Sm, Yb). The nature of the cation M modifies the

equilibrium between the acid and basic functions and thus determines the catalytic performances. The better equilibrium allowing reaching the highest butanol yield was obtained with the Pd-containing mixed oxide. A good correlation was found between the amount of basic sites of medium and high strength and the selectivity to butanol. On the other hand the presence of a large amount of acid sites increases the selectivity to 1,1-diethoxyethane and acetaldehyde. The addition of water to the reaction mixture has a detrimental influence on the selectivity to butanol. The Pd-containing catalyst exhibited a remarkable stability during the reaction.

IV.2. Catalytic conversion of ethanol over CuMgAlO mixed oxide catalysts obtained from LDH precursors

In the previous section we have shown that Cu and Pd-based catalysts obtained from LDH precursors were the most active in the series studied, but, while the later was quite selective to butanol, the former gave both butanol and 1,1-diethoxyethane as main products. Taking it into consideration and because the Cu-based catalyst is less expensive than the Pd-based one, it has been further studied. Thus, a series of CuMgAlO mixed oxides with different copper contents (1 – 20 at %) and Mg/Al ratios ($1 \leq Mg/Al \leq 5$) were prepared from LDH precursors, characterized and tested as catalysts in ethanol conversion, the results obtained being published in Ref. [29] and resumed below. The physico-chemical properties of the catalysts are reported in Table IV.4.

Table IV.4. Physico-chemical characteristics of the calcined catalysts.

Catalyst	Calcination temp. (°C)	Surface area ($m^2.g^{-1}$) [After catalytic test]	Pore volume (cm^3g^{-1})	Copper content[a] (at %)	Total basicity (mmol CO_2 g^{-1})
CuO	550	004	-	-	-
MgAl(3)O	550	224	0.35	-	-
Cu1MgAl(3)O	550	189	0.28	01.1	1.85
Cu3MgAl(3)O	550	174 [175]	0.32	-	-
Cu5MgAl(3)O	550	180	0.23	06.7	1.58
Cu10MgAl(3)O	550	200	0.31	12.3	1.20
Cu20MgAl(3)O	550	140	0.26	22.9	0.89
Cu5MgAl(5)O	550	150	0.49	-	-
Cu5MgAl(1)O	550	182 [146][b]	0.32	-	-
Cu7MgAl(3)O	250	013	0.02	-	-
Cu7MgAl(3)O	350	222	0.31	-	-
Cu7MgAl(3)O	450	187	0.31	-	-
Cu7MgAl(3)O	550	176 [180]	0.32	-	-
Cu7MgAl(3)O	650	170	0.21	-	-

[a] Determined by EDX.

[b] After 100 h reaction run.

Fig. IV.2 shows the effect of the Cu content in the CuxMgAl(3)O samples on their catalytic performances. Note that with MgAl(3)O (Cu-free) catalyst, the conversion was ~ 0.3 %, the major product being 1,1-diethoxyethane. For the sake of comparison, the catalytic properties of CuO are also reported on Fig. IV.2. An optimum of conversion of 4.5 % was observed for the catalyst with 7 % Cu content. This volcano shape can account for a decrease of the conversion due to a too low number of active sites below 7 % of copper, and to the increase of the CuO average crystallite sizes above [29].

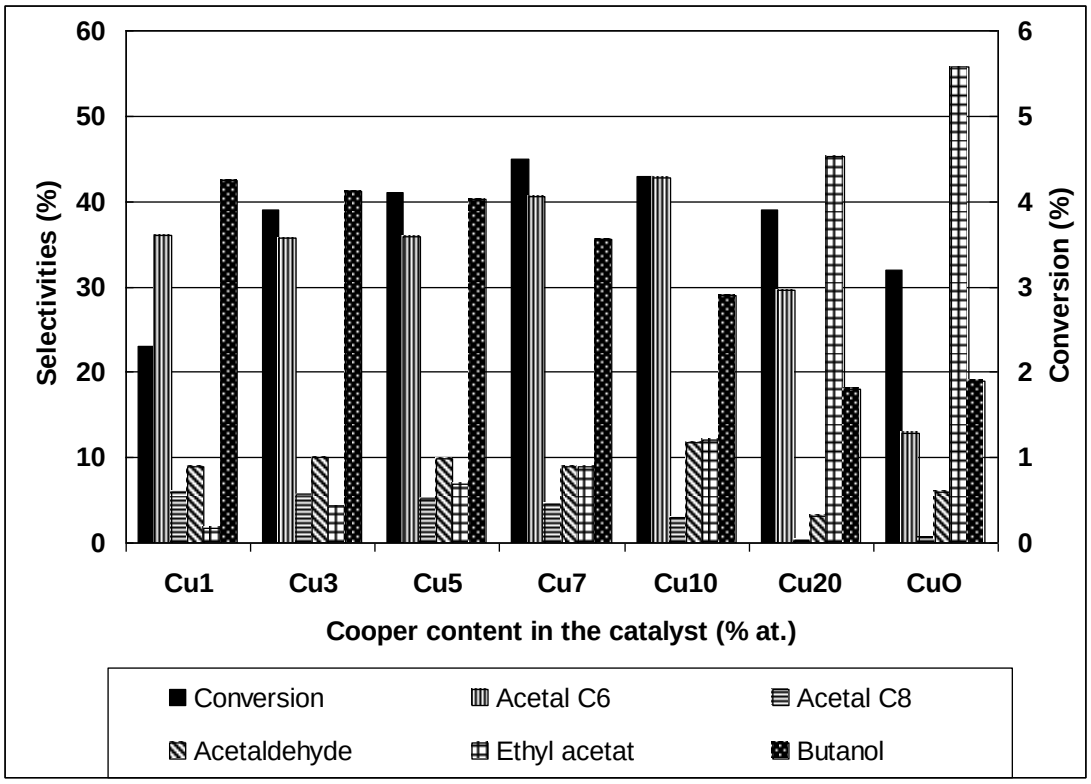

Figure IV.2. Influence of the Cu content on the performances of the CuxMgAl(3)O catalysts. Reaction conditions: 200 °C, 5 h.

Regarding the selectivities for the two main products of reaction, butanol and 1,1-diethoxyethane, they behave differently with increasing copper loading and the CuO crystal size. The selectivity for butanol indeed decreases regularly from ~ 42 % to ~ 18 %, while that of 1,1-diethoxyethane goes through a maximum value at 10 % Cu. At high Cu content (Cu20MgAl(3)O) and for CuO, a marked decrease for both butanol and 1,1-diethoxyethane selectivities to the

benefit of ethyl acetate was observed. Moreover, in these cases, 2-butanol was also observed among the reaction products, the 1-butanol/2-butanol molar ratio being equal to 3.9 and 3.5 for Cu20MgAl(3)O and CuO, respectively. We also note that the selectivity into ethyl acetate increased continuously with the copper content in the catalysts, becoming the main reaction product for Cu20MgAl(3)O and CuO. The 1,1-diethoxybutane selectivity, always lower than 7 %, decreased when the Cu content in the catalyst was increased, becoming almost zero for the CuO catalyst. The acetaldehyde and butyraldehyde selectivities varied irregularly as a function of the Cu content in the catalyst, between 3.2 and 11.7 % and between 1.4 and 3.5 %, respectively. We note that butyraldehyde was not observed on CuO. Traces of crotonaldehyde were observed only for the systems with Cu contents lower than 5 %. Note that XRD patterns of the catalysts after 5 h of reaction were similar to those before reaction, therefore showing no structural evolution [29].

As underlined above the acidity of the catalysts is not correlated to the copper content. Moreover, the catalytic properties were not correlated to their acidity. By contrast, a direct relationship was evidenced between the basicity of these catalysts and the selectivity for *n*-butanol: the selectivity for *n*-butanol increased when the number of strong basic sites increased, as shown in Fig. IV.3. No relationship was found between basicity and 1,1-diethoxyethane selectivity. This suggests that acetaldehyde self-condensation would be the rate determining step of the reaction leading to *n*-butanol. Moreover, this reaction probably involves stronger basic sites than those required for the condensation between acetaldehyde and ethanol leading to 1,1-diethoxyethane.

The effect of the Mg/Al ratio in the Cu5MgAl(y)O samples on the catalytic performances has also been studied. The ethanol conversion remained practically unchanged at ~ 4 % when the Mg/Al ratio was increased from 1 to 5. At the same time, the selectivity in butanol slightly decreased from 42 to 39.5 %, while the selectivity in 1,1-diethoxyethane increased from 32 to 39 %. The selectivities in minor products varied erratically but within a narrow range. These results show that the Mg/Al ratio does not influence the catalytic activity, and only slightly the selectivity. However, the different structural properties previously reported for this series of samples can hinder the influence of the Mg/Al ratio [29].

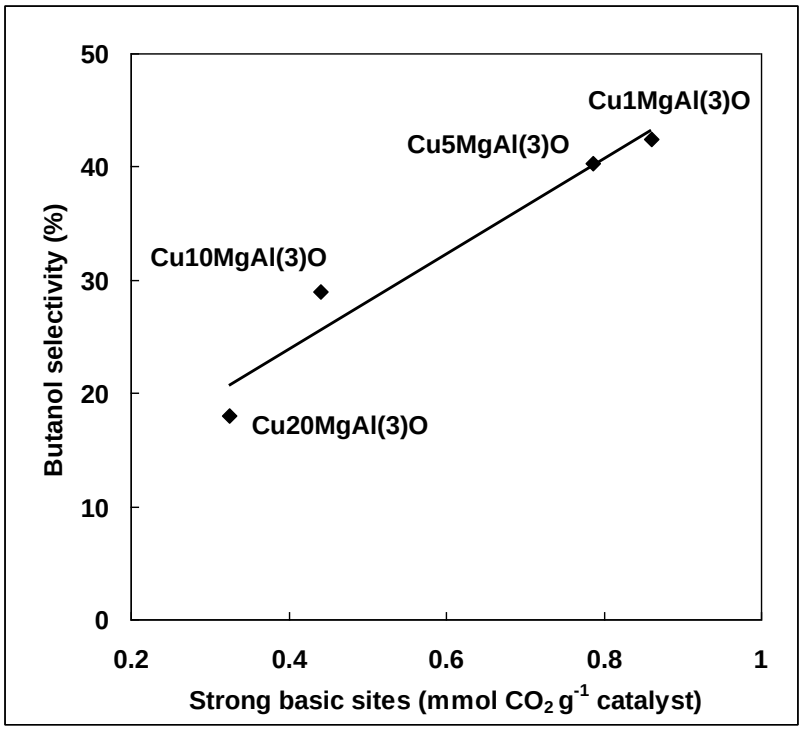

Figure IV.3. Selectivity for *n*-butanol versus the number of strong basic sites in CuxMgAl(3)O catalysts.

The effect of the calcination temperature of the LDH precursors on the catalytic properties was studied using Cu7MgAl(3)O. The results are presented in Fig. IV.4. Up to 350 °C the conversion remained lower than 1 %. It must be noted that, as already shown, the catalyst is in the lamellar form in this case. The conversion then increased with the calcination temperature. The maximum was reached at 550 °C, the catalyst being in the mixed oxide form. The selectivities for butanol and 1,1-diethoxyethane showed opposite behaviors, the former increasing regularly with the calcination temperature. The highest butanol yields were obtained for calcination temperatures above 450 °C. We note that with the catalyst calcined at 650 °C, methyl ethyl ketone was observed among the reaction products.

The stability of the catalyst was checked by carrying out the reaction with Cu7MgAl(3)O calcined at 550 °C, three times successively. The conversion remained almost similar in each run and only minor changes of selectivities were observed. It can be considered that the catalytic properties are maintained after three successive reactions.

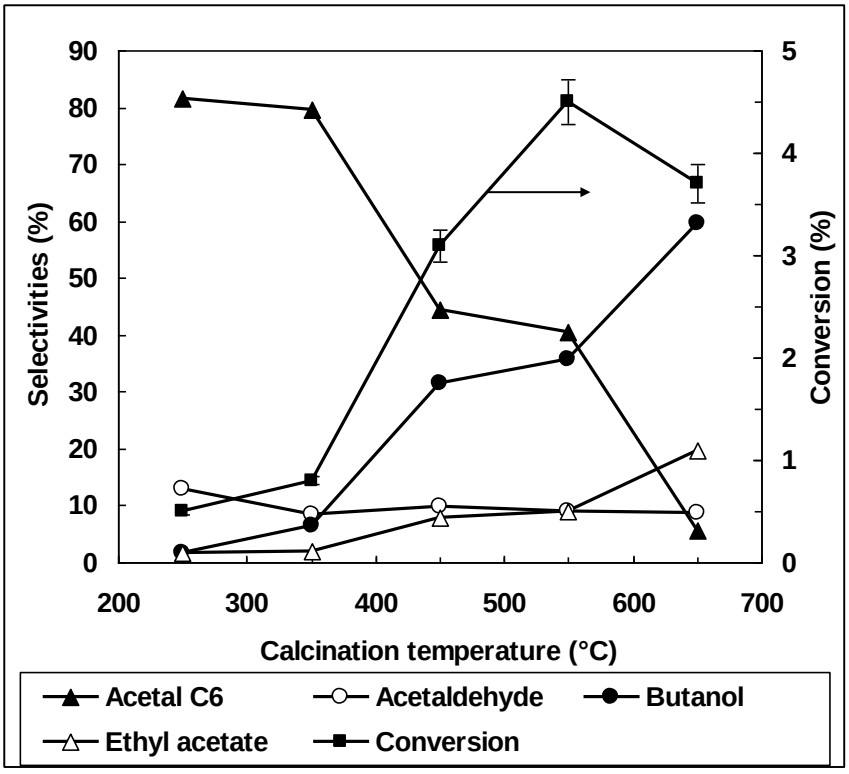

Figure IV.4. Influence of the calcination temperature of the LDH precursor on the catalytic properties of Cu7MgAl(3)O. Reaction conditions: 200 °C, 5 h.

It is worth noting that when the reaction temperature was increased in the range from 200 to 260 °C for the Cu5MgAl(5)O catalyst, the ethanol conversion increased from ~ 4 % to 9 %. At the same time, the selectivity for butanol increased up to 80 % at the expense of acetals. These results may be compared with those reported by Ndou et al. [5] where the best selectivity for butanol was ~ 18 % for an ethanol conversion of ~ 56 % at 450 °C.

When the reaction time increased from 2 h to 100 h for the reaction performed at 200 °C, the conversion increased from 2.6 to 11.1 % and the selectivity for butanol reached 67.6 % while that for 1,1-diethoxyethane decreased.

The influence of the addition of water, as well as its removal from the reaction medium, was also studied (Table IV.5). The addition of water to the reaction mixture, which is also a by-product of the reaction, has a negative effect on the catalytic activity, as expected from the reversibility of all the processes involved. The selectivity into acetaldehyde, a primary dehydrogenation product, and 1,1-diethoxyethane increased in the presence of water, while that into butanol dramatically decreased in all cases studied. This is in agreement with the

transformation of the Lewis strong basic sites O^{2-} into weaker Brønsted OH^- sites due to the presence of water.

Table IV.5. Influence of water on the catalytic properties of different CuMgAlO mixed oxides. Reaction temperature: 200 °C.

Catalyst	Solvent	t (h)	Conv (%)	Selectivities (%) [a]						
				C6	C8	Et-al	Bu-al	Cr-al	Bu-ol	EA
Cu1MgAl(3)O	Ethanol	5	2.3	36.0	6.0	9.0	3.0	1.7	42.4	1.8
Cu1MgAl(3)O	Ethanol 96%	5	0.5	53.5	-	46.5	-	-	-	-
Cu5MgAl(1)O	Ethanol	25	7.3	28.4	4.6	4.6	0.8	-	50.5	10.9
Cu5MgAl(1)O	Ethanol 96%	25	1.5	36.8	2.7	36.8	4.1	5.2	3.8	10.8
Cu7MgAl(3)O	Ethanol	5	4.5	40.5	4.6	9.0	1.4	-	35.6	8.9
Cu7MgAl(3)O	Ethanol [b]	5	7.2	24.9	3.5	15.3	3.7	0.5	47.4	8.7

[a] C6: 1,1-diethoxyethane; C8: 1,1-diethoxybutane; Et-al: acetaldehyde; Bu-al: butyraldehyde; Cr-al: crotonaldehyde; EA: ethyl acetate; DET: diethyl ether.

[b] New run with a fresh catalyst after drying on $MgSO_4$.

An attempt was also made to remove water from the reaction medium to try to displace the equilibrium and push the conversion further. After a typical test, the reaction mixture, separated by filtration, was dried using $MgSO_4$ treated at 250 °C overnight under nitrogen, and after a new separation by filtration, re-engaged in the autoclave in the presence of a fresh catalyst loaded for a new run. A significant increase of the conversion accompanied by an increase of the selectivity for butanol and a decrease of the selectivity for 1,1-diethoxyethane was observed (Table IV.5). These results are in accordance with the preservation of Lewis stronger basic sites O^{2-} due to the removal of water.

In conclusion, the orientation of the transformation towards butanol or acetal depends on the reaction conditions and of the composition of mixed oxides, mainly the copper content. The reaction is oriented towards butanol at higher reaction temperatures or at longer reaction times. At 200 °C the ethanol conversion amounted to ~ 11 % when the reaction time was set at 100 h. At the same time the selectivity for butanol was increased to ~ 70 %. The ethanol conversion and the

selectivity for butanol reached ~ 9 % and ~ 80 %, respectively, when the reaction temperature was set at 260 °C. Calcination of the precursor at 550 °C gives a material characterized by an optimum of catalytic activity. Contrarily to the Mg/Al ratio, which does not play a very important role on the catalytic properties of the studied catalysts, the copper content proves very important. An optimum for the Cu contents in the CuMgAlO mixed oxides between 5 and 10 atomic percent with respect to the cationic species was observed. Over catalysts with high loadings in copper or pure copper oxide, the main pathway is the condensation of ethanol with acetaldehyde resulting in ethyl acetate formation. The strong and the total basicity of the catalysts decreased with increasing the copper content and the selectivity for *n*-butanol increased when the number of strong basic sites increased. The structural and textural features of the catalysts used in 5 h catalytic runs remained unchanged. When the reaction time was increased to 100 h, a supplementary crystallization accompanied by a decrease of the specific surface area of the solid was observed. The presence of water in the reaction mixture (either produced by the reaction or added with the feed) has a negative effect on the catalytic activity of the catalysts suggesting the need of continuously removing water from the reaction medium.

IV.3. Cyanoethylation of methanol over transition-metal containing Mg-Al hydrotalcites and their corresponding mixed oxides

At present, much attention is paid to the development of benign catalytic processes in chemical synthesis, leading to high yields and selectivities of products with easy separation and recovery of the catalysts. Regarding base catalyzed reactions, the solids obtained from hydrotalcite-like precursors, particularly the mixed oxides derived from their thermal decomposition, give rise to a growing interest. This is due to their tunable acid-base properties mainly depending on the composition, the activation temperature and, for some of them, their rehydration ability [30-32].

Layered double hydroxides (LDHs) belong to the anionic clays family [33] and have the general formula $M^{2+}_{1-x}M^{3+}_{x}(OH)_2(A^{n-})_{x/n} \cdot mH_2O$, where M^{2+} and M^{3+} cations are six-coordinated to hydroxyl groups forming brucite-like sheets which stack to create a layered structure. Counter-anions A^{n-} are intercalated in the inter-layer space to compensate the charge introduced by the M^{3+} cations replacing some M^{2+} cations in the layers [30, 33-35]. The LDHs and their derived mixed oxides are increasingly used as catalysts in different base catalyzed and redox reactions [36-39]. Recently, much attention has been indeed paid on redox catalysts obtained from transition metal-containing LDHs [40-44]. In contrast, the acid-base properties of this type of LDHs and of their derived mixed oxides have been scarcely investigated. This is why we decided to investigate the acido-basic properties of a series of multicationic M/Mg/Al LDHs with M = Mn, Fe, Co, Ni, Cu, Zn prepared by the classical coprecipitation method in alkaline media and of their corresponding mixed oxides obtained by calcination at 550 °C and to study their catalytic properties in the cyanoethylation of methanol as model of base catalyzed reaction. The results obtained have been published in Ref. [45].

The cyanoethylation reaction, generally performed in the presence of a base compound [46, 47], has been catalyzed in homogeneous phase by alkali hydroxides [47] and alkoxides [48] and, more interesting for clean processes, with heterogeneous catalysts such as anion exchange resins, alkaline earth oxides, KF or KOH supported on alumina [49], Mg-Al LDH and MgAlO mixed oxides obtained by thermal decomposition of this latter [50, 51]. The cyanoethylation of monohydric alcohols with acrylonitrile is a conjugated addition giving β-alkoxypropionitrile according to the equation:

$$CH_3OH \quad + \quad CH_2 = CH - CN \quad \xrightarrow{base} \quad CH_3 - O - CH_2 - CH_2 - CN$$

The reaction product is an important intermediate in the synthesis of drugs and organic compounds of industrial interest [49, 50, 52-54]. Hydrogenation of β-alkoxypropionitrile indeed leads to amines, and hydrolysis, to different types of carboxylic acids. Cyanoethylation with different alcohols is not inhibited by adsorption of carbon dioxide at room temperature on the surface of the solids because the alcohols are more strongly adsorbed [55].

A mechanism in 3 steps has been previously proposed for the heterogeneous cyanoethylation reaction of alcohols [49, 56]. It can be briefly described as follows:

(1) $B^- : \quad + \quad CH_3OH \quad \rightarrow \quad B^- : H^+ \quad + \quad CH_3O^-$

(2) $CH_3O^- \quad + \quad CH_2 = CH - CN \quad \rightarrow \quad CH_3 - O - CH_2 - \ddot{C}^- H - CN$

(3) $CH_3 - O - CH_2 - \ddot{C}^- H - CN \quad + \quad B^- : H^+ \quad \rightarrow \quad CH_3 - O - CH_2 - CH_2 - CN \quad + \quad B^- :$

In the first step, abstraction of a proton from the hydroxyl group of the alcohol by the basic sites of the catalyst produced an alkoxide anion which is stabilized on a conjugated acid site. The adsorbed alkoxide then reacts in a second step with the acrylonitrile to give an adsorbed 3-alkoxypropanenitrile anion. This latter is finally protonated in a third step to yield 3-alkoxypropanenitrile with regeneration of the basic site. This mechanism obviously point out the main role played by the acid-base pairs on the reactivity.

It is worth noting that high activities and selectivities have been recently reported in the cyanoethylation reaction of ethanol with acrylonitrile using mixed oxides derived from LDHs modified with rare earth cations [52, 53]. However, only few studies concerning cyanoethylation of methanol were already published in the open literature and, to the best of our knowledge, anyone with LDH containing transition metal cations as catalysts [49, 50, 56].

Pure, more or less crystallized LDH phase was identified in the LDH precursors with cell parameters c = 24.94 Å and a = 3.05 Å. Except for Fe-containing mixed oxide, only pure Mg(Al)O phase with the periclase-like structure was detected in the MMgAlO mixed oxides. Weak reflections that can correspond to both Fe_2O_3 and $FeAl_2O_4$ phases, whose peaks are superimposed, were observed for FeMgAlO catalyst [45]. The physico-chemical characteristics of the mixed oxides are resumed in Table IV.6.

Table IV.6. Chemical composition, textural and structural characteristics of the mixed oxides.

Catalyst	M/(M+Mg+Al) atomic ratio		Mg/Al atomic ratio		Specific surface area (m^2/g)	Pore volume (cm^3/g)	Cell parameter *a* (Å)
	theor.	exp.	theor.	exp.			
MgAlO	-	-	3.0	3.3	224	0.35	4.19
MnMgAlO	0.05	0.06	3.0	2.8	167	0.22	4.19
FeMgAlO	0.05	0.07	3.0	2.5	213	0.25	4.19
CoMgAlO	0.05	0.07	3.0	2.5	205	0.37	4.18
NiMgAlO	0.05	0.06	3.0	2.4	194	0.31	4.20
CuMgAlO	0.05	0.07	3.0	3.1	180	0.23	4.19
ZnMgAlO	0.05	0.06	3.0	2.8	179	0.33	4.20

The TG-DTG analysis suggested that, for using a mixed oxide catalyst having a clean surface, the LDH precursor must be calcined just before the catalytic run at a temperature higher than 500 °C [45].

It is well known that the mixed oxides obtained via thermal decomposition of LDH precursors posses several sorts of active sites [8, 57-59]. Weak Brønsted basic sites are associated with surface OH^- groups; medium-strength Lewis sites are related to Mg^{2+}–O^{2-} and Al^{3+}–O^{2-} acid-base pairs; while strong Lewis basic sites are due to the presence of low coordinated O^{2-}. Medium strength acid-base Lewis pairs are the major species in these materials. The relative equilibrium between Lewis acid and base sites was expected to vary upon introduction of M^{2+} transition metal cations in the structure. These variations are a key point to understand the catalytic behavior in general and in the cyanoethylation reaction in particular. Therefore, the number and strength of sites of the materials were investigated by CO_2 and NH_3-TPD for probing the basic and acid sites, respectively. The results obtained are resumed in Tables IV.7 and IV.8. They confirmed that introduction of transition metal cations in MgAlO was able to modify the acid-base properties of the mixed oxides, particularly the equilibrium between the medium-strength sites. These latter corresponded to the acid-base pairs whose number was indeed increased when M^{2+}–O^{2-} pairs with M^{2+} = Mn^{2+}; Fe^{2+}; Co^{2+}; Ni^{2+}; Cu^{2+}; Zn^{2+} were introduced due to the higher electronegativity of M^{2+} cations as compared to Mg^{2+}.

Table IV.7. Number of basic sites of different strength for MMgAlO mixed oxides, derived from TPD of CO_2.

Catalyst	Number of basic sites (mmol/g)			Total number	
	Weak (%)	Medium (%)	Strong (%)	(mmol/g)	(mmol/m^2)
MgAlO	0.4 (21.0)	0.9 (47.4)	0.6 (31.6)	1.9	0.0085
MnMgAlO	0.4 (28.6)	0.5 (35.7)	0.5 (35.7)	1.4	0.0084
FeMgAlO	0.5 (31.2)	0.6 (37.6)	0.5 (31.2)	1.6	0.0075
CoMgAlO	0.5 (29.4)	0.6 (35.3)	0.6 (35.3)	1.7	0.0083
NiMgAlO	0.3 (21.4)	0.5 (35.7)	0.6 (42.8)	1.4	0.0072
CuMgAlO	0.4 (25.0)	0.4 (25.0)	0.8 (50.0)	1.6	0.0089
ZnMgAlO	0.3 (23.0)	0.5 (38.5)	0.5 (38.5)	1.3	0.0072

Table IV.8. Number of acid sites of different strength for MMgAlO mixed oxides, derived from TPD of NH_3.

Catalyst	Number of acid sites (mmol/g)			Total number	
	Weak (%)	Medium (%)	Strong (%)	(mmol/g)	(mmol/m^2)
MgAlO	0.6 (46.1)	0.2 (15.4)	0.5 (38.5)	1.3	0.0058
MnMgAlO	0.7 (20.6)	1.5 (44.1)	1.2 (35.3)	3.4	0.0204
FeMgAlO	1.1 (30.6)	1.7 (47.2)	0.8 (22.2)	3.6	0.0169
CoMgAlO	0.9 (29.0)	1.7 (54.9)	0.5 (16.1)	3.1	0.0151
NiMgAlO	0.9 (45.0)	0.8 (40.0)	0.3 (15.0)	2.0	0.0103
CuMgAlO	0.6 (26.1)	1.0 (43.5)	0.7 (30.4)	2.3	0.0127
ZnMgAlO	0.4 (33.3)	0.3 (25.0)	0.5 (41.7)	1.2	0.0067

The results of the catalytic cyanoethylation reaction of methanol on the dried LDH samples showed high selectivities of 99-100 % in β-metoxypropionitrile (CH_3-O-CH_2-CH_2-CN), while the conversions were quite low. These latter remained in all cases lower than 5 % after 5 h of reaction and ranked as follows: MgAl-LDH > CoMgAl-LDH ≈ CuMgAl-LDH ≈ MnMgAl-LDH > FeMgAl-LDH ≈ ZnMgAl-LDH > NiMgAl-LDH (Fig. IV.5). It should be noted that with MgAl-LDH the conversion was lower than in the cyanoethylation reaction with ethanol (~ 20 % at 5h) [52]. This suggested that the proton abstraction which is easier on methanol with higher

acidic character than ethanol was not the rate limiting step, being likely the stability of the alkoxide anion. Besides, the lower conversion values observed for MMgAl-LDHs compared to the MgAl-LDH sample must be related to the lower intrinsic basic character of the former samples which decreased their ability to abstract a proton from the hydroxyl group of methanol (Eq. (1)). That was due to the higher electronegativity of the transition metal cations than Mg^{2+} which decreased the electron density on the hydroxyls groups of the MMgAl-LDH layers. Assuming that these latter are the catalytic sites, their activity decreased.

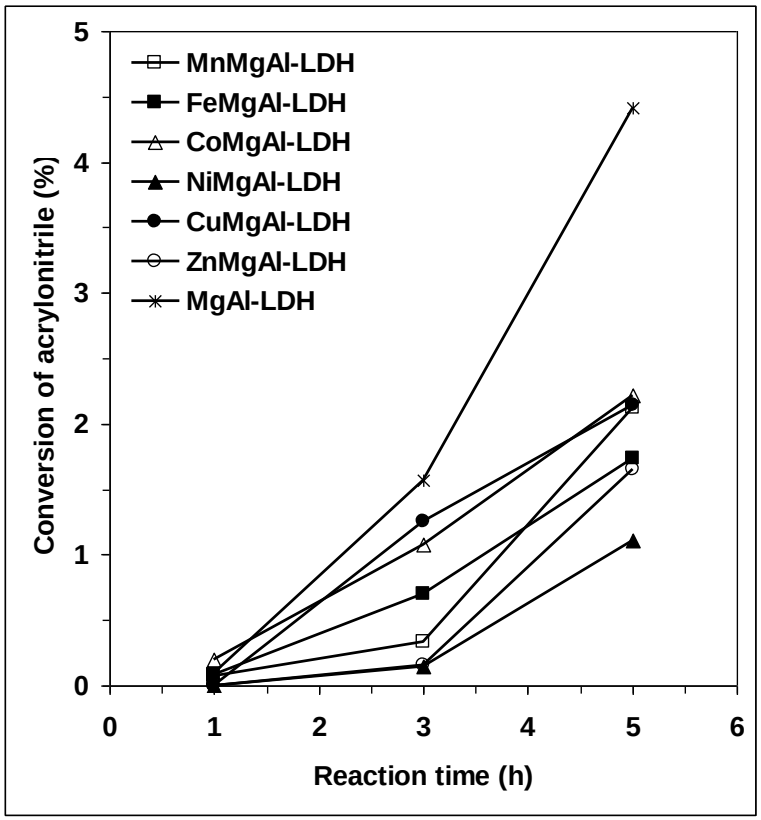

Figure IV.5. The activity of the MMgAl-LDH samples in the cyanoethylation reaction of methanol with acrylonitrile. Reaction conditions: temperature 90 °C; methanol-to-acrylonitrile molar ratio = 3; 3 % w/w catalyst.

As previously reported in cyanoethylation reactions, the mixed oxides were much more active than the LDH precursors [52-54]. The conversion reached 100 % after 5 h of reaction for MgAlO and went from 60 to 11 % for transition metal-containing catalysts as it can be seen in Fig. IV.6. The conversions reached with the different mixed oxides ranked as follows: MgAlO >

CoMgAlO > CuMgAlO > MnMgAlO > NiMgAlO > FeMgAlO > ZnMgAlO. This order of conversions was similar than that already observed for the precursors, except in the case of NiMgAlO where equilibrium between basic and acid sites would be better than in FeMgAlO and ZnMgAlO.

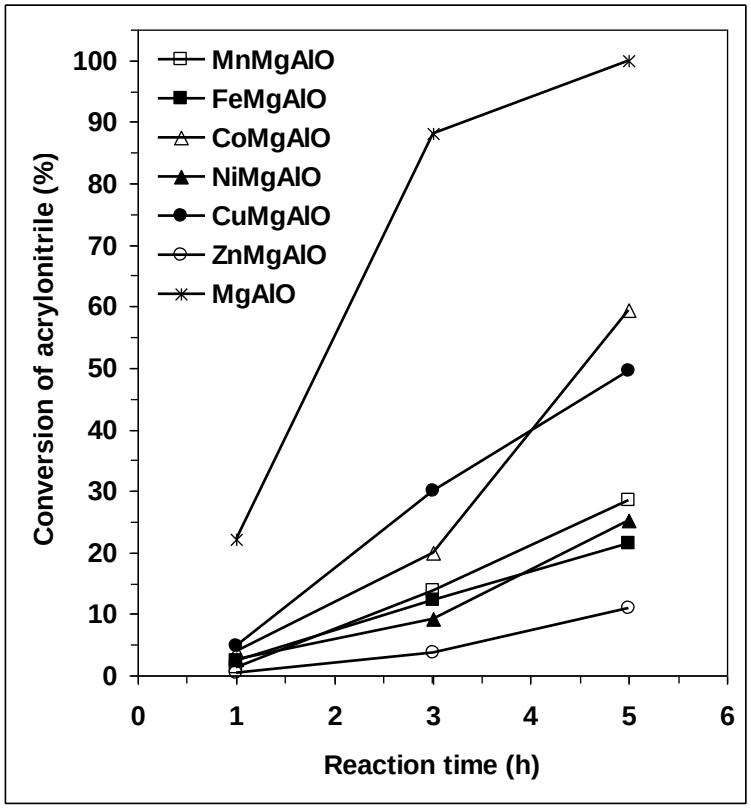

Figure IV.6. The activity of the MMgAlO mixed-oxides in the cyanoethylation reaction of methanol with acrylonitrile. Reaction conditions: temperature 90 °C; methanol-to-acrylonitrile molar ratio = 3; 3 % w/w catalyst.

The acrylonitrile conversions obtained with the different mixed oxides after 5 h of reaction have been correlated to the total number of basic and acid sites (Fig. IV.7). One can note the different behavior of MgAlO and of the MMgAlO mixed oxides. The highest conversion obtained with MgAlO was in line with the higher concentration of basic sites, particularly of medium and high strength, in this sample (Table IV.7). The first step of proton abstraction on methanol is obviously the most easily performed with this catalyst. For the MMgAlO mixed oxide catalysts the conversion also increased with the total number of basic sites, though being lower than with MgAlO (Fig. IV.7a).

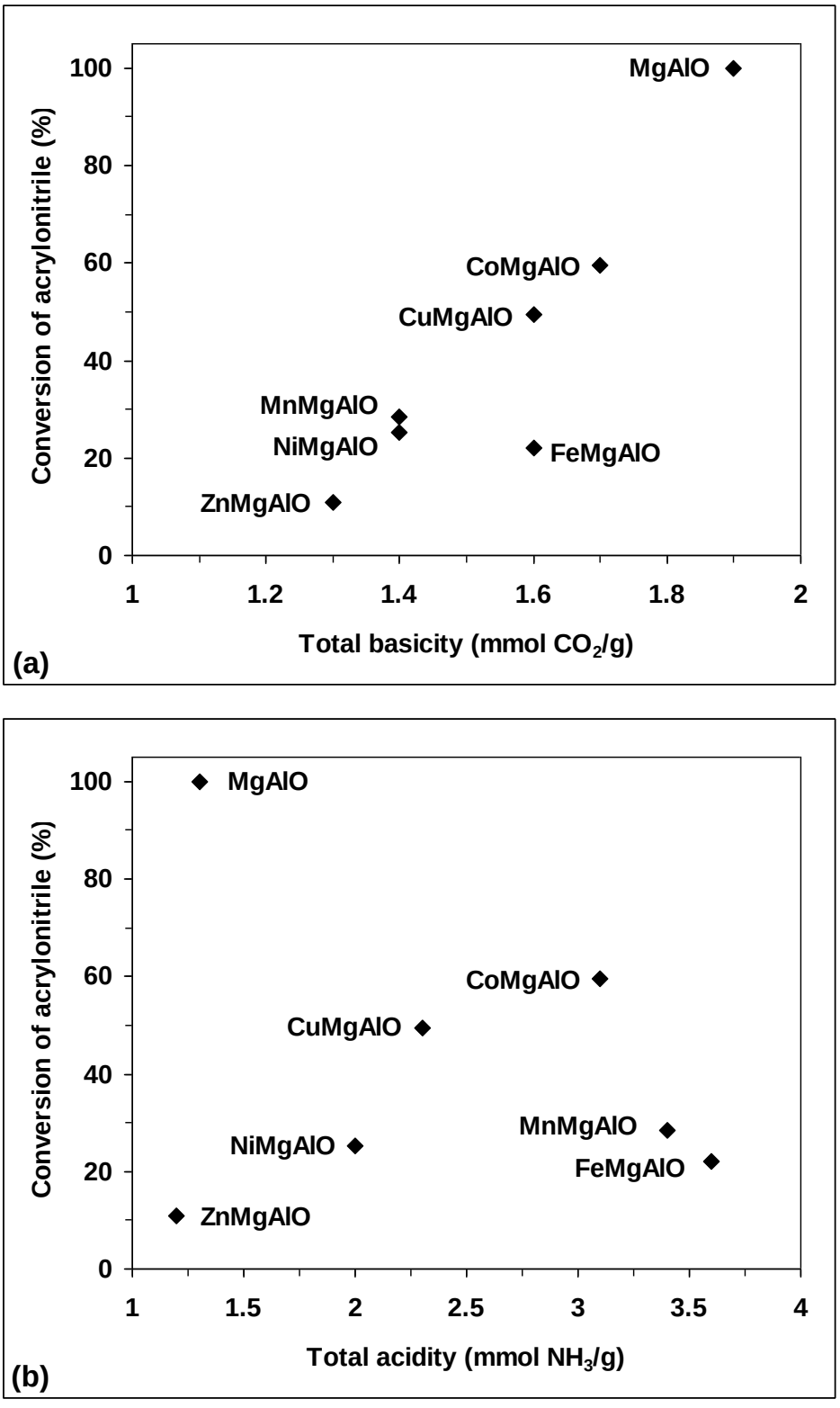

Figure IV.7. Acrylonitrile conversion versus number of basic sites (a) and acid sites (b) in the catalyst.

A different behavior was observed regarding the evolution of the conversion in function of the number of acid sites (Fig. IV.7b). It was indeed going through a maximum for an intermediate value. For these mixed oxides exhibiting a lower number of basic sites, particularly of medium and high strength, than MgAlO, the methoxide anions were highly stabilized on the acid sites and their reaction with acrylonitrile (Eq. (2)) became rate-limiting as previously reported [52]. The stabilization of the methoxide anion was too weakly achieved when a low number of acid sites were present while, on the contrary, the methoxide anions are too strongly stabilized when this number of sites became high. In both cases the conversion decreased.

In conclusion, CO_2 and NH_3-TPD experiments showed that introduction of transition metal cations modify the acid-base equilibrium in the M-MgAlO mixed oxides (M = Mn, Fe, Co, Ni, Cu and Zn) toward an improvement of the acid character. Mixed oxides were much more active in the cyanoethylation reaction of methanol than their corresponding LDH precursors, both being quite selective for β-metoxypropionitrile. For the as-prepared LDH samples the conversions were below 5 % after 5 h of reaction and ranked as follows: MgAl-LDH > CoMgAl-LDH ≈ CuMgAl-LDH ≈ MnMgAl-LDH > FeMgAl-LDH ≈ ZnMgAl-LDH > NiMgAl-LDH. The acrylonitrile conversion reached 100 % after 5 h of reaction for MgAlO mixed oxide, but decreased after introduction of the transition metal cations. The conversions reached with the metal cation containing mixed oxides ranked as follows: MgAlO > CoMgAlO > CuMgAlO > MnMgAlO > NiMgAlO > FeMgAlO > ZnMgAlO. They increased with the number of basic sites of the samples and went through a maximum in function of the number of acid sites. This confirmed the main role played by the equilibrium between the two types of sites.

IV.4. Esterification of acetic acid with *n*-butanol using molybdenum and vanadium oxides supported on γ-alumina

Nowadays, there is a great interest in the esterification reaction because organic esters are largely used in the production of plastic derivatives, perfumery, agro-chemistry and other branches of fine chemistry [60].

The esterification reaction is an extremely slow reaction and needs the addition of a catalyst in order to obtain high actual yields. The most common catalysts used for an esterification reaction are strong mineral acids such as sulfuric and hydrochloric acids as well as sulfonic acids [61]. Their catalytic activity is high, but they have several disadvantages, such as their corrosive nature, the existence of side reactions and they are often hardly separated from the reaction mixture. The use of solid acid catalysts offers an alternative as they can be easily separated from the liquid reaction mixture by filtration or decantation and, thus, reused, they have high selectivity and, last but not least, they are environmentally friendly. The solid catalysts mostly used in esterification reactions are classical solid acids including ion-exchange resins [62-66], zeolites [67-69], superacids like sulphated zirconia [70, 71] and heteropoly acids (HPA, both supported and unsupported) [72-75]. However, they have shown some limitations in application to esterification including low thermal stability (ion-exchange resins), resistance to mass transfer (zeolites) and loss of the active phase (sulphated zirconia and HPA) [71, 73, 76]. For these reasons, there is significant interest in developing new solid acid catalysts for esterification reactions. Note that the commercially available solid acid catalysts have been comparatively studied in the esterification of acetic acid with butanol [76].

It is well known [77] that oxides of elements with valence five or higher, such as tungsta, molybdena, vanadia, phosphoric anhydride and niobia, present strong to very strong Brønsted acidity which make them good candidates as acid catalysts. Some of them have already been studied as catalysts for esterification [78-81] and transesterification [82-84] reactions. Thus, $Nb_2O_5/SiO_2–Al_2O_3$ has been studied as catalyst for the esterification reaction of acetic acid with ethanol, *n*-butanol and iso-pentanol showing conversions of 83, 87 and 91 %, respectively, and 100 % selectivity for esters (8 h reaction time) [78]. WO_3/USY showed good catalytic performances (conversion above 74 % at 200 °C and reaction time 2 h) in the esterification of oleic acid with ethanol [79], and WO_3/ZrO_2 was an effective catalyst in the esterification of the

free fatty acids from dark oil to fatty acid methyl esters with conversion of 96 % at 150 °C (2 h reaction time) [80]. MoO_3 supported onto a thin alumina film has found to give 62 % conversion and 100 % selectivity for ester in the esterification reaction of acetic acid with ethanol [81]. Unsupported and silica-supported V_2O_5 catalysts have been tested in the transesterification reaction of dimethyl oxalate with phenol, the unsupported system showing relatively good performances (35 % dimethyl oxalate conversion and total selectivities to methyl phenyl oxalate and diphenyl oxalate exceeding 75 %) [82], but, to the best of our knowledge, there are no studies investigating alumina-supported V_2O_5 as catalysts for the esterification reaction. Moreover, neither alumina-supported V_2O_5 nor alumina-supported MoO_3 were studied as catalysts for the esterification of acetic acid with *n*-butanol. The reaction product, *n*-butyl acetate is an important chemical having extensive applications in the industry being used in large quantities as a solvent in the lacquer industry and coating manufacture, extractant and dehydrator [60, 85, 86]. Additionally, it is able to replace the toxic and teratogenic ethoxy ethyl acetate, which is often used as a solvent [87].

Thus, the catalytic properties of molybdenum and vanadium oxides supported on γ-alumina in the esterification of *n*-butanol with acetic acid have been for the first time studied and compared with those of γ-alumina support. The effects of the reaction time, the molar ratio between the reactants, the speed of agitation and the catalyst loading on the reaction were investigated. The obtained results were published in Refs. [88, 89] and are resumed below.

IV.4.1. Study of molybdenum oxide supported on γ-alumina

The physico-chemical characteristics of the catalysts were resumed in Table IV.9.

Table IV.9. Physico-chemical properties of the catalysts.

Catalyst	Phase identified by XRD	BET surface area (m^2/g)	Total pore volume (cm^3/g)	Total acidity (mmol/g)
Al_2O_3	γ-Al_2O_3	227	0.38	0.124
5Mo-Al_2O_3	γ-Al_2O_3	196	0.35	0.360
10Mo-Al_2O_3	γ-Al_2O_3	178	0.30	0.520

The conversion of acetic acid at 100 °C as a function of the reaction time over Al_2O_3, 5Mo-Al_2O_3 and 10Mo-Al_2O_3 catalysts as well as in the absence of a catalyst is shown in Fig. IV.8. The selectivity of *n*-butyl acetate was, in all cases, 100 %. This means that the conversion of acetic acid can represent the yield of *n*-butyl acetate. As expected, the conversion of acetic acid was higher in the presence of a catalyst than without a catalyst and increased remarkably with the prolonging of the reaction time. The activities at 120 min of reaction time are compared in the following. As known, esterification is a typical acid catalyzed reaction, and the acidity of the catalyst would exert a great influence on the catalytic activity. The highest conversion (62.6 %) of acetic acid over 10Mo-Al_2O_3 catalyst may thus be due to its high acid site density (Table IV.9) comparatively with 5Mo-Al_2O_3 (conversion 41.4 %) and Al_2O_3 (conversion 32.2 %) catalysts that have lower acid site densities. Nevertheless, when the site-time yields (STY, mol/mol H^+/s), are compared, the alumina support shows an activity higher (STY = 0.246 mol/mol H^+/s) than 5Mo-Al_2O_3 and 10Mo-Al_2O_3 samples for which STY are 0.105 and 0.110 mol/mol H^+/s, respectively. This is in line with the fact that γ-alumina possesses stronger acid sites than the supported molybdenum oxide samples, as shown from the NH_3-TPD experiments [88].

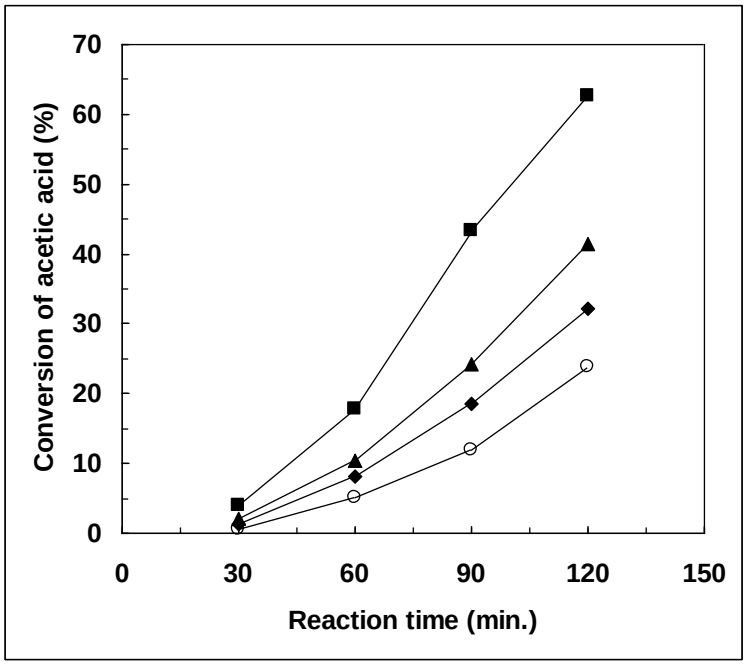

Figure IV.8. Conversion of acetic acid as a function of the reaction time in the catalytic and non-catalytic reaction. Reaction conditions: temperature 100 °C, acetic acid-to-*n*-butanol molar ratio = 1:1, 0.7 wt. % catalyst. (○ – non-catalytic, ♦ – Al_2O_3, ▲ – 5Mo-Al_2O_3, ■ – 10Mo-Al_2O_3).

The effect of mole ratio of reactants on the esterification of acetic acid with *n*-butanol for catalytic and non-catalytic reactions has also been studied. For all *n*-butanol to acetic acid mole ratios, the only product observed was *n*-butyl acetate. With the increase in *n*-butanol to acetic acid mole ratio from 1:1 to 2:1 and to 3:1, the conversion increased in all cases because, as expected based on the Le Châtelier principle, the increase of the alcohol amount enhances the conversion of the acid. The conversion of acetic acid reached 81 % in the presence of 10Mo-Al_2O_3 catalyst for an *n*-butanol to acetic acid mole ratio equal to 3:1 and a reaction time of 120 min.

It is worth noting that no effect of the speed of agitation in the range 450–750 rpm on the conversion of acetic acid was observed indicating no resistance to mass transfer to the external surface of the catalyst. On the other hand, when the mass fraction of the catalyst was increased from 0.5 to 1 % the conversion tended to a plateau for mass fractions of the catalyst around 1 % suggesting that this is the optimal mass fraction of the catalyst in the reaction medium.

We checked the stability of the 10Mo-Al_2O_3 catalyst by carrying out the reaction three times successively. It was concluded that the catalyst can be reused as there is no loss in catalytic activity and product selectivity at least during three cycles.

In conclusion, molybdenum oxide supported on γ-alumina acts as an efficient stable solid acid catalyst for the esterification of acetic acid with *n*-butanol. In all the esterification reactions the selectivity was 100 % while the conversion reached about 81 % in the presence of 10Mo-Al_2O_3 sample within 120 min of reaction time for an *n*-butanol to acetic acid mole ratio equal to 3 at 100 °C. The conversion increased following the order: Al_2O_3 < 5Mo-Al_2O_3 < 10Mo-Al_2O_3 in line with the total acid site density measured by NH_3-TPD. The optimal mass fraction of the catalyst in the reaction medium was around 1 %. The catalytic properties of the 10Mo-Al_2O_3 catalyst are maintained after three successive reactions.

IV.4.2. Study of vanadium oxide supported on γ-alumina

The physico-chemical characteristics of the catalysts were resumed in Table IV.10.

Table IV.10. The physico-chemical characteristics of the catalysts.

Catalyst	Surface area (m^2/g)	Phases identified by XRD	Chemical composition[a] (wt. %) by EDX		Number of acid sites (mmol/g)		
			V	Al	W & M[b]	Strong	Total
Al_2O_3	227	γ-Al_2O_3	-	-	0.097	0.027	0.124
5V-Al_2O_3	178	γ-Al_2O_3	15.30	45.58	0.076	0.094	0.170
10V-Al_2O_3	147	γ-Al_2O_3, V_2O_5	20.75	40.34	0.068	0.182	0.250
10V-Al_2O_3 used[c]	-	-	8.32	50.55	0.060	0.150	0.210

[a] Oxygen in balance.

[b] Weak and Medium strength.

[c] Reaction conditions: 0.7 wt % catalyst, temperature 100 °C, *n*-butanol-to-acetic acid molar ratio = 3:1 and reaction time 120 min.

The conversion of acetic acid as a function of the reaction time over Al_2O_3, 5V-Al_2O_3 and 10V-Al_2O_3 catalysts as well as in the absence of a catalyst is shown in Fig. IV.9a. As expected, the conversion of acetic acid was higher in the presence of a catalyst than without a catalyst and increased remarkably with the prolonging of the reaction time. The selectivity of *n*-butyl acetate was, in all cases, 100 %. The activities at 120 min of reaction time are compared in the following. As known, esterification is a typical acid catalyzed reaction, and the acidity of the catalyst would exert a great influence on the catalytic activity. The highest conversion (62.6 %) of acetic acid over 10V-Al_2O_3 catalyst may thus be due to its higher acid site density and strength (Table IV.10) compared with 5V-Al_2O_3 (conversion 38.7 %) and Al_2O_3 (conversion 32.2 %) catalysts that have both lower acid site densities and strengths. Note that the catalytic performances of the V_2O_5/Al_2O_3 catalysts were comparable with those of the MoO_3/Al_2O_3 catalysts with similar transition-metal loadings and measured in similar reaction conditions. With increasing the reaction time from 120 to 210 min for 10V-Al_2O_3 catalyst, the conversion of acetic acid increased from 62.6 % to 87.7 % without a change in the selectivity for *n*-butyl acetate (Fig. IV.9b).

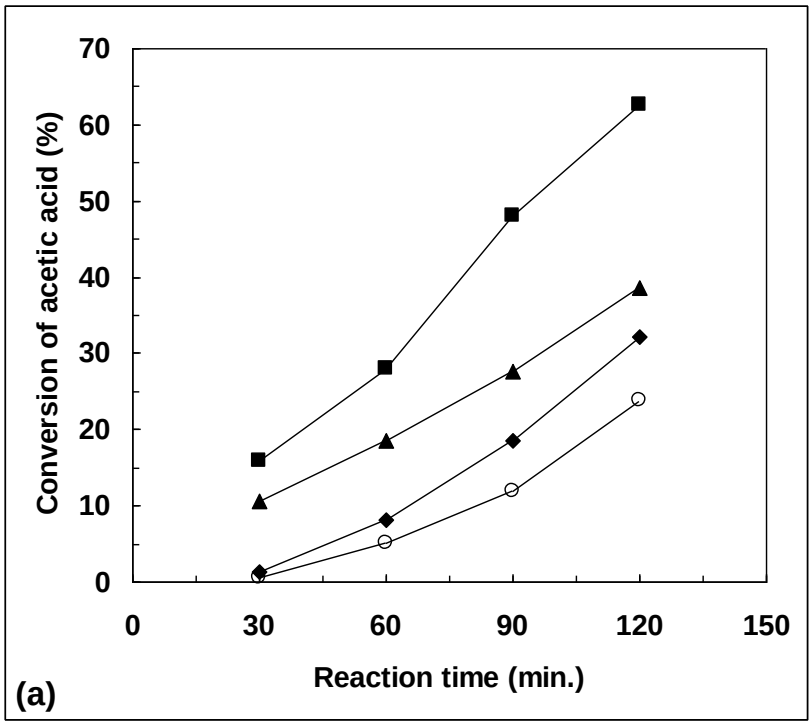

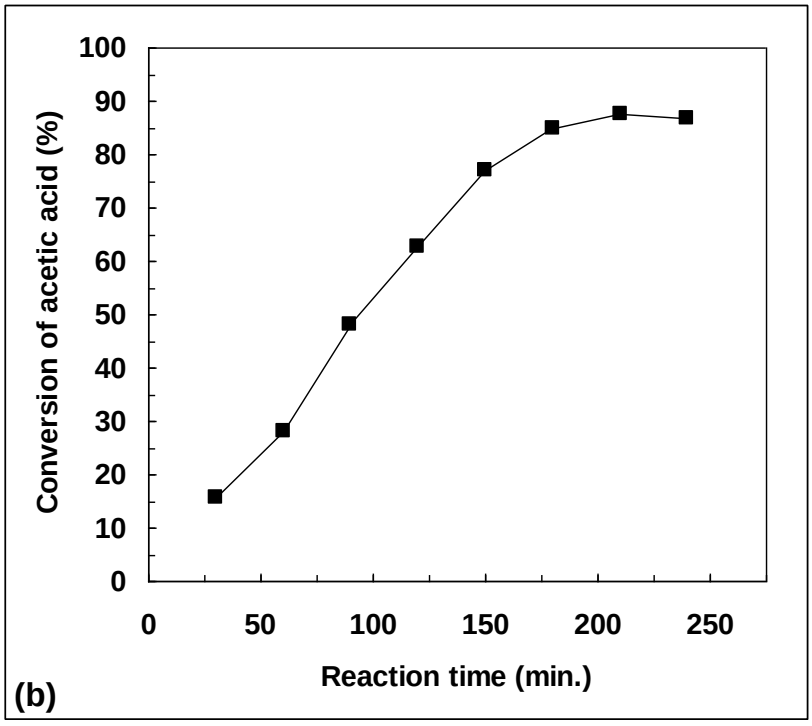

Figure IV.9. Conversion of acetic acid as a function of the reaction time in the catalytic and non-catalytic esterification reaction at 120 min (a) and 240 min (b). Reaction conditions: *n*-butanol-to-acetic acid molar ratio = 1:1, temperature 100 °C, 0.7 wt % catalyst. (○ – non-catalytic, ♦ – Al_2O_3, ▲ – 5V-Al_2O_3, ■ – 10V-Al_2O_3).

The effects of different feed ratio on acetic acid conversion over 5V-Al_2O_3 and 10V-Al_2O_3 catalysts were studied. By increasing the *n*-butanol-to-acetic acid mole ratio from 1:1 to 2:1 the conversion increased, as expected, for both catalysts. Nevertheless, by further increasing the mole ratio to 3:1, a decrease in conversion was observed probably due to the leaching of vanadia from alumina support in line with the observed loss of vanadium and decrease of the number of acid sites of the catalyst after the catalytic test (Table IV.10). This phenomenon has already been observed during the esterification of acetic acid with *n*-butanol on montmorillonite-supported dodecatungstophosphoric acid catalyst [75].

It is worth noting that no effect of the speed of agitation in the range 450–750 rpm on the conversion of acetic acid was observed indicating no resistance to mass transfer to the external surface of the catalyst. On the other hand, when the mass fraction of the catalyst was increased from 0.5 to 1 wt % the conversion tended to a plateau for mass fractions higher than 0.7 % suggesting that this is the optimal mass fraction of the catalyst in the reaction medium.

We checked the stability of the 10V-Al_2O_3 catalyst by carrying out the reaction three times successively. The results obtained, presented in Fig. IV.10, show a loss of activity of the 10V-Al_2O_3 catalyst with its subsequent reuse. Thus, for a reaction time of 2 h the conversion of 62.6 % in the first run decreased to 52.0 % in the second run and to 47.6 % in the third run. This decrease in catalytic activity is probably due to the subsequent leaching of vanadia from the alumina support into the liquid phase during the catalytic reactions as suggested by the EDX chemical analysis of the catalyst after the catalytic test (Table IV.10). Note that the selectivity for *n*-butyl acetate remained 100 %.

In conclusion, vanadium oxides supported on γ-alumina containing well dispersed VO_x species on the alumina support act as relatively efficient solid acid catalysts for the esterification of acetic acid with *n*-butanol. In all the esterification reactions the selectivity for butyl acetate was 100 %. The conversion increased following the order: Al_2O_3 < 5V-Al_2O_3 < 10V-Al_2O_3 in line with the total acid site density and strength measured by NH_3-TPD. There was no resistance to mass transfer to the external surface of the catalyst and the optimal catalyst loading in the reaction medium was around 0.7 %. Although the selectivity for butyl acetate remained 100 %, the catalytic activity of the 10V-Al_2O_3 catalyst decreased after three successive reactions because of the leaching of vanadia from the alumina support.

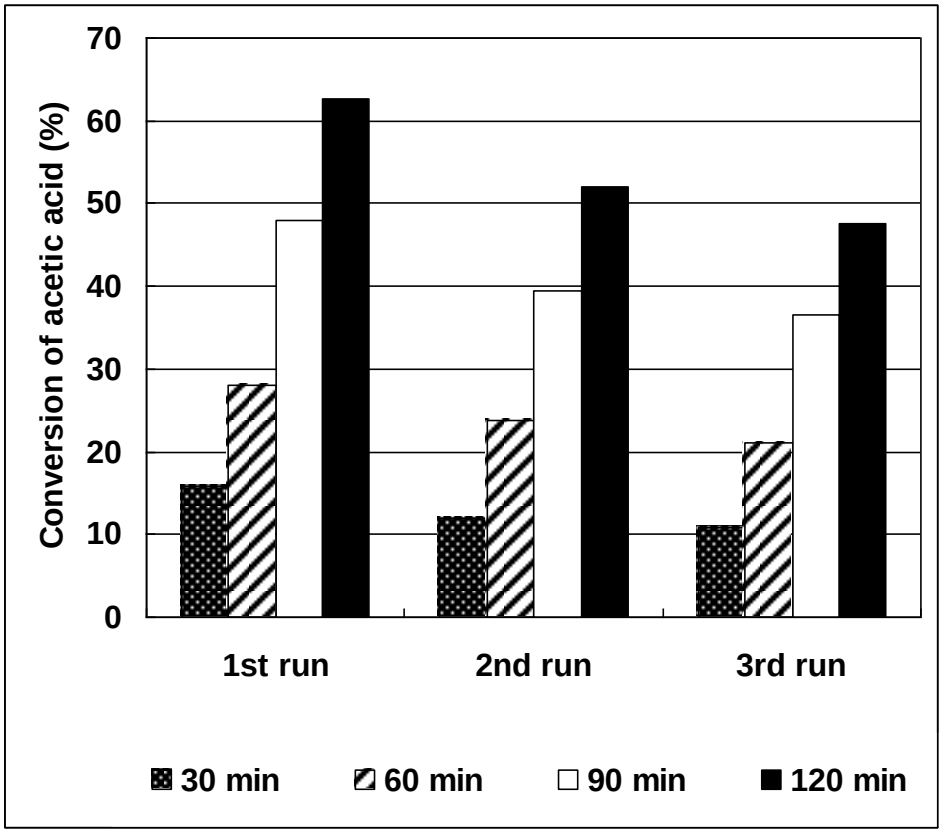

Figure IV.10. Reusability of the 10V-Al_2O_3 catalyst. Reaction conditions: *n*-butanol-to-acetic acid molar ratio = 1:1, temperature 100 °C, 0.7 wt % catalyst.

It is noteworthy that based on the fact that the addition of MoO_3 to V_2O_5/Al_2O_3 could increase its surface acidity [90] and, consequently, its catalytic activity in the esterification reaction and that Mo and V could interact on the support surface [91, 92] resulting in an increased catalyst stability, we have also studied MoO_3-V_2O_5/Al_2O_3 catalysts for the esterification of acetic acid with *n*-butanol, a paper being just accepted for publication [93]. A good reusability of the catalysts after three reaction cycles was indeed observed and a local interaction between molybdenum and vanadium on the catalyst surface has been evidenced. Moreover, compared with V_2O_5/Al_2O_3 with similar vanadia loadings, the MoO_3-V_2O_5/Al_2O_3 catalysts showed not only an increased stability during the esterification reaction, but also an improved catalytic activity.

SECTION B. PROSPECTIVE

This page intentionally left blank

RESEARCH AND ACADEMIC CAREER DEVELOPMENT PLAN

In this section, different research subjects in the field of Catalysis by Oxides that I intend to tackle in the future in the Laboratory of Chemical Technology and Catalysis of the University of Bucharest are described and justified based on a literature survey. They are in line with my main research directions as presented in the previous section, but new research topics are also envisaged.

The production of ethylene by catalytic oxidative dehydrogenation (ODH) of ethane is an attractive alternative route, exhibiting particular economic, technological and environmental interest. It has been studied over a wide range of catalytic materials, such as rare-earth oxides [1, 2], alkaline/alkaline-earth metal oxides [3-6], perovskites [7-10] and single and multicomponent transition metal oxide-based materials [11-16], but no material is yet suitable for industrial implementation. Among the systems studied, the NiO-based ones constitute one the most promising catalytic materials for ethane ODH, their good performance being first reported by Schuurman et al. [17]. One of the strategies used for improving the NiO catalytic performance was to dope it with various elements, such as Li, Mg, Al, Ga, Ti, Nb, Ta. Among these, it was found that Ni–Nb exhibited the highest ethylene selectivity (90 %) while Ni–Li the lowest (19 %) [18]. However, it has recently been shown that Ni-Nb-O system loses its catalytic activity due to the continuous reduction of the NiO oxygen over-stoichiometry in the reaction conditions and to the formation of the $NiNb_2O_6$ phase thermodynamically stable at the reaction temperature [19]. Based on these results, we consider that the strategy of doping NiO could be extended to other elements that could decrease the unselective electrophilic oxygen species on the NiO surface, leading to enhanced activity in the selective conversion of ethane to ethylene. Moreover, based on our previous results presented in Chapter I, the phosphatation of NiO is also envisaged.

Iron phosphate is known to be a highly active and selective catalyst for the oxidative dehydrogenation (ODH) of molecules containing active hydrogen, i.e. hydrogen at the α-position of an electron-attracting group, like isobutyric acid, lactic acid, glycolic acid etc. [20]. It was also

found to be active and selective for the gas-phase ammoxidation of methylpyrazine to cyanopyrazine [21] as well as for the ODH of ethane into ethylene, and in this case the ethylene yields approached 50 % [22]. Based on these results we intend to study iron phosphate as well as transition metal-doped iron phosphate as catalysts for the ODH of propane. Doping iron phosphate with small amounts of transition metals is envisaged in order to improve its catalytic performances [23] and to study the effects of such doping on the catalytic properties.

In recent years, many efforts were directed towards the design of catalytic materials based on single [24-27] and mixed [28-32] transition-metal based oxides to replace noble metal catalysts for VOCs abatement. In that context, there have been only few studies investigating nanospinel ferrites although they were shown to be effective catalysts for the total oxidation of VOCs [33-35] as well as for CO oxidation [36]. Moreover, we have recently shown for the first time that cobalt ferrite is a good catalyst for the total oxidation of propane [37]. Nevertheless, to our knowledge, no systematic study investigating nanosized spinel ferrites as catalysts for light alkanes' total oxidation has ever been undertaken. For these reasons we have in mind a systematic study of a series of simple AFe_2O_4 and mixed $A_xB_{1-x}Fe_2O_4$ nanostructured spinel ferrites as catalysts in the total oxidation reaction of methane. Ferrites are potential catalysts for this reaction due to their redox activity and their stability under oxidative conditions [33]. A spinel-type ferrite structure [38], presents two types of interstitial sites: tetrahedral and octahedral; these sites are surrounded by four and six oxygen atoms, respectively. The formula of the spinel ferrites is AFe_2O_4 where the A^{II} ions occupy the tetrahedral and Fe^{III} ions the octahedral positions. In fact, most of the ferrite properties depend on the cation distribution in the tetrahedral or octahedral sites in the spinel structure. The cation distribution is responsible of the number of vacancies and the non-stoichiometry, altering bulk and surface properties of the corresponding system, which is of special interest for catalysis [39]. These structural properties provide opportunities to extensively tune redox and electronic properties by varying the chemical composition of the ferrites to optimize their catalytic properties. Moreover, the identity of divalent metal component (A) inevitably affects the catalytic performance of metal ferrites [40]. Interesting divalent metal components (A) could be Mn, Co, Ni and Cu because they form spinel-type ferrite phases readily and are all reported in the literature as active components in oxide based catalysts for light alkanes and other VOCs combustion [41]. On the other hand, synergetic

effects in mixed $A_xB_{1-x}Fe_2O_4$ spinel ferrite catalysts rationalized on the basis of enhanced electron transfer and oxygen non-stoichiometry in these oxides are expected. Indeed, mixed $A_xB_{1-x}Fe_2O_4$ spinel ferrites with an optimum *x* value were already shown to be more active catalysts than simple ferrites [42]. This is why we expect even better catalytic performances for mixed $A_xB_{1-x}Fe_2O_4$ nanospinel ferrites in the total oxidation of methane. Note that a funding request for this research topic has already been made to the Executive Agency for Higher Education, Research, Development and Innovation Funding (UEFISCDI) within the frame of *IDEAS* Program - Exploratory Research Projects.

An interesting way to obtain mixed oxides catalysts is through the use of layered double hydroxides (LDH) as precursors [43]. Indeed after a calcination treatment mixed oxides with unique properties, such as high surface area, good thermal stability, good homogeneity and basic properties, are formed [43]. For an efficient catalytic system for methane total oxidation, the activity results from a cooperative effect between a large surface area combined with a high degree of metal dispersion. For obtaining LDH-derived mixed oxides with good metal dispersion and high catalytic activity the active metal must be placed in the brucite-like layers of the precursor structure [44]. We have shown [45] that in the case of LDH-derived Cu-Mg-Al mixed oxides, only the highly dispersed copper species were catalytically active. On the other hand, it is well known [46] that the introduction of high quantities of Cu^{2+} into the brucite-like layers is possible only in the presence of other elements as zinc. Taking these into consideration as well as the fact that trimetallic Zn-Cu-Al and Mn-Cu-Al LDH-derived catalysts were already found to be highly active in toluene combustion [47], we decided to increase the copper dispersion in the LDH-derived Cu-based catalysts in order to improve their catalytic performances by adding Zn. Moreover, taking into consideration that catalysts containing both Cu and Mn as active components were found to have comparable activities with the nobel metal-based ones in ethanol and acetaldehyde combustion [48, 49], we also decided to study Cu-Zn-Mn LDH-derived oxides as catalysts in methane total oxidation. We mention that we are already performing this work in our laboratory under the frame of the Postdoctoral Research Project entitled “New LDH-derived trimetallic mixed oxides, catalysts for light alkanes combustion” financed by UEFISCDI.

Single transition metal-oxides, used as catalysts for VOCs combustion, are commonly supported on materials with high surface areas and good thermal stability, such as alumina, ceria, ceria-zirconia, ceria-titania, zirconia, titania and silica, in order to ensure and maintain a high degree of dispersion of the catalytic active species [50-53]. Among them, ceria is one of the most suitable supports for this type of catalysts. Cerium oxide itself has a high catalytic activity in oxidation reactions, provided by the redox couple Ce^{4+}/Ce^{3+}, which leads to an outstanding oxygen storage capacity (OSC) coupled with high oxygen mobility in the crystal structure, making more oxygen available for the oxidation processes [54-57]. Moreover, the interaction between the transition metal ions and ceria lattice is crucial for the catalytic activity as shown for Cu-Ce-O composite oxides for which the capacity of ceria in governing the catalytic behavior by assisting the Cu^{2+}/Cu^{+} couples through Ce^{4+}/Ce^{3+} cycles plays a key role [58]. On the other hand, mesoporous nano-structured ceria possesses certain specific physical properties compared to the conventional one. Thus, along with an increased surface area, a remarkable enhancement of the OSC and potentially of the catalytic activity of cerium oxide has been observed when the particle size was reduced down to nanoscale, because of the large number of lattice defects such as oxygen vacancies, which provide an increased number of active sites for gas-solid catalysis [59, 60]. Taking these into consideration, we believe that the cheap but active transition metal oxides, such as MnO_x, CoO_x, NiO, CuO, well dispersed on high surface area ordered mesoporous nano-structured ceria with its own activity in oxidation processes, could lead to highly efficient catalysts for methane combustion. For this reason this will be one of our research topics in the future.

Obviously, as all the oxide-based catalysts proposed to be studied are semiconductors and the redox reactions they catalyze, i.e. the ODH and total oxidation of light alkanes, are connected with their electronic properties [61], we will characterize them by electric conductivity measurements for evidencing the relationship existing between their catalytic activity and their redox and electronic properties. We also intend to develop this technique by coupling the electric conductivity measurements set-up with a mass spectrometer for identifying the species existing in the gas phase simultaneously with the transformations occurring in the solid under different reactant sequences in conditions close to those used during catalysis. This will allow us to complete the electric conductivity measurements data and to better explain the catalytic

properties of the materials studied. It is worth noting that researchers from laboratories abroad already proposed to me collaborations for characterizing oxide-based catalysts by electric conductivity measurements.

We also have in mind the problem of biodiesel production by catalytic transesterification of vegetable oils or animal fats, as the biodiesel type fuels from renewable energy sources such as vegetable oils are believed to be the future fuels for the transportation sector instead of the liquid fossil fuels [62]. Transesterification is a well established and common method for biodiesel production from vegetable and other fatty oils [63, 64]. It is a catalytic process consisting in changing triglycerides with light alcohols (mainly methanol and ethanol) into alkyl ester and glycerol. Even though homogeneous alkaline and acidic catalysts are usually used in transesterification reactions, they have some disadvantages compared to heterogeneous catalysts which are cheap and available, stable at high temperatures and pressures and are easy to regenerate. This is why, in last decade, numerous solid acid and base catalysts were used in transesterification reactions including zeolites [65-67], functionalized oxides [68-70], heteropoly acids [71-73] and, respectively, alkali earth metal oxides [74, 75], doped and mixed metal oxides [76-78] and calcined MgAl-hydrotalcites [79-81]. Unfavorable catalyst morphology and leaching of active sites are the major problems of the solid acid catalysts while the solid base catalysts are very sensitive to water, CO_2 and free fatty acids. However, improving the preparation route and treatment steps of LDH-derived MgAl mixed oxides could transform them into industrially used catalysts for biodiesel production [62]. This is why, we intend to prepare and study as catalysts for the transesterification reaction LDH-derived MgAl and more basic LnMgAl mixed oxides (Ln = rare earth cation), but also MMgAl mixed oxides (M = transition metal) in which the equilibrium between acid and basic sites can be modified [82] due to the higher electronegativity of M^{2+} cations as compared to Mg^{2+} with consequences on both catalytic activity and sensitivity to CO_2 and free fatty acids. We have in mind the preparation of organic compounds-intercalated LDH precursors which could lead by appropriate thermal treatments to high surface area mesoporous mixed oxides with interesting catalytic performances.

Finally, the dry reforming of methane (DRM) has attracted our interest as it has attracted wide interest over the past few years because of its positive environmental and industrial impact.

The environmental viewpoint stems from the fact that CO_2 and CH_4, two of the main greenhouse gases that cause global warming and climate change [83], can be consumed by reforming reactions leading to a significant reduction in their concentrations in the atmosphere [84]. From the industrial point of view, the DRM reaction is attractive as it produces synthesis gas with a higher purity and a lower H_2/CO ratio than does either partial oxidation or steam reforming of methane [85], being, therefore, suitable for the Fischer-Tropsch synthesis of long chain hydrocarbons and oxygenates [86, 87]. Furthermore, it can be carried out with natural gas from fields containing large amounts of CO_2, without its pre-separation from the feed [88] and it has lower operating costs [89]. However, due to the endothermic nature of the DRM reaction (temperature as high as 800°C is required for high conversion of reactants), the main obstacle to the industrial implementation of this process is that there are no commercial catalysts that can operate at these elevated temperatures without suffering from carbon deposition, the major problem which leads to catalytic deactivation. The noble metals and nickel were found to be highly active catalysts for DRM reaction [90]. However, the noble metals tend to have better resistance than Ni to carbon-deposition, but their high cost and limited availability makes them unsuitable for large-scale applications [91]. Therefore, an important challenge is to increase the resistance of nickel supported catalysts to deactivation by carbon deposition, because nickel has activity and selectivity comparable to those of noble metals but at much less cost. One method of inhibiting carbon deposition is to control the nickel loading [92] and the size of the ensembles of metal atoms on the surface, because the ensembles necessary for carbon formation are larger than those needed for CH_4 reforming [93]. Another factor which greatly affects the coking tendency is the type of the support. Suitable supports have to be resistant to the high temperature applied and to maintain the metal dispersion of the catalyst during operation. In this respect, many materials were investigated as supports for Ni-based catalysts in the DRM reaction, such as: TiO_2 [94], SiO_2 [95], La_2O_3 [96], MgO [97] etc., but the most commonly used support was γ-Al_2O_3 [98, 99]. Moreover, the support must have the proper surface acid-base properties, which also affects the carbon deposition [100, 101]. As long as wet impregnation of the active metals on different supports is not fully reproducible and may give rise to some heterogeneity in the distribution of metal on the surface leading to a lower dispersion of metallic species and favoring coke deposition [102], an appropriate strategy of preparation of catalysts is required. In this respect, LDH can be used as precursors for catalysts supports, since they lead to oxides with high surface

area, basic properties and small crystal size with good dispersion of the metal loaded as active phase as already shown for NiMgAl mixed oxide [103]. Moreover, this method leads to materials with better resistance to sintering than the corresponding supported catalysts [104, 105]. To our knowledge, no systematic study investigating the effect of nickel loading on the catalytic performances of the unpromoted and transition metal-promoted LDH-derived Ni-based catalyst in the DRM reaction has ever been undertaken. This is why we intend to do this, using as promoters transition metals such as Co, Cu etc. as it has already been shown that they increased the catalytic activity of the Ni/Al_2O_3 catalysts in the DRM reaction [106]. Moreover, we consider that the promoting effect of the transition metals can be increased based on the ability of the LDH structure to accommodate many of them [107]. In this manner better LDH-derived Ni-containing catalysts for DRM reaction could be obtained.

All the research topics described above that I intend to tackle during my future university career involve the study of catalytic processes catalyzed by redox or acid-base oxides having as a main objective to find and develop new active and selective catalysts and to explain their catalytic behavior. If the proposed catalysts will not be so efficient for industrial applications, explaining their catalytic properties in correlation with their physico-chemical characteristics will open new ways for further improve their catalytic efficiency and will be a step forward for discovering new active oxide-based catalysts for the processes studied. All these topics will be the object of project proposals submitted to both national and European/international funding agencies. Of course, undergraduate and graduate students will be included in the research teams of the projects and will be encouraged to contribute and participate in a synergistic level. In this manner they will develop personal and professional skills integrated with training in specific research skills that will open to them future career perspectives.

Finally, it is worth noting that I already give at the University of Bucharest the following courses entitled *Catalytic Materials* and *Microporous and Mesoporous Materials for Catalysis*, at master and bachelor level, respectively. They are strongly related to my research work, and for this reason I already included in my lectures certain of my relevant research results and I will continue to do that in the future. Moreover, all the laboratory works at master level involve studies of catalytic materials related to my current research interests.

This page intentionally left blank

REFERENCES

This page intentionally left blank

Section A

Chapter I

1. E.A. Mamedov, V. Cortés Corberán, Appl. Catal. A 127 (1995) 1.
2. F. Cavani, N. Ballarini, A. Cericola, Catal. Today 127 (2007) 113.
3. http://www.uhde.eu/fileadmin/documents/brochures/uhde_brochures_pdf_en_12.pdf
4. J. Haber, Appl. Catal. A 113 (1994) 199.
5. S. Wang, K. Murata, T. Hayakawa, S. Hamakawa, K. Suzuki, Appl. Catal. A 196 (2000) 1.
6. I. Takahara, M. Saito, Chem. Lett. (1996) 973.
7. K. Nakagawa, M. Okamura, N. Ikenaga, T. Suzuki, T. Kobayashi, Chem. Commun. (1998) 1025.
8. K. Nakagawa, C. Kajita, N. Ikenaga, T. Kobayashi, G. M. Nishitani, T. Ando, T. Suzuki, Chem. Lett. (2000) 1100.
9. O. V. Krylov, A. K. Mamedov, S. R. Mirzabekova, Catal. Today 24 (1995) 371.
10. O. V. Krylov, A. K. Mamedov, S. R. Mirzabekova, Ind. Eng. Chem. Res. 34 (1995) 474.
11. K. Nakagawa, C. Kajita, N.-O. Ikenaga, M. Nishitani-Gamo, T. Ando, T. Suzuki, Catal. Today 84 (2003) 149.
12. S. Ge, C. Liu, S. Zhang, Z. Li, Chem. Eng. J. 94 (2003) 121.
13. G. Raju, B.M. Reddy, B. Abhishek, Y.H. Mo, S.E. Park, Appl. Catal. A 423-424 (2012) 168.
14. F. Dury, E. M. Gaigneaux, P. Ruiz, Appl. Catal. A 242 (2003) 187.
15. F. Dury, M. A. Centeno, E. M. Gaigneaux, P. Ruiz, Catal. Today 81 (2003) 95.
16. O. Demoulin, F. Dury, M. Navez, E.M. Gaigneaux, P. Ruiz, Catal. Today 91–92 (2004) 27.
17. O. Demoulin, I. Seunier, F. Dury, M. Navez, R. Rachwalik, B. Sulikowski, S. R. Gonzalez-Carrazan, E. M. Gaigneaux, P. Ruiz, Catalysis Today 99 (2005) 217.
18. N. Mimura, M. Okamoto, H. Yamashita, S. T. Oyama, K. Murata, J. Phys. Chem. B 110 (2006) 21764.
19. H. Li, Y. Yue, C. Miao, Z. Xie, W. Hua, Z. Gao, Catal. Comm. 8 (2007) 1317.
20. S. Sato, M. Ohhara, T. Sodesawa, F. Nozaki, Appl. Catal. 37 (1988) 207.
21. M. Sugino, H. Shimada, T. Turuda, H. Miura, N. Ikenaga, T. Suzuki, Appl. Catal. A 121 (1995) 125.

22. N. Mimura, M. Saito, Catal. Lett. 58 (1999) 59.
23. N. Mimura, M. Saito, Catal. Today 55 (2000) 173.
24. D.Y. Hong, J.S. Chang, J.H. Lee, V.P. Vislovskiy, S.H. Jhung, S.E. Park, Y.H. Park, Catal. Today 112 (2006) 86.
25. S. Wang, Z. H. Zhu, Energy & Fuels 18 (2004) 1126.
26. M.B. Ansari, S.E. Park, Energy Environ. Sci. 5 (2012) 9419.
27. I.C. Marcu, I. Sandulescu, J.M.M. Millet, J. Mol. Catal. A 203 (2003) 241.
28. I.C. Marcu, I. Sandulescu, J.M.M. Millet, Appl. Catal. A 227 (2002) 309.
29. F. Urlan, I.C. Marcu, I. Sandulescu, Catal. Commun. 9 (2008) 2403.
30. I.C. Marcu, J.M.M. Millet, J.M. Herrmann, Catal. Lett. 78 (2002) 273.
31. I.C. Marcu, I. Sandulescu, Y. Schuurman, J.M.M. Millet, Appl Catal A 334 (2008) 207.
32. I.C. Marcu, I. Sandulescu, Rev. Chim. 55 (2004) 423.
33. G.T. Click, B.J. Barone, U. S. Patent 4,515,899 (1985).
34. J.M.M. Millet, Catal. Rev. Sci. Eng. 40 (1998) 1.
35. J.E. Miller, M.M. Gonzales, L. Evans, A.G. Sault, C. Zhang, R. Rao, G. Whitwell, A. Maiti, D. King-Smith, Appl. Catal. A 231 (2002) 281.
36. A. Argent, P.G. Harrison, J. Chem. Soc., Chem. Commun. (1986) 1058.
37. A. Maiti, N. Govind, P. Kung, D. King-Smith, J. E. Miller, C. Zhang G. Whitwell, J. Chem. Phys. 117 (2002) 8080.
38. A. Kaddouri, C. Mazzocchia, E. Tempesti, Appl. Catal. A 169 (1998) L3.
39. J. El-Idrissi, M. Kacimi, F. Bozon-Verduraz, M. Ziyad, Catal. Lett. 56 (1998) 221.
40. A.E.C. Palmqvist, E.M. Johansson, S.G. Jaras, M. Muhammeda, Catal. Lett. 56 (1998) 69.
41. K. Otsuka, W. Ye, M. Nakamura, Appl. Catal. A 183 (1999) 317.
42. A. Trovarelli, C. de Leitenburg, M. Boaro, G. Dolcetti, Catal. Today 50 (1999) 353.
43. C. Larese, M. Lopez Granados, R. Mariscal, J.L.G. Fierro, P.S. Lambrou, A.M. Efstathiou, Appl. Catal. B 59 (2005) 13.
44. C. Larese, F. Cabello Galisteo, M. López Granados, R. Mariscal, J.L.G. Fierro, P.S. Lambrou, A.M. Efstathiou, J. Catal. 226 (2004) 443.
45. I.C. Marcu, M.N. Urlan, Á. Rédey, I. Săndulescu, CR Chim. 13 (2010) 365.
46. E. Cremer *in* Advances in Catalysis and Related Subjects (W. G. Frankenburg, Ed.), vol. VII, Academic Press, 1967, p. 75.

47. V. Iannazzo, G. Neri, S. Galvagno, M. Di Serio, R. Tesser, E. Santacesaria, Appl. Catal. A 246 (2003) 49.
48. Y. Takita, X. Qing, A. Takami, H. Nishiguchi, K. Nagaoka, Appl. Catal. A 296 (2005) 63.
49. P.M. Michalakos, M.C. Kung, I. Jahan, H.H. Kung, J. Catal. 140 (1993) 226.
50. J.L. Callahan, R.K. Grasselli, AIChE J. 9 (1963) 755.
51. R.K. Grasselli, Top. Catal. 15 (2001) 93.
52. R.K. Grasselli, D.D. Suresh, K. Knox, J. Catal. 18 (1970) 356.
53. R.K. Grasselli, D.D. Suresh, J. Catal. 25 (1972) 273.
54. S. Royer, D. Duprez, ChemCatChem 3 (2011) 24.
55. I.T. Trotuş, C.M. Teodorescu, V.I. Pârvulescu, I.C. Marcu, ChemCatChem (2013) DOI: 10.1002/cctc.201200699.
56. M. López Granados, F. Cabello Galisteo, P.S. Lambrou, R. Mariscal, J. Sanz, I. Sobrados, J.L.G. Fierro, A.M. Efstathiou, J. Catal. 239 (2006) 410.
57. S.A. D'Ippolito, M.A. Bañares, J.L. Garcia Fierro, C.L. Pieck, Catal. Lett. 122 (2008) 252.
58. S.A. Karakoulia, K.S. Triantafyllidis, A.A. Lemonidou, Micropor. Mesopor. Mater. 110 (2008) 157.
59. S. Sugiyama, T. Osaka, Y. Hirata, K.I. Sotowa, Appl. Catal. A 312 (2006) 52.
60. S. Dźwigaj, I. Gressel, B. Grzybowska, K. Samson, Catal. Today 114 (2006) 237.
61. S.N. Koc, G. Gurdag, S. Geissler, M. Guraya, M. Orbay, M. Muhler, J. Mol. Catal. A 225 (2005) 197.
62. E. Heracleous, M. Machli, A.A. Lemonidou, I.A. Vasalos, J. Mol. Catal. A 232 (2005) 29.
63. M.A. Bañares, S.J. Khatib, Catal. Today 96 (2004) 251.
64. T. Davies, S. H. Taylor, J. Mol. Catal. A 220 (2004) 77.
65. B. Zhaorigetu, W. Li, H. Xu, R. Kieffer, Catal. Lett. 94 (2004) 125.
66. S.M. Al-Zahrani, B.Y. Jibril, A.E. Abasaeed, Catal. Lett. 85 (2003) 57.
67. O.V. Buyevskaya, D. Wolf, M. Baerns, Catal. Today 62 (2000) 91.
68. W. Zhang, X. Zhou, D. Tang, H. Wan, K. Tsai, Catal. Lett. 23 (1994) 103.
69. D. Tichit, B. Coq, CATTECH 7 (2003) 206.
70. G. Mitran, A. Urda, N. Tanchoux, F. Fajula, I.C. Marcu, Catal. Lett. 131 (2009) 250.
71. Y. He, H. Ji, J. Xu, L. Wang, J. Nat. Gas Chem. 18 (2009) 359.
72. M.I. Khan, S. Deb, C.L. Marshall, Catal. Lett. 128 (2009) 256.

73. M.N. Taylor, A.F. Carley, T.E. Davies, S.H. Taylor, Top. Catal. 52 (2009) 1660.
74. I.V. Mishakov, E.V. Ilyina, A.F. Bedilo, A.A. Vedyagin, React. Kinet. Catal. Lett. 97 (2009) 355.
75. M. Olea, I. Sack, V. Balcaen, G.B. Marin, H. Poelman, K. Eufinger, D. Poelman, R. De Gryse, J.S. Paul, B.F. Sels, P.A. Jacobs, Appl. Catal. A 318 (2007) 37.
76. A. Albuquerque, L. Marchese, L. Lisi, H. O. Pastore, J. Catal. 241 (2006) 367.
77. S. Dźwigaj, I. Gressel, B. Grzybowska, K. Samson, Catal. Today 114 (2006) 237.
78. Y.M. Liu, W.L. Feng, T.C. Li, H.Y. He, W.L. Dai, W. Huang, Y. Cao, K.N. Fan, J. Catal. 239 (2006) 125.
79. B. Mitra, I.E. Wachs, G. Deo, J. Catal. 240 (2006) 151.
80. B. Solsona, J.M. López Nieto, U. Díaz, Micropor. Mesopor. Mater. 94 (2006) 339.
81. L.A. Palacio, A. Echavarría, L. Sierra, E.A. Lombardo, Catal. Today 107–108 (2005) 338.
82. S.N. Koc, G. Gurdag, S. Geissler, M. Muhler, Ind. Eng. Chem. Res. 43 (2004) 2376.
83. F.C. Calaza, M.F. Gomez, L.A. Arrua, O.A. Ferrettia, M.C. Abello, React. Kinet. Catal. Lett. 81 (2004) 259.
84. Y. Liu, J. Wang, G. Zhou, M. Xian, Y. Bi, K. Zhen, React. Kinet. Catal. Lett. 73 (2001) 199.
85. M.C. Abello, M.F. Gomeza, O. Ferretti, Appl. Catal. A 207 (2001) 421.
86. K. Chen, S. Xie, A.T. Bell, E. Iglesia, J. Catal. 198 (2001) 232.
87. R.B. Watson, U.S. Ozkan, J. Catal. 191 (2000) 12.
88. B.Y. Jibril, M.C. Al-Kinany, S.H. Al-Khowaiter, S.A. Al-Drees, H.A. Al-Megren, M.A. Al-Dosari, R.H. Al-Rasheed, S.M. Al-Zahrani, A.E. Abasaeed, Catal. Commun. 7 (2006) 79.
89. Q. Ge, B. Zhaorigetu, C. Yu, W. Li, H. Xu, Catal. Lett. 68 (2000) 59.
90. L. Jalowiecki-Duhamel, A. Ponchel, C. Lamonier, A. D'Huysser, Y. Barbaux, Langmuir 17 (2001) 1511.
91. S. Wang, K. Murata, T. Hayakawa, S. Hamakawa K. Suzuki, J. Chem. Technol. Biotechnol. 76 (2001) 265.
92. Y. Wu, Y. He, T. Chen, W. Weng, H. Wan, Appl. Surf. Sci. 252 (2006) 5220.
93. Y. Brik, M. Kacimi, M. Ziyad, F. Bozon-Verduraz, J. Catal. 202 (2001) 118.
94. R. Bulánek, K. Novoveská, B. Wichterlová, Appl. Catal. A 235 (2002) 181.

95. V. Cortés Corberán, M.J. Jia, J. El-Haskouri, R.X. Valenzuela, D. Beltrán-Porter, P. Amorós, Catal. Today 91–92 (2004) 127.
96. S. Blanco, S.R.G. Carrazán, V. Rives, Appl. Catal. A 342 (2008) 93.
97. A. Węgrzyn, A. Rafalska-Łasocha, B. Dudek, R. Dziembaj, Catal. Today 116 (2006) 74.
98. M.J. Holgado, F.M. Labajos, M.J S. Montero, V. Rives, Mater. Res. Bull. 38 (2003) 1879.
99. M.J. Holgado, V. Rives, M.S. San Román, Appl. Catal. A 214 (2001) 219.
100. K. Bahranowski, G. Bueno, V. Cortés Corberán, F. Kooli, E.M. Serwicka, R.X. Valenzuela, K. Wcisło, Appl. Catal. A 185 (1999) 65.
101. R. Dula, K. Wcisło, J. Stoch, B. Grzybowska, E.M. Serwicka, F. Kooli, K. Bahranowski, A. Gaweł, Appl. Catal. A 230 (2002) 281.
102. J. M. López Nieto, Top. Catal. 41 (2006) 3.
103. M. A. Chaar, D. Patel, H. H. Kung, J. Catal. 109 (1988) 463.
104. S. Tanasoi, G. Mitran, N. Tanchoux, T. Cacciaguerra, F. Fajula, I. Săndulescu, D. Tichit, I.C. Marcu, Appl. Catal. A 395 (2011) 78.
105. F. Basile, G. Fornasari, M. Gazzano, A. Vaccari, Appl. Clay Sci. 16 (2000) 185.
106. R.E. Kirk, D.F. Othmer, Encyclopedia of Chemical Technology, 4th edition, vol. 22, John Wiley & Sons, New York, 1994, p. 183.
107. G. Mitran, T. Cacciaguerra, S. Loridant, D. Tichit, I.C. Marcu, Appl. Catal. A 417-418 (2012) 153.
108. B. Solsona, T.E. Davies, T. Garcia, I. Vázquez, A. Dejoz, S.H. Taylor, Appl. Catal. B 84 (2008) 176.
109. F.E. Trigueiro, C.M. Ferreira, J.C. Volta, W.A. Gonzalez, P.G. Pries de Oliveria, Catal. Today 118 (2006) 425.
110. C. Trionfetti, I. V. Babich, K. Seshan, L. Lefferts, Appl. Catal. A 310 (2006) 105-113.
111. J. E. Miller, N. B. Jackson, L. Evans, A. G. Sault, M. M. Gonzales, Catal. Lett. 58 (1999) 147.
112. Z. Jiang, J. Yu, J. Cheng, T. Xiao, M. O. Jones, Z. Hao, P. P. Edwards, Fuel Proc. Technol. 91 (2010) 97.

Chapter II

1. T. Garcia, B. Solsona, D.M. Murphy, K.L. Antcliff, S.H. Taylor, J. Catal. 229 (2005) 1.
2. L.D. Pfefferle, L.C. Pfefferle, Catal. Rev. Sci. Eng. 29 (1987) 219.
3. T.V. Choudhary, S. Banerjee, V.R. Choudhary, Appl. Catal. A 234 (2002) 1.
4. M.R. Morales, B.P. Barbero, L.E. Cadus, Appl. Catal. B 67 (2006) 229.
5. R.M. Heck, R.J. Farrauto, Catalytic Air Pollution Control. Commercial Technology, Van Nostrand Reinhold, New York, 1995.
6. R. Craciun, B. Nentwich, K. Hadjiivanou, H. Knozinger, Appl. Catal. A 243 (2003) 67.
7. L.G. Tejuca, J.L.G. Fierro, J.M.D. Tascon, Adv. Catal. 35 (1989) 237.
8. L. Fabrini, A. Kryukov, S. Capelli, G. L. Chiarello, I. Rosetti, C. Oliva, L. Forni, J. Catal. 232 (2005) 247.
9. M. Alifanti, M. Florea, V. Cortes-Corberan, U. Endruschat, B. Delmon, V. I. Parvulescu, Catal. Today 112 (2006) 169.
10. I. Popescu, A. Urda, T. Yuzhakova, I.C. Marcu, J. Kovacs, I. Săndulescu, CR Chim. 12 (2009) 1072.
11. S. Cimino, L. Lisi, R. Pirone, G. Russo, M. Turco, Catal. Today 59 (2000) 19.
12. F. Cavani, F. Trifiró, A. Vaccari, Catal. Today 11 (1991) 173.
13. A. Vaccari, Appl. Clay Sci. 14 (1999) 161.
14. F. Kovanda, T. Rojka, J. Dobesova, V. Machovic, P. Bezdicka, L. Obalova, K. Jiratova, T. Grygar, J. Solid State Chem. 179 (2006) 812.
15. R. Dula, R. Janik, T. Machej, J. Stoch, R. Grabowski, E.M. Serwicka, Catal. Today 119 (2007) 327.
16. Z. Jiang, J. Yu, J. Cheng, T. Xiao, M. O. Jones, Z. Hao, P.P. Edwards, Fuel Proc. Technol. 91 (2010) 97.
17. Z. Jiang, Z. Hao, J. Yu, H. Hou, C. Hu, J. Su, Catal. Lett. 99 (2005) 157.
18. Z. Jiang, L. Kong, Z. Chu, L.J. France, T. Xiao, P.P. Edwards, Fuel 96 (2012) 257.
19. S. Tanasoi, G. Mitran, N. Tanchoux, T. Cacciaguerra, F. Fajula, I. Săndulescu, D. Tichit, I.C. Marcu, Appl. Catal. A 395 (2011) 78.
20. M. Iamarino, R. Chirone, L. Lisi, R. Pirone, P. Salatino, G. Russo, Catal. Today 75 (2002) 317.
21. M. Bosomoiu, G. Bozga, D. Berger, C. Matei, Appl. Catal. B 84 (2008) 758.

22. F. Diehl, J. Barbier Jr., D. Duprez, I. Guibard, G. Mabilon, Appl. Catal. B 95 (2010) 217.
23. S. H. Taylor, S. R. O'Leary, Appl. Catal. B 25 (2000) 137.
24. M. Marion, E. Garbowski, M. Primet, J. Chem. Soc. Faraday Trans. 86 (1990) 3027.
25. P. Park, J. Ledford, Appl. Catal. B 15 (1998) 221.
26. L. Kundakovic, M. Flytzani-Stephanopoulos, Appl. Catal. A 171 (1998) 13.
27. M. Dongare, V. Ramaswamy, C. Gopinath, A. Ramaswamy, S. Scheurell, M. Brueckner, E. Kemnitz, J. Catal. 199 (2001) 209.
28. G. Águila, F. Gracia, J. Cortés, P. Araya, Appl. Catal. B 77 (2008) 325.
29. Z. Wang, H. Wan, B. Liu, X. Zhao, X. Li, H. Zhu, X. Xu, F. Ji, K. Sun, L. Dong, Y. Chen, J. Colloid Interf. Sci. 320 (2008) 520.
30. S. Tanasoi, N. Tanchoux, A. Urdă, D. Tichit, I. Săndulescu, F. Fajula, I.C. Marcu, Appl. Catal. A 363 (2009) 135.
31. A. Alejandre, F. Medina, P. Salagre, X. Correig, J.E. Sueiras, Chem. Mater. 11 (1999) 939.
32. J.W. Veldsink, G.F. Versteeg, W.P.M. van Swaaij, Chem. Eng. J. 57 (1995) 273.
33. J.B. Silva, C.F. Diniz, R.M. Lago, N.D.S. Mohallem, J. Non-Cryst. Solids 348 (2004) 201.
34. J.C. Lou, Y.J. Tu, J. Air Waste Manag. Assoc. 55 (2005) 1809.
35. M. Florea, M. Alifanti, V.I. Parvulescu, D. Mihaila-Tarabasanu, L. Diamandescu, M. Feder, C. Negrila, L. Frunza, Catal. Today 141 (2009) 361.
36. O.A. Fouad, K.S. Abdel Halim, M.M. Rashad, Top. Catal. 47 (2008) 61.
37. A. Urdă, A. Herraïz, Á. Rédey, I.C. Marcu, Catal. Commun. 10 (2009) 1651.
38. J.G. McCarthy, Y.F. Chang, V.L. Wong, M.E. Johansson, Prepr. Am. Chem. Soc. Div. Petrol. Chem. 42 (1997) 158.
39. M. Baldi, E. Finocchio, F. Millela, G. Busca, Appl. Catal. B 16 (1998) 43.
40. H. Will, P. Scholz, B. Ondruschka, Top. Catal. 29 (2004) 175.

Chapter III

1. J.M. Herrmann in B. Imelik and J.C. Védrine (eds.), Catalyst Characterization, Physical Techniques for Solid Materials, Plenum Press, New York, 1994, ch. 20.
2. H. Ponceblanc, J.M.M. Millet, G. Coudurier, J.M. Herrmann, J.C. Védrine, J. Catal. 142 (1993) 373.
3. J.M. Herrmann, J. Disdier, F.G. Freire, M.F. Portela, J. Chem. Soc., Faraday Trans. 91 (1995) 2343.
4. J.M. Herrmann, P. Vernoux, K.E. Béré, M. Abon, J. Catal. 167 (1997) 106.
5. I.C. Marcu, J.M.M. Millet, J.M. Herrmann, Catal. Lett. 78 (2002) 273.
6. I.C. Marcu, I. Săndulescu, Y. Schuurman, J.M.M. Millet, Appl. Catal. A 334 (2008) 207.
7. L.M. Madeira, J.M. Herrmann, F.G. Freire, M.F. Portela, F.J. Maldonado, Appl. Catal. A 158 (1997) 243.
8. L.M. Madeira, J.M. Herrmann, J. Disdier, M.F. Portela, F.G. Freire, Appl. Catal. A 235 (2002) 1.
9. J.M. Herrmann, F. Villain, L.G. Appel, Appl. Catal. A 240 (2003) 177.
10. G. Mitran, A. Urdă, I. Săndulescu, I.C. Marcu, React. Kinet. Mech. Catal. 99 (2010) 135.
11. J.M.M. Millet, I.C. Marcu, J.M. Herrmann, J. Mol. Catal. A 226 (2005) 111.
12. J.M. Herrmann, J. Disdier, Catal. Today 56 (2000) 389.
13. J.M. Herrmann, New J. Chem. 36 (2012) 883.
14. A. Trovarelli (Ed.), Catalysis by ceria and related materials, Imperial College Press, London, 2005.
15. M. Mogensen, N.M. Sammes, G.A. Tompsett, Solid State Ionics 129 (2000) 63.
16. C. Bozo, N. Guilhaume, J.M. Herrmann, J. Catal. 203 (2001) 393.
17. I. Popescu, I.T. Trotuş, I.C. Marcu, Appl. Catal. B 128 (2012) 55.
18. L.F. Heckelsberg, A. Clark, G.C. Bailey, J. Phys. Chem. 60 (1956) 559.
19. J.M. Herrmann, J. Catal. 118 (1989) 43.
20. J.M. Herrmann, J.L. Portefaix, M. Forissier, F. Figueras, P. Pichat, J. Chem. Soc., Faraday Trans. 75 (1979) 1346.
21. J.M. Herrmann, J. Disdier, Catal. Today 20 (1994) 135.
22. M. Boaro, A. Trovarelli, J.H. Hwang, T.O. Mason, Solid State Ionics 147 (2002) 85.

23. E.J.W. Verwey, P.W. Haijman, F.C. Romeijn, G.W. van Oosterhout, Philips Res. Rep. 5 (1950) 173.
24. S. Mars, N. van Krevelen, Chem. Eng. Sci., Special Sup. 9 (1954) 41.
25. I.C. Marcu, M.N. Urlan, Á. Rédey, I. Săndulescu, CR Chim. 13 (2010) 365.
26. V. Raghavan, Materials science and engineering: a first course, 5th edition, Prentice-Hall of India Private Limited, New Delhi, 2004, p. 368.
27. Y. Takita, X. Qing, A. Takami, H. Nishiguchi, K. Nagaoka, Appl. Catal. A 296 (2005) 63.
28. I. Popescu, I. Săndulescu, Á. Rédey, I.C. Marcu, Catal. Lett. 141 (2011) 445.
29. J.R. Ebner, US Patent 4,405,498 (1983).
30. A.T. Guttmann, R.K. Grasselli, J.F. Brazdil, US Patent 4,746,641 (1988).
31. A.T. Guttmann, R.K. Grasselli, J.F. Brazdil, US Patent 4,788,317 (1988).
32. R. Nilsson, T. Lindblad, A. Andersson, J. Catal. 148 (1994) 501.
33. T. Birchall, A.E. Sleight, Inorg. Chem. 15 (1976) 868.
34. S. Hansen, K. Stahl, R. Nilsson, A. Andersson, J. Solid State Chem. 102 (1993) 340.
35. H. Roussel, B. Mehlomakulu, F. Belhadj, E. van Steen, J.M.M. Millet, J. Catal. 205 (2002) 97.
36. Z. Tianshu, P. Hing, J. Mater. Sci.: Mater. Electron. 10 (1999) 509.
37. F.J. Berry, M.E. Brett, J. Chem. Soc., Dalton Trans. (1983) 9.
38. C.M. Osburn, R.W. West, J. Chem. Solids 32 (1971) 1331.
39. J.M. Herrmann, J.L. Portefaix, React. Kinet. Catal. Lett. 12 (1979) 51.
40. B. Benaïchouba, J.M. Herrmann, React. Kinet. Catal. Lett. 22 (1983) 209.
41. K. Aika, H. Lundsford, J. Phys. Chem. 81 (1977) 1393.
42. D.L. Nguyen, Y. Ben Taarit, J.M.M. Millet, Catal. Lett. 90 (2003) 65.
43. R.K. Grasselli in G. Ertl, H. Knözinger, J. Weitkamp (Eds.), Handbook of Heterogeneous Catalysis, vol. 5, Wiley–VCH, 1997, p. 2307.
44. A. Andersson, S.L.T. Andersson, G. Centi, R.K. Grasselli, M. Sanati, F. Trifiro, Stud. Surf. Sci. Catal. 7 (1992) 691.
45. G. Centi, S. Perathoner, Stud. Surf. Sci. Catal. 92 (1995) 59.

Chapter IV

1. J. Frankaerts, G.F. Froment, Chem. Eng. Sci. 19 (1964) 807.
2. A. Pelso, M. Moresi, C. Mustachi, B. Soracco, Can. J. Chem. Eng. 57 (1979) 159.
3. J. Edwards, J. Nicolaidis, M.B. Cultip, C.O. Bennett, J. Catal. 50 (1977) 24.
4. C. Yang, Z. Meng, J. Catal 142 (1993) 37.
5. A.S. Ndou, N. Plint, N.J. Coville, Appl. Catal. A 251 (2003) 337.
6. E. Iglesia, D.G. Barton, J.A. Biscardi, M.J.L. Gines, S.L. Soled, Catal Today 38 (1997) 339.
7. M.J.L. Gines, E. Iglesia, J. Catal. 176 (1998) 155.
8. J.I. Di Cosimo, V.K. Diez, M. Xu, E. Iglesia, C.R. Apesteguia, J. Catal. 178 (1998) 499.
9. H. Hattori, Chem. Rev. 95 (1995) 537.
10. V.M.T.M. Silva, A.E. Rodrigues, Chem. Eng. Sci. 56 (2001) 1255.
11. M.F. Gomez, L.A. Arrua, M.C. Abello, React. Kinet. Catal. Lett. 73 (2001) 143.
12. M. Natarajan, E.A. Frame, T. Asmus, W. Clark, J. Garbak, M.A. Gonzalez, E. Liney, W. Piel, J.P. Wallace III, SAE Tech. Pap. Ser. (2001) 2001-01-3631.
13. A.S. Cheng, R.W. Dibble, B.A. Buchholz, SAE Tech. Pap. Ser. (2002) 2002-01-1705.
14. M. Kaufhold, M. El-Chabawi, Huels Chemische Werke AG, US Patent 5,527,969 (1996).
15. T. Aizawa, H. Nakamura, K. Wakabayashi, T. Kudo, H. Hasegawa, Showa Denko KK, US Patent 5,362,918 (1994).
16. J.I. Di Cosimo, C.R. Apesteguia, M.J.L. Gines, E. Iglesia, J. Catal. 190 (2000) 261.
17. A.M. Hilmen, M. Xu, M.J.L. Gines, E. Iglesia, Appl. Catal. A 169 (1998) 355.
18. R.E. Kirk, D.F. Othmer, Encyclopedia of Chemical Technology, 4^{th} ed., vol. 4, John Wiley & Sons, New York, 1994, p. 696.
19. G. Gregorio, G.F. Pregaglia, R. Ugo, J. Organomet. Chem. 37 (1972) 385.
20. P.L. Burk, R.L. Pruett, K.S. Campo, J. Mol. Catal. 33 (1985) 15.
21. C. Carlini, G.M. Di, M. Marchionna, M. Noviello, G.A.M. Raspolli, G. Sbrana, J. Mol. Catal. A 184 (2002) 273.
22. C. Carlini, M. Di Girolamo, A. Macinai, M. Marchionna, M. Noviello, A.M.R. Galletti, G. Sbrana, J. Mol. Catal. A 200 (2003) 137.
23. C. Carlini, A. Macinai, M. Marchionna, M. Noviello, A.M.R. Galletti, G. Sbrana, J. Mol. Catal. A 206 (2003) 409.
24. C. Carlini, A. Macinai, A.M.R. Galletti, G. Sbrana, J. Mol. Catal. A 212 (2004) 65.

25. C. Carlini, C. Flego, M. Marchionna, M. Noviello, A.M.R. Galletti, G. Sbrana, F. Basile, A. Vaccari, J. Mol. Catal. A 220 (2004) 215.
26. I.C. Marcu, N. Tanchoux, F. Fajula, D. Tichit, Catal. Lett. 143 (2013) 23.
27. S. Abelló, F. Medina, X. Rodríguez, Y. Cesteros, P. Salagre, J.E. Sueiras, D. Tichit, B. Coq, Chem. Commun. (2004) 1096.
28. S. Abelló, F. Medina, D. Tichit, J. Pérez-Ramírez, J.C. Groen, J.E. Sueiras, P. Salagre, Y. Cesteros, Chem. Eur. J. 11 (2005) 728.
29. I.C. Marcu, D. Tichit, F. Fajula, N. Tanchoux, Catal. Today 147 (2009) 231.
30. F. Cavani, F. Trifirò, A. Vaccari, Catal. Today 11 (1991) 173.
31. J. Palomeque, J. Lopez, F. Figueras, J. Catal. 211 (2002) 150.
32. K. Yamaguchi, K. Ebitani, K. Kaneda, J. Org. Chem. 64 (1999) 2966.
33. A. Vaccari, Appl. Clay Sci. 14 (1999) 161.
34. A.H. Padmasri, A. Venugopal, V.D. Kumari, K.S. Rama Rao, P. Kanta Rao, J. Mol. Catal. A 188 (2002) 255.
35. F.B. Sels, E.D. De Vos, P.A. Jacobs, Catal. Rev. 43 (2001) 443.
36. Y. Ono, T. Baba, Catal. Today 38 (1997) 321.
37. F. Zhang, X. Xiang, F. Li, X. Duan, Catal. Surv. Asia 12 (2008) 253.
38. G. Centi, S. Perathoner, Micropor. Mesopor. Mat. 107 (2008) 3.
39. S.P. Newman, W. Jones, New J. Chem. 22 (1998) 105.
40. G. Mitran, T. Cacciaguerra, S. Loridant. D. Tichit, I.C. Marcu, Appl. Catal. A 417-418 (2012) 153.
41. F. Kovanda, K. Jirátová, Appl. Clay Sci. 53 (2011) 305.
42. S. Tanasoi, G. Mitran, N. Tanchoux, T. Cacciaguerra, F. Fajula, I. Săndulescu, D. Tichit, I.C. Marcu, Appl. Catal. A 395 (2011) 78.
43. Z. Jiang, J. Yu, J. Cheng, T. Xiao, M.O. Jones, Z. Hao, P.P. Edwards, Fuel Proc. Technol. 91 (2010) 97.
44. C. Resini, T. Montanari, L. Barattini, G. Ramis, G. Busca, S. Presto, P. Riani, R. Marazza, M. Sisani, F. Marmottini, U. Costantino, Appl. Catal. A 355 (2009) 83.
45. O.D. Pavel, D. Tichit, I.C. Marcu, Appl. Clay Sci. 61 (2012) 52.
46. H.A. Bruson, 1949. Cyanoethylation. In: Organic Reactions, vol. 5. John Wiley & Sons, Inc., New York, p. 80.

47. J.H. Mac Gregor, C. Pugh, J. Chem. Soc. (1945) 535.
48. W.P. Unlermoheln, J. Am. Chem. Soc. 67 (1945) 1505.
49. H. Kabashima, H. Hattori, Catal. Today 44 (1998) 277.
50. P.S. Kumbhar, J. Sanchez-Valente, F. Figueras, Chem. Commun. 10 (1998) 1091.
51. K.K. Rao, F. Figueras, J. Sancez-Valente, M. Gravelle, J. Catal. 173 (1998) 115.
52. R. Bîrjega, O.D. Pavel, G. Costentin, M. Che, E. Angelescu, Appl. Catal. A 288 (2005) 185.
53. E. Angelescu, O.D. Pavel, M. Che, G. Costentin, Catal. Commun. 5 (2004) 647.
54. O.D. Pavel, R. Bîrjega, M. Che, G. Costentin, E. Angelescu, S. Şerban, Catal. Commun. 9 (2008) 1974.
55. H. Hattori, Appl. Catal. A 222 (2001) 247.
56. J.S. Valente, H. Pfeiffer, E. Lima, J. Prince, J. Flores, J. Catal. 279 (2011) 196.
57. V.K. Diez, C.R. Apesteguia, J.I. Di Cosimo, Catal. Today 63 (2000) 53.
58. A. Corma, V. Fornes, M.R. Martin-Aranda, F. Rey, F., J. Catal. 134 (1992) 58.
59. F. Prinetto, G. Ghiotti, R. Durand, D. Tichit, J. Phys. Chem. B 104 (2000) 11117.
60. R.E. Kirk, D.F. Othmer, Encyclopedia of Chemical Technology, 4th ed., vol. 9, John Wiley & Sons, New York, 1994, p. 797.
61. R.E. Kirk, D.F. Othmer, Encyclopedia of Chemical Technology, 4th ed., vol. 9, John Wiley & Sons, New York, 1994, p. 755.
62. M.R. Altıokka, A. Citak, Appl. Catal. A 239 (2003) 141.
63. W.T. Liu, C.S. Tan, Ind. Eng. Chem. Res. 40 (2001) 3281.
64. G.D. Yadaw, M.B. Thathagar, React. Funct. Polym. 52 (2002) 99.
65. M.J. Lee, J.Y. Chiu, H.M. Lin, Ind. Eng. Chem. Res. 41 (2002) 2882.
66. M. Altıokka, A. Çitak, Appl. Catal. A 239 (2003) 141.
67. I. Hoek, T.A. Nijhuis, A.I. Stankiewich, J.A. Moulijn, Appl. Catal. A 266 (2004) 109.
68. S.R. Kirumakki, N. Nagaraju, S. Narayanan, Appl. Catal. A 273 (2004) 1.
69. F. Zang, J. Wang, C. Yuan, X. Ren, Sci. China Ser B-Chem., 49 (2006) 140.
70. S. Ardizzone, C. L. Bianchi, V. Ragaini, B. Vercelli, Catal. Lett. 62 (1999) 59.
71. S. Khire, P.V. Bhagwat, M. Fernandes, P.B. Gangundi, H. Vadalia, Indian J. Chem. Technol. 19 (2012) 342.
72. J.H. Sepúlveda, J.C. Yori, C.R. Vera, Appl. Catal. A 288 (2005) 18.
73. F. Zhang, J. Wang, C. Yuan, X. Ren, Sci. China: Ser. B Chem. 49 (2006) 140.

74. K.M. Parida, S. Mallick, J. Mol. Catal. A 275 (2007) 77.
75. S.K. Bhorodwaj, M.G. Pathak, D.K. Dutta, Catal. Lett. 133 (2009) 185.
76. T.A. Peters, N. Benes, A. Holmen, J. Keurentjes, Appl. Catal. A 297 (2006) 182.
77. G. Busca in J.L.G. Fierro (Ed.), Metal Oxides: Chemistry and Applications, CRC Press, Boca Raton, 2006, ch. 9.
78. V.S. Braga, I.C.L. Barros, F.A.C. Garcia, S.C.L. Dias, J.A. Dias, Catal. Today 133–135 (2008) 106.
79. A.A. Costa, P.R.S. Braga, J.L. de Macedo, J.A. Dias, S.C.L. Dias, Micropor. Mesopor. Mater. 147 (2012) 142.
80. Y.M. Park, S.H. Chung, H.J. Eom, J.S. Lee, K.Y. Lee, Biores. Technol. 101 (2010) 6589.
81. R. Wan, S.C. Li, Y.P. Yuan, T.Y. Li, C.H. Du, Modern Chem. Ind. 30 (Suppl. 1) (2010) 37.
82. J. Gong, X. Ma, S. Wang, M. Liu, X. Yang, G. Xu, J. Mol. Catal. A 207 (2004) 215.
83. A.V. Biradar, S.B. Umbarkar, M.K. Dongare, Appl. Catal. A 285 (2005) 190.
84. R.F. Brandão, R.L. Quirino, V.M. Mello, A.P. Tavares, A.C. Peres, F. Guinhos, J.C. Rubim, P.A.Z. Suarez, J. Braz. Chem. Soc. 20 (2009) 954.
85. G.B. Varadwaj, K.M. Parida, Catal. Lett. 141 (2011) 1476.
86. S. Blagov, S. Parada, O. Bailer, P. Moritz, D. Lam, R. Weinand, H. Hasse, Chem. Eng. Sci. 61 (2006) 753.
87. S. Steinigeweg, J. Gmehling, Ind. Eng. Chem. Res. 41 (2002) 5483.
88. G. Mitran, É. Makó, Á. Rédey, I.C. Marcu, Catal. Lett. 140 (2010) 32.
89. G. Mitran, É. Makó, Á. Rédey, I.C. Marcu, CR Chim. 15 (2012) 793.
90. N. Haddad, E. Bordes-Richard, L. Hilaire, A. Barama, Catal. Today 126 (2007) 256.
91. M.A. Bañares, S.J. Khatib, Catal. Today 96 (2004) 251.
92. M. Roy, H. Ponceblanc, J.C. Volta, Top. Catal. 11/12 (2000) 101.
93. G. Mitran, O.D. Pavel, I.C. Marcu, J. Mol. Catal. A (2013) DOI: 10.1016/j.molcata.2013.01.001.

Section B

1. S.A.R. Mulla, O.V. Buyevskaya, M. Baerns, J. Catal. 197 (2001) 43.
2. O.V. Buyevskaya, D. Wolf, M. Baerns, Catal. Today 62 (2000) 91.
3. H.M. Swana, A. Toebes, J.R.H. Ross, Catal. Today 13 (1992) 201.
4. D.J. Wang, M.P. Rosynek, J.H. Lunsford, J. Catal. 151 (1995) 155.
5. S.J. Conway, J.H. Lunsford, J. Catal. 131 (1991) 513.
6. L. Leveles, S. Fuchs, K. Seshan, J.A. Lercher, L. Lefferts, Appl. Catal. A 227 (2002) 287.
7. H.X. Dai, C.F. Ng, C.T. Au, J. Catal. 189 (2000) 52.
8. H.X. Dai, C.F. Ng, C.T. Au, J. Catal. 193 (2000) 65.
9. J.E. Miller, A.G. Sault, D.E. Trudell, T.M. Nenoff, S.G. Thoma, N.B. Jackson, Appl. Catal. A 201 (2000) 45.
10. H.X. Dai, C.T. Au, Y. Chan, K.C. Hui, Y.L. Leung, Appl. Catal. A 213 (2001) 91.
11. K.A. Zemski, D.R. Justes, A.W. Castleman, Jr., J. Phys. Chem. A 105 (2001) 10237.
12. B. Solsona, A. Dejoz, T. Garcia, P. Concepcion, J.M. López Nieto, M.I. Vaazquez, M.T. Navarro, Catal. Today 117 (2006) 228.
13. K.I. Nakamura, T. Miyake, T. Konishi, T. Suzuki, J. Mol. Catal. A 260 (2006) 144.
14. X. Li, E. Iglesia, Appl. Catal. A. 334 (2008) 339.
15. J.M. López Nieto, P. Botella, M.I. Vázquez, A. Dejoz, Chem. Commun. (2002) 1906.
16. P. Botella, E.G. González, A. Dejoz, J.M. López Nieto, M.I. Vázquez, J. González-Calbet, J. Catal. 225 (2004) 428.
17. Y. Schuurman, V. Ducarme, T. Chen, W. Li, C. Mirodatos, G.A. Martin, Appl. Catal. A 163 (1997) 227.
18. E. Heracleous, A.A. Lemonidou, J. Catal. 270 (2010) 67.
19. B. Savova, S. Loridant, D. Filkova, J.M.M. Millet, Appl. Catal. A 390 (2010) 148.
20. M. Ai, Kinet. Catal. 44 (2003) 198.
21. P. Nagaraju, C. Srilakshmi, N. Pasha, N. Lingaiah, I. Suryanarayana, P.S. Sai Prasad, Appl. Catal. A 334 (2008) 10.
22. J.E. Miller, M.M. Gonzales, L. Evans, A.G. Sault, C. Zhang, R. Rao, G. Whitwell, A. Maiti, D. King-Smith, Appl. Catal. A 231 (2002) 281.
23. M. Ai, Appl. Catal. A 234 (2002) 235.

24. U. Zavyalova, P. Scholz, B. Ondruschka, Appl. Catal. A 323 (2007) 226.
25. S.C. Kim, W.G. Shim, Appl. Catal. B 79 (2008) 149.
26. A.R. Gandhe, J.S. Rebello, J.L. Figueiredo, J.B. Fernandes, Appl. Catal. B 72 (2007) 129.
27. F. Wyrwalski, J.M. Giraudon, J.F. Lamonier, Catal. Lett. 137 (2010) 141.
28. M.R. Morales, B.P. Barbero, L.E. Cadus, Appl. Catal. B 67 (2006) 229.
29. M. Alifanti, M. Florea, V.I. Parvulescu, Appl. Catal. B 70 (2007) 400.
30. U. Zavyalova, B. Nigrovski, K. Pollok, F. Langenhorst, B. Müller, P. Scholz, B. Ondruschka, Appl. Catal. B 83 (2008) 221.
31. N. van Vegten, T. Baidya, F. Krumeich, W. Kleist, A. Baiker, Appl. Catal. B 97 (2010) 398.
32. Z. Jiang, L. Kong, Z. Chu, L.J. France, T. Xiao, P.P. Edwards, Fuel 96 (2012) 257.
33. J.B. Silva, C.F. Diniz, R.M. Lago, N.D.S. Mohallem, J. Non-Cryst. Solids 348 (2004) 201.
34. J.C. Lou, Y.J. Tu, J. Air Waste Manag. Assoc. 55 (2005) 1809.
35. M. Florea, M. Alifanti, V.I. Parvulescu, D. Mihaila-Tarabasanu, L. Diamandescu, M. Feder, C. Negrila, L. Frunza, Catal. Today 141 (2009) 361.
36. O.A. Fouad, K.S. Abdel Halim, M.M. Rashad, Top. Catal. 47 (2008) 61.
37. A. Urdă, A. Herraïz, Á. Rédey, I.C. Marcu, Catal. Commun. 10 (2009) 1651.
38. J. Haber, Catal. Sci. Technol. 2 (1981) 13.
39. J.A. Toledo-Antonio, N. Nava, M. Martínez, X. Bokhimi, Appl. Catal. A 234 (2002) 137.
40. H. Lee, J.C. Jung, H. Kim, Y.M. Chung, T.J. Kim, S.J. Lee, S.H. Oh, Y.S. Kim, I.K. Song, Catal. Lett. 124 (2008) 364.
41. T.V. Choudhary, S. Banerjee, V.R. Choudhary, Appl. Catal. A 234 (2002) 1.
42. C.S. Hwang, N.C. Wang, Mat. Chem. Phys. 88 (2004) 258.
43. J.F. Lamonier, A.B. Boutoundou, C. Gennequin, M.J. Perez-Zurita, S. Siffert, A. Aboukais, Catal. Lett. 118 (2007) 165.
44. R. Dula, R. Janik, T. Machej, J. Stoch, R. Grabowski, E.M. Serwicka, Catal. Today 119 (2007) 327.
45. S. Tanasoi, N. Tanchoux, A. Urda, D. Tichit, I. Sandulescu, F. Fajula, I.C. Marcu, Appl. Catal. A 363 (2009) 135.
46. F. Trifiro, A. Vaccari, G. Del Piero, Stud. Surf. Sci. Catal. 39 (1988) 571.
47. L.A. Palacio, J. Velásquez, A. Echavarría, A. Faro, F.R. Ribeiro, M.F. Ribeiro, J. Hazard. Mater. 177 (2010) 407.

48. R.W. McCabe, P.J. Mitchell, Ind. Eng. Chem. Prod. Res. Dev. 23 (1984) 196.
49. L.J. Pettersson, A.M. Wahlberg, S.G. Jaras, Stud. Surf. Sci. Catal. 116 (1998) 465.
50. L.M. Gandía, M.A.Vicente, A. Gil, Appl. Catal. B 38 (2000) 295.
51. P.O. Larsson, H. Berggren, A. Andersson, O. Augustsson, Catal. Today 35 (1997) 137.
52. P. Fornasiero, E. Fonda, R. De Monte, G. Vlaic, J. Kašpar, M. Graziani, J. Catal. 187 (1999) 177.
53. K.J.A. Raj, B Viswanathan, Indian J. Chem. A 49 (2010) 401.
54. M. Haneda, T. Mizushima, N. Kakuta, A. Ueno, Bull. Chem. Soc. Jpn. 67 (1994) 2617.
55. H.J. Kwon, J.H. Baik, Y.T. Kwon, I.S. Nam, S.H. Oh, Chem. Eng. Sci. 62 (2007) 5042.
56. D.C. Sayle, S.A. Maicaneanu, G.W. Watson, J. Am. Chem. Soc. 124 (2002) 11429.
57. W.P. Dow, Y.P. Wang, T.J. Huang, Appl. Catal. A 190 (2000) 25.
58. F. Zamar, A. Trovarelli, G. Dolcetti, J. Chem. Soc. Chem. Commun. (1995) 965.
59. L.X. Yin, Y.Q. Wang, G.S. Pang, Y. Koltypin, A. Gedanken, J. Colloid Interface Sci. 246 (2002) 78.
60. S. Bernal, G. Blanco, M.A. Cauqui, P. Corchado, J.M. Pintado, J.M. Rodriguez-Izquierdo, Chem. Commun. (1997) 1545.
61. J.M. Herrmann, Catal. Today 112 (2006) 73.
62. A.K. Endalew, Y. Kiros, R. Zanzi, Biomass Bioenergy 35 (2011) 3787.
63. J.M. Marchetti, V.U. Miguel, A.F. Errazu, Renew. Sust. Energy Rev. 11 (2007) 1300.
64. H. Fukuda, A. Kondo, H. Noda, J. Biosci. Bioeng. 92 (2001) 405.
65. A. Brito, M.E. Borges, N. Otero, Energy Fuels 21 (2007) 3280.
66. Q. Shu, B. Yang, H. Yuan, S. Qing, G. Zhu, Catal. Commun. 8 (2007) 2159.
67. M. Sasidharan, R. Kumar, J. Mol. Catal. A 210 (2004) 93.
68. M. Zabeti, W.M.A.W. Daud, M.K. Aroua, Fuel Proc. Technol. 90 (2009) 770.
69. R. Jothiramalingam, M.K. Wang, Ind. Eng. Chem. Res. 48 (2009) 6162.
70. K.I. Mbaraka, R.R. Daniela, V.S.Y. Lin, B.H. Shanks, J. Catal. 219 (2003) 329.
71. K. Suwannakarn, E. Lotero, K. Ngaosuwan, J.G. Goodwin Jr., Ind. Eng. Chem. Res. 48 (2009) 2810.
72. A. Zieba, L. Matachowski, J. Gurgul, E. Bielanska, A. Drelinkiewicz, J. Mol. Catal. A 316 (2010) 30.
73. S. Furuta, H. Matsuhashi, K. Arata, Biomass Bioenergy 30 (2006) 870.

74. P.D. Patil, V.G. Gude, S. Deng, Ind. Eng. Chem. Res. 48 (2009) 10850.
75. R.S. Watkins, A.F. Lee, K. Wilson, Green. Chem. 6 (2006) 335.
76. W. Xie, Z. Yang, H. Chun, Ind. Eng. Chem. Res. 46 (2007) 7942.
77. N. Boz, M. Kara, Chem. Eng. Commun. 196 (2009) 80.
78. A. Kawashima, K. Matsubara, K. Honda, Bioresour. Technol. 99 (2008) 3439.
79. A. Brito, M.E. Borges, M. Garin, A. Henandez, Energy Fuels 23 (2009) 2952.
80. D.G. Cantrell, L.J. Gillie, A.F. Lee, K. Wilson, Appl. Catal. A 287 (2005) 183.
81. H.Y. Zeng, X. Deng, Y.J. Wang, K.B. Liao, AIChE J. 55 (2009) 1229.
82. O.D. Pavel, D. Tichit, I.C. Marcu, Appl. Clay Sci. 61 (2012) 52.
83. Kyoto protocol reference manual on accounting of emissions and assigned amount, United Nations Framework Convention on Climate Change (2008) 106.
84. Y.H. Hu, E. Ruckenstein, Adv. Catal. 48 (2004) 297.
85. S. Teuner, Hydrocarb. Process. 64 (1985) 107.
86. A.M. Gadalla, B. Bower, Chem. Eng. Sci. 43 (1988) 3049.
87. J.R. Rostrup-Nielsen, Stud. Surf. Sci. Catal. 81 (1993) 25.
88. M.C.J. Bradford, M.A. Vannice, Catal. Rev. Sci. Eng. 41 (1999) 1.
89. J.R.H. Ross, A.N.J. van Keulen, M.E.S. Hegarty, K. Seshan, Catal. Today 30 (1996) 193.
90. O. Tokunaga, S. Ogasawara, React. Kinet. Catal. Lett. 39 (1989) 69.
91. T. Inui, Catalysis, Royal Soc. Chem. 16 (2002) 133.
92. E. Ruckenstein, Y.H. Hu, J. Catal. 162 (1996) 230.
93. J.R. Rostrup-Nielsen, Stud. Surf. Sci. Catal. 68 (1991) 85.
94. K. Nagaoka, K. Takanabe, K. Aika, Chem. Commun. (2002) 1006.
95. J. Nakamura, K. Aikawa, K. Sato, T. Uchijima, Catal. Lett. 25 (1994) 265.
96. X.E. Verykios, Int. J. Hydrogen Energ. 28 (2003) 1045.
97. J.R. Rostrup-Nielsen, J. Catal. 144 (1993) 38.
98. S.B. Wang, G.Q. Lu, Appl. Catal. A 169 (1998) 271.
99. Z.X. Cheng, X.G. Zhao, J.L. Li, Q.M. Zhu, Appl. Catal. A 205 (2001) 31.
100. Z.L. Zhang, X.E. Verykios, Catal. Today 21 (1994) 589.
101. T. Horiuchi, K. Sakuma, T. Fukui, Y. Kubo, T. Osaki, T. Mori, Appl. Catal. A 144 (1996) 111.
102. A. Fonseca, E.M. Assaf, J. Power Sources 142 (2005) 154.

103. R. Lanza, J.A. Velasco, S.G. Jaras, Catalysis, Royal Soc. Chem. 23 (2011) 50.
104. A.I. Tsyganok, T. Tsunoda, S. Hamakawa, K. Suzuki, K. Takehira, T. Hayakawa, J. Catal. 213 (2003) 191.
105. A. Bhattacharyya, V.W. Chang, D.J. Schumacher, Appl. Clay Sci. 13 (1998) 317.
106. J.S. Choi, K.I. Moon, Y.G. Kim, J.S. Lee, C.H. Kim, D.L. Trimm, Catal. Lett. 52 (1998) 43.
107. C. Forano, T. Hibino, F. Leroux, C. Taviot-Gueho in F. Bergaya, B.K.G. Theng and G. Lagaly (Eds.), Handbook of Clay Science, Developments in Clay Science, Elsevier, Amsterdam, vol. 1, 2006, p. 1021.